ATOM INTERACTIONS
WITH SOLID SURFACES

JOE N. SMITH Jr.

ATOM INTERACTIONS
WITH SOLID SURFACES

PROEFSCHRIFT

TER VERKRIJGING VAN DE GRAAD VAN DOCTOR IN DE WISKUNDE
EN NATUURWETENSCHAPPEN AAN DE RIJKSUNIVERSITEIT TE LEIDEN,
OP GEZAG VAN DE RECTOR MAGNIFICUS, DR. J. GOSLINGS, HOOG-
LERAAR IN DE FACULTEIT DER GENEESKUNDE, TEN OVERSTAAN VAN
EEN COMMISSIE UIT DE SENAAT TE VERDEDIGEN OP DONDERDAG
28 MEI 1970 TE KLOKKE 16.15 UUR

DOOR

JOE NELSON SMITH Jr.

GEBOREN TE WASHINGTON, D.C. IN 1932

Promotoren: professor dr J. Kistemaker
en   professor dr J. Los.

TABLE OF CONTENTS

TABLE OF CONTENTS

INTRODUCTION

In the interaction of low energy ($\le$ 1 eV) atomic beams with solid surfaces, diverse processes may occur depending on the particular nature of the atom-surface system under consideration. Excluding chemical reaction of the impinging atom with the surface, or with atoms of other species adsorbed on the surface, the subsequent re-emission of the atom is determined by its life history in the region of the surface. To adequately describe the history, one needs to know the interaction time τ, between the atom and the surface, the interaction potential, $V(r)$, and the mechanism of energy transfer between the atom and the surface. Implicit in knowledge of these parameters is the nature of the force existing between the atom and the surface (e.g. van der Waals, co-valent, ionic etc.), the phonon spectrum and electronic band structure of the solid (at its free surface), and the corresponding electronic configuration of the interacting atom, and the perturbation of these properties due to the interaction itself.

Experimentally, the initial and final state of the atom can be well defined and from such measurements one attempts to infer the mechanism of interaction with the surface that gave rise to the observed change of state of the atom. This procedure is full of uncertainties because similar determinations of the initial and final state of the other collision partner, the surface, are not measurable. Indeed the properties of an ideal free surface of a solid material are not known accurately and the properties of a real surface, under experimental conditions, are usually very poorly defined indeed.

At the present level of technology, one must resort to differential experiments in order to attempt to determine the properties of the surface that influence its interaction with a gas atom. Thus one determines the change in state of the atom, as a result of the interaction, by altering the properties of the surface in a known way. For example one may alter the crystal structure of the surface or the degree of surface contamination and determine the influence of these perturbations on the final state of the gas atom, or one may study the interaction of the same species of gas with a variety of surfaces under the same experimental conditions.

In the succeeding chapters of this work, this "differential" approach to the question of surface properties on the atom-surface interaction is developed. Chapters 1, 2 and 3 describe experiments concerned with the scattering of rare gases from solid surfaces. Chapter 1 presents a critical review of work in

this field performed prior to 1967, including the work of the present author.
The experiments reported in chapter 2 emphasize the importance of considering
interaction time and the thermal motion of the lattice in determining the
final state of the reflected gas atom. The experiments reported in chapter 3
demonstrate that thermal energy atomic beam scattering from surfaces yields
information about the amplitude of the interaction potential in the plane of
the surface and suggests the influence of normal modes of vibration on the
scattering.

While revealing a great deal about the role played by the surface in the
atom-surface interaction, the type of experiments reported in chapters 1
through 3 are not amenable to a direct determination of the interaction time
or magnitude of the force of attraction between the atom and the surface.
Chapter 4 describes experiments concerned with the surface ionization of pot-
assium on tungsten, in which the interaction time, τ, and bond energy, Q, are
measured directly, as a function of the degree and type of surface contamina-
tion. These later experiments demonstrate rather explicitly that the nature
of the bonding of the adsorbed contaminant to the surface has a dramatic
effect on interaction of the atom with the surface and these results are shown
to be in agreement with inferences that were made in the earlier work (cf.
chapters 1 - 3).

In addition to thus providing supplementary information on the perturbation
of the atom-surface interaction produced by various types of contamination,
the surface ionization experiments on the K/W system reported in chapter 4
provide a deeper insight into the physical interpretation of the pre-exponential
factor, τ_o, defined by the relation $\tau = \tau_o \exp Q/kT$, than has heretofore been
obtained experimentally. In addition, an interrelation between τ_o and Q is
strongly suggested by these results.

In order to continue this study of τ_o and Q similar experiments were under-
taken for the Na/W system and are reported in chapter 5. While time did not
permit these latter experiments to be carried to completation, several im-
portant observations were made and are reported in chapter 5, along with sug-
gestions for further experimental study and analysis.

Following chapter 5 is a summary of the work reported in this thesis and
a presentation of the conclusions that may be derived therefrom. Finally, the
curriculum vitae of the author is given.

CHAPTER I

MOLECULAR BEAM SCATTERING FROM SOLID SURFACES*†

Joe N. Smith, Jr. and Howard Saltsburg

General Atomic Division, General Dynamics Corporation
John Jay Hopkins Laboratory for Pure and Applied Science
San Diego, California

A general review of molecular-beam
solid-surface scattering experiments
is given with particular emphasis upon
recent studies of directed scattering.
A general improvement in experimental
techniques has made these data more
amenable to theoretical interpretation.
On the other hand, these refinements
demonstrate quite dramatically the de-
ficiencies in such studies, particularly
with regard to the solid surface, and
these deficiencies are reviewed along
with suggestions for further work. Com-
parison of experiment with theory, where
applicable, is also made. The studies
cited are restricted to beam energies
< 1 eV and exclude chemical reaction
and molecular dissociation and
reconstitution.

INTRODUCTION

The simplest conceptual picture of the primary process in the interaction between a gas and a solid surface, that of the collision of a single gas particle with a coupled lattice of other particles, can be realized experimentally with molecular beam techniques.

The advantages accruing from this experimental approach have been well documented[1] and result from the ability to control or to specify the initial state of the incident molecules. This initial state is defined in terms of the molecular velocity, mass, incident angle, internal energy and other intrinsic properties, such as polarizability and electric and magnetic moments, which affect the gas-surface interaction.

The interaction can be considered to be a two-body collision although one of the bodies is very large, and has a complex internal energy structure; as a result, the interaction is more complex than that between two isolated atoms. At large distances, for example, the attractive portion of the potential varies more slowly for a gas atom-surface system than for an atom-atom system. Further, even in an ideal lattice the properties of surface particles are different from those of the bulk particles, yet they are coupled via lattice forces.

From an energy-transfer standpoint, one may define, conceptually, two extremes in molecule-surface collision phenomena, i.e. completely elastic scattering (no internal energy change in either the gas molecule or the lattice) and trapping (permanent adsorption and complete energy accommodation). In the former case, if the obvious geometrical criteria are met, diffraction may be observed. For the latter case, re-emission does not occur. Between these limiting conditions, as the trapping condition is approached (on an energy-transfer basis), the re-emission which occurs tends to become more diffuse. However, as will be discussed later, Knudsen or cosine scattering need not be associated with an accommodation coefficient, AC, of unity. Similarly, for elastic collisions, the AC for translational energy transfer need not vanish (i.e., the Baule model); by definition, however, the AC for internal energy transfer (rotation, vibration, and phonon excitation) must be zero. In the range 0 < AC < 1, the spatial distribution of a scattered beam is indicative of the dynamical response of the gas-surface system to the collision and it is this type of scattering (directed scattering) to which the major portions of this review is devoted.

In the main, molecular beam studies of gas-surface interactions have been limited to a study of the changes in some characteristic property of the gas induced by the collision while the solid surface is relegated to a less precise descriptive role. This is due, of course, to the relative ease of studying, experimentally, the gas particle in collision compared with studying the solid. This is a serious experimental deficiency which has not yet been resolved and, as a result, our quantitative understanding of even relatively simple collision processes is far from complete. Nevertheless, many qualitative features of the collision process can be deduced and these will be discussed.

This review will be limited to molecular beam studies of scattering and energy transfer in neutral gas-solid collisions where molecular dissociation and reconstitution, and chemical reaction and condensation, do not occur. In the following sections a brief review of experimental techniques will be given, followed by a summary of the experimental observations together with suggestions for future studies.

EXPERIMENTAL TECHNIQUES

Beam Generation

Several classes of molecular beam sources are available, each class having a characteristic energy range and maximum beam flux. To date, nearly all molecular beam-surface interaction experiments have utilized conventional oven beam sources which limit beam energies to ≤ 0.50 eV, and which yield only modest fluxes ($\leq 10^{14}$ particles/cm^2-sec). Under proper operating conditions the beam, using such a source, has a Maxwellian distribution in velocity. Aerocynamic nozzle beams are beginning to find application in surface studies where an energy range of 0.5 to 5 eV is desired. Nozzle beam sources deliver high fluxes ($\sim 10^{18}$-10^{19} particle/cm^2-sec) and the beams are essentially monoenergetic, although the exact distribution of speeds must be determined experimentally. The current status of nozzle-beam development has been reviewed by Knuth[2] and French[3]. To obtain very high energy beams (> 100 eV), neutralized ion beams have been used[4] and attempts are being made to lower these energies to below 10 eV[5]. In principle, energy-selected beams may be obtained in this way, but the fluxes are severely limited by space charge spreading of the parent ion beam at the lower energies. Sodickson,

Carpenter, and Davidson[6] have proposed a new technique utilizing a container filled with the desired beam gas which is accelerated to high velocity, then ruptured (in vacuum), allowing the gas to emerge. Velocities of 10^6 cm/sec and instantaneous fluxes of 10^{25} molecules/cm^2-sec appear feasible. However, beam contamination and low repetition rates seem to be serious problems with this technique.

Detectors

Electron impact ionization of the neutral species, and measurement of the resulting ion current, provide the nearly universal method of detecting molecular beams, although specialized methods exist for low ionization potential species[1], reactive species[7], and easily condensable species[8]. Electron impact detectors may be designed to measure either the beam flux, J [9], or the beam density, n [10]. Estimates of the mean velocity, $\bar{v}$, may be made by simultaneous comparison of the beam flux and beam density, since $\bar{v} = J/n$ [11,12]; using modulated beams, the transit time of the beam over a known path may be determined by phase shift measurements[13,14]. A more sophisticated approach involves the measurement of the velocity distribution of the beam: time-of-flight techniques utilizing pulsed beams and waveform analysis[15,16], the Stern-Gerlach effect[17], and slotted-disc velocity selectors (SDVS) of various types[18,19] have also been employed.

The gross response of the solid to the time-averaged effect of numerous molecule-surface collisions has been determined in a limited number of experiments. Thus sensitive torsion balances have been employed to determine momentum transfer to a surface by a beam[10,20,21] and energy transfer has been determined by measuring the temperature rise of a piezoelectric crystal upon which the desired target material has been plated[22].

Surface Preparation

In all studies of gas-surface interactions, the nature of the surface is of prime importance, and represents, by far, the greatest complication in such experiments. Experiments performed on "engineering" surfaces are, for this reason, most difficult to discuss in terms of fundamental phenomena. Even in the case of experiments employing single crystals, however, the problem is only partially resolved due to the influence of surface contamination, for it was

shown clearly by Roberts[23] that adsorbed gases had very pronounced effects on energy transfer in the gas-solid system.

The earliest molecular beam scattering experiments utilized cleavage faces of alkali-halide single crystals[24-26]; more recently, metal single crystals[27,28] have been investigated. In these experiments, the orientation of the crystal was determined and in some cases separate studies of surface structures were made but no in-situ studies of the structure at the surface were made in conjunction with the beam experiment. It is, however, frequently possible to infer, with considerable reliability, the gross structure of the surface from other previous studies.

The problem of surface contamination has received much attention in recent years, though applications of clean surface techniques to beam scattering experiments are limited. Roberts[29] has reviewed several techniques for generating clean surfaces in ultrahigh vacuum (UHV). Cleavage of LiF crystals under vacuum conditions has been used by Crews[26] and conventional UHV techniques have been employed by Hinchen and Foley[13]. Another approach to the problem, developed by Smith and Saltsburg[27], utilized continuous deposition of metal surfaces at a rate faster than the contamination rate resulting from background gas adsorption. Further, the substrate material and temperature were chosen so as to permit epitaxial growth of single crystals.

In all these recent studies, serious attempts at characterization of the scattering surface (gross crystallography and surface contamination from the gas phase) were made, but complete understanding of all the relevant parameters is not yet at hand as is indicated below.

SUMMARY OF EXPERIMENTAL RESULTS

Scattering studies may be divided into three categories based upon the spatial behavior of the scattered beam: diffraction, diffuse scattering, and directed scattering. Each has been observed and although a full theoretical description still is not available, the experimental observations can be understood qualitatively and in some cases semi-quantitatively.

Only a limited number of beam scattering studies in which energy transfer is studied have been reported, although much work is in progress.

Diffraction

A necessary, but not sufficient, condition for diffraction is a fully elastic collision between a gas atom and a lattice, resulting in zero energy transfer to the lattice. The geometrical criteria for the observation of diffraction is the proper relationship between the de Broglie wavelength of the gas atom, the lattice spacing, and the angle of incidence, and is independent of the interaction potential and, of course, lattice dynamical considerations. First-order diffraction has been observed for H atoms on LiF[7], and H_2 and He on LiF[24,26, 30,31]. Zabel[25] has reported poorly resolved diffraction peaks for He, Ne and A from NaCl although, in the plane-of-incidence, diffraction was observed only for He and there is some question about the origin of the peaks seen in Ne and A. In recent experiments on metal single crystals, first-order diffraction peaks have not been observed, although a significant degree of specular reflection was found for He and H_2 on Ag[32].

Diffraction peaks observed in scattering from alkali halides were shown to result from coherent scattering from a two-dimensional net of like ions in the surface of the crystal; no evidence of diffraction from the interior of the crystal has been obtained. Estermann and Stern[24], Zabel[25], and Crews[26] showed that the width of the diffraction peak was a result of the (assumed) Maxwellian velocity distribution of the incident beams. Using mono-energetic beams, Estermann, Frisch and Stern[30] verified the de Broglie wavelength of He to within 1%. The use of a smooth single crystal for the observation of diffraction appears to be a necessary but not sufficient condition since diffraction is observed for He on LiF but not on Au and Ag crystals. Further, the variation in intensity of the scattered specular beam for different alkali halides[7] indicates that the criteria for a satisfactory diffraction surface are not well defined and that even on cleavage faces of alkali halides, significant inelastic interactions occur.

The effect of surface contamination on the geometrical aspects of diffraction is minimal since both Estermann and Stern and Crews, utilizing rather different vacuum conditions, were able to observe diffraction peaks of He on LiF. Even here, however, significant inelastic effects are observed and have been described (selective adsorption,[33]).

Diffuse Scattering

Diffuse scattering is characterized by the intensity of the scattered beam flux varying as the cosine of the angle between the direction of observation and the target normal. Although widely observed, detailed interpretation is difficult. Any process in which the particle spends a significant time in interaction with the surface (relative to a single elastic collision) may lead to diffuse scattering. Though usually associated with microscopically rough surfaces or grossly contaminated surfaces, it has been observed for NH_3 scattered from a clean (111) plane of Ag, this same surface displays highly directed scattering of He[34]. Diffuse reflection has been observed for N_2 scattered from contaminated Al under conditions where multiple specular reflections could be distinguished from diffuse re-emission, and the latter was found to be the predominant mechanism[35]. Although the spatial randomization is complete in diffuse scattering, energy accommodation need to be. An accommodation coefficient of 0.35 has been reported for A diffusely scattered by Ni[11]. Finally, surfaces, from which diffuse scattering at thermal energies would be expected, may behave differently at higher energies. Thus, a complex lobular pattern has been observed for 1 eV a scattered from dirty brass[36].

Directed Scattering - General Observations

Directed scattering (also referred to as lobular scattering) of molecular beams from solid surfaces is the result of the complex dynamical interaction of the gas-solid system when a free atom or molecule collides with a crystalline lattice. The scattered beam has a spatial distribution which is not generally describable in terms of superposition of diffuse scattering and specular reflection (or diffraction). In this context specular reflection is to be distinguished from specularly directed reflection. The latter implies that the angular divergence of the scattered beam is very much greater than that of the incident beam. Directed scattering is consequently a function of the parameters of the system which are related to the interaction potential and lattice dynamics. Although directed scattering has been observed on many kinds of surfaces --clean, contaminated, single and polycrystalline with all the possible permutations-- the qualitative trends of the scattering are essentially the same.

Before describing the basic phenomenology of directed scattering it will be well to note the sensitivity of scattering distributions to the condition of the target surface, in terms of surface structure and contamination. This has perhaps been best demonstrated using expitaxially grown Au films[27]. For He, the effect of surface contamination is shown in Fig. 1. Using a He beam (300°K) incident at 50° upon (111) plane of Au, whose temperature was fixed at 560°K, scattering distributions were measured during deposition (i.e. upon a clean crystal) and following cessation of deposition, during which time the surface became contaminated. Curve A was obtained during the continuous deposition of Au, and the scattered beam in this case is relatively narrow and specularly directed. The evaporation was then terminated abruptly and the intensity of the scattered beam at the specular angle ($\theta_r = 50°$) was observed to decrease, accompanied by an increase in the width of the scattered beam. Curve B, obtained approximately 30 minutes later, is the limiting steady-state distribution. The increased dispersion in the scattered beam (curve A to B) was shown to be a direct result of contamination of the Au surface from the ambient vacuum background ($\approx 10^{-7}$ torr). Note that even the contaminated surface (curve B) exhibits specularly directed scattering. With argon a similar comparison shows that the dispersion in the scattered beam produced by contamination is considerably less than with He and the scattered beam is shifted by about 10° toward the target normal upon contamination. With Ag targets, also produced by continuous evaporation, the effects of contamination upon the beam scattering are negligible, i.e., when evaporation is terminated, the scattering of all gases studied remains virtually unchanged for several hours. This striking stability of epitaxially grown Ag films has been discussed by Saltsburg and Smith[34] and recent LEED studies of epitaxially grown Ag show the existence of very stable structures resulting from oxygen adsorption[37]. One further observation is relevant. In all metal surface systems (including Ag and Au crystals) from which molecular beams have been scattered, at ambient pressures in the region of 10^{-7} torr, there exists a temperature below which the surface exhibits diffuse reflection. This is a reversible transition and is always in the region of 200°C. The most reasonable explanation lies in a contaminant adsorption since only in the UHV work of Hinchen and Foley is this effect not seen.

The effect of gross crystal structure of the surface is exhibited for the scattering of He from Au (Fig. 2). Both scattering distributions A and B were
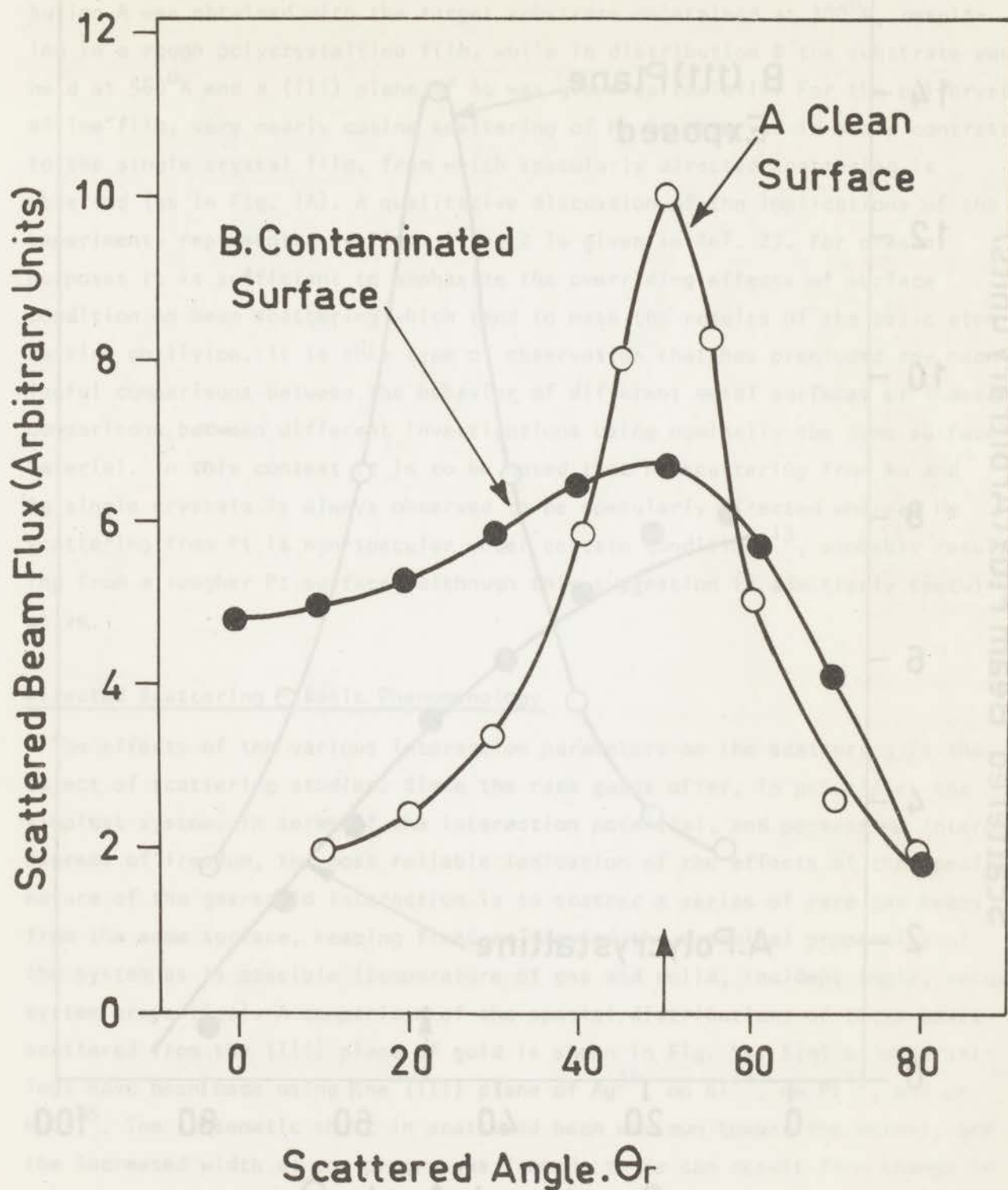
Fig. 1 - He scattering from the (111) plane of Au, (A) during, and (B) after
deposition (P ~ 5 x 10^{-7} torr). Θ_i = 50° measured from target normal,
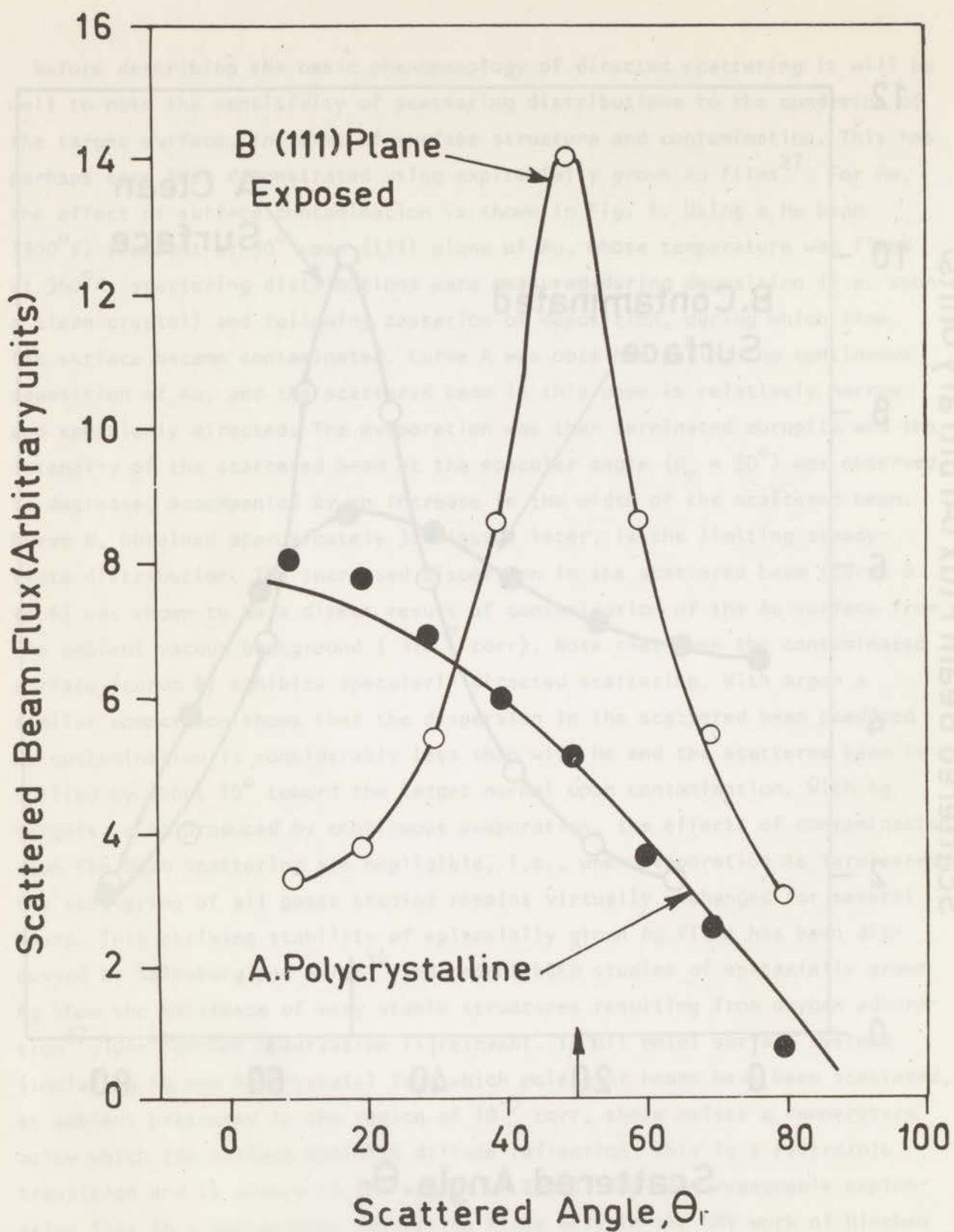T_B = 300°, T_T = 560°K. Ref. 27.

Fig. 2 - He scattering from clean Au; $\theta_i = 50^\circ$ for both (A) and (B). Ref. 27.

obtained during Au deposition, and hence represent clean surfaces. Distri-
bution A was obtained with the target substrate maintained at 300°K, result-
ing in a rough polycrystalline film, while in distribution B the substrate was
held at 560°K and a (111) plane of Au was grown epitaxially. For the polycryst-
alline film, very nearly cosine scattering of He is observed in sharp contrast
to the single crystal film, from which specularly directed scattering is
observed (as in Fig. 1A). A qualitative discussion of the implications of the
experiments represented by Figs. 1 and 2 is given in Ref. 27. For present
purposes it is sufficient to emphasize the overriding effects of surface
condition on beam scattering which tend to mask the results of the basic atom-
lattice collision. It is this type of observation that has precluded any mean-
ingful comparisons between the behavior of different metal surfaces or indeed
comparisons between different investigations using nominally the same surface
material. In this context it is to be noted that He scattering from Au and
Ag single crystals is always observed to be specularly directed whereas He
scattering from Pt is non-specular under certain conditions[13], probably result-
ing from a rougher Pt surface, although this suggestion is admittedly specul-
ative.

Directed Scattering - Basic Phenomenology

The effects of the various interaction parameters on the scattering is the
object of scattering studies. Since the rare gases offer, in principle, the
simplest system, in terms of the interaction potential, and possess no internal
degrees of freedom, the most reliable indication of the effects of the specific
nature of the gas-solid interaction is to scatter a series of rare gas beams
from the same surface, keeping fixed as many of the dynamical properties of
the system as is possible (temperature of gas and solid, incident angle, vacuum
system properties). A comparison of the spatial distributions of these gases
scattered from the (111) plane of gold is shown in Fig. 3a. Similar observat-
ions have been made using the (111) plane of Ag[34], on Ni[11], on Pt[13], and on
NaCl[25]. The systematic shift in scattered beam maximum toward the normal, and
the increased width as one progresses from He to Xe can result from change in
either the mass of the gas atom or the interaction energy between the atom and
the surface, due to polarization forces. The "hard-cube" model[38] has been used
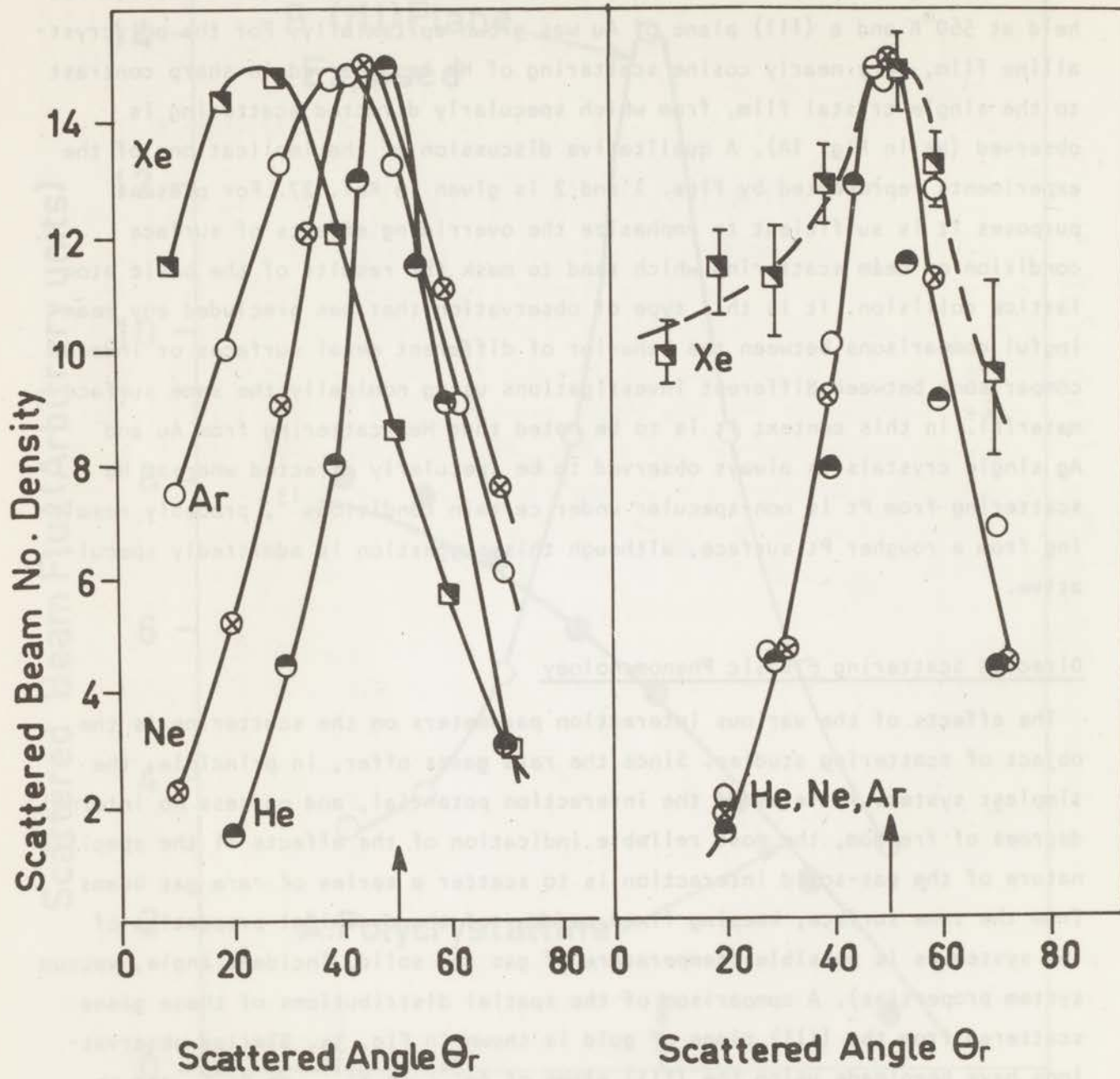to examine the separate effects of the change in mass of the gas atom and the

Fig. 3 - Rare gas scattering from Au(111) measured during Au deposition;
(a) $T_B = 300°K$, $T_T = 560°K$, $\theta_i = 50°$; (39) (b) $T_B = 2500°K$, $T_T = 560°K$, $\theta_i = 50°$. Ref. 39.

change in well depth, assuming a square well interaction potential. A factor of 10 increase in either mass or well depth results in a shift in the position of the scattered beam, by $\sim$ 10 deg, toward the target normal. For the series of rare gases on Au (Fig. 3a), the mass change is a factor of 32 and the heat of adsorption (assumed proportional to well depth) varies by 12, making the distinction less evident this case.

Results of studies with Ne, CH_4, and NH_3 scattered from (111) Ag imply, however, that ΔH is the dominant factor, for in this case a transition from highly directed scattering to nearly diffuse scattering for gases of similar mass, but greatly different heat of adsorption, is seen[34]. In these experiments, the Ne distribution was quite narrow and nearly specularly directed while NH_3 was diffusely scattered; the CH_4 distribution was intermediate between these two extremes. The dominance of the role of the interaction potential in these results is inferred by noting that the mass increases by only 20%, going from CH_4 to Ne, but the heat of adsorption decreases by a factor of $\sim$ 8 between NH_3 and Ne.

Of obvious importance, in addition to the interaction potential, is the beam energy and for the rare gases on Au, a comparison of Fig. 3a with Fig. 3b exhibits the effects of beam temperature on the scattering. For He, Ne and A the scattered beam, which was subspecular (lying between the target normal and the specular angle) at 300°K becomes specularly directed at 2500°K. In addition, the Ne and A distributions have narrowed sufficiently so that for the three lighter gases the distributions essentially coincide. For Xe, although the position of maximum intensity has shifted to the specular angle, considerable scattering near the normal is observed. It is possible to subtract a diffuse scattering (cosine) distribution from the hot Xe distribution (Fig. 3b) and the remaining distribution very nearly coincides with the distribution for the lighter gases, implying an apparent superposition of diffuse and specularly directed scattering. This result is not too surprising if one considers the considerably stronger interaction of Xe with the metal surface as compared with He, Ne, and A; crude energy transfer calculations based upon hard sphere and lattice models reinforce this conclusion invoking transient adsorption or trapping as the origin of the diffuse component[39].

All experiments involving changes in the beam temperature, T_B, or solid temperature, T_S, result in a nearly universal observation that, as the ratio
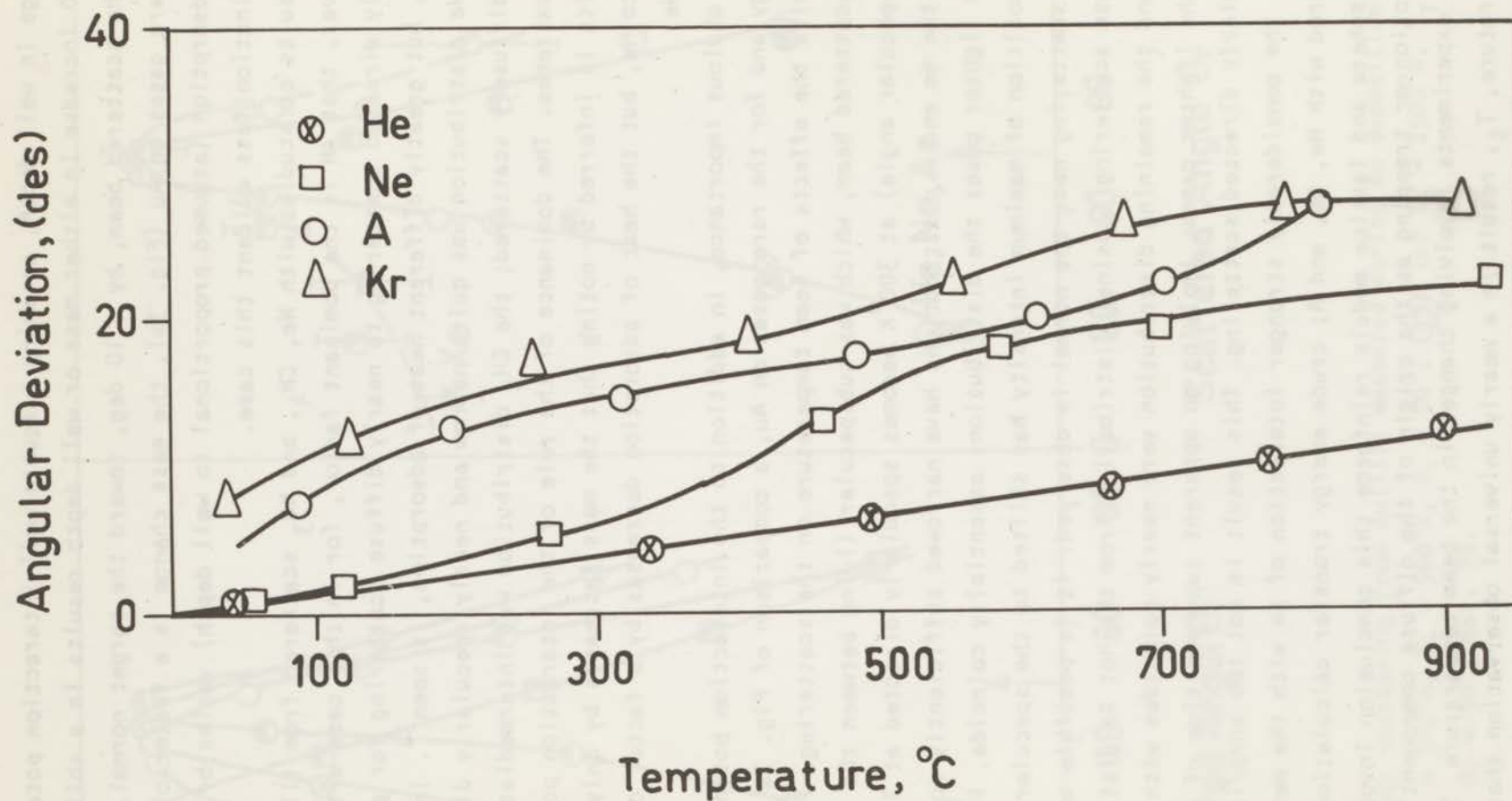
Fig. 4 - Rare gas scattering from annealed polycrystalline Pt. The angular
deviation is the displacement of the position of maximum intensity
in the scattered beam toward the target normal from the specular
angle; $T_B = 300°K$, $\theta_i = 67.5°$ (measured from target normal) Ref. 13.
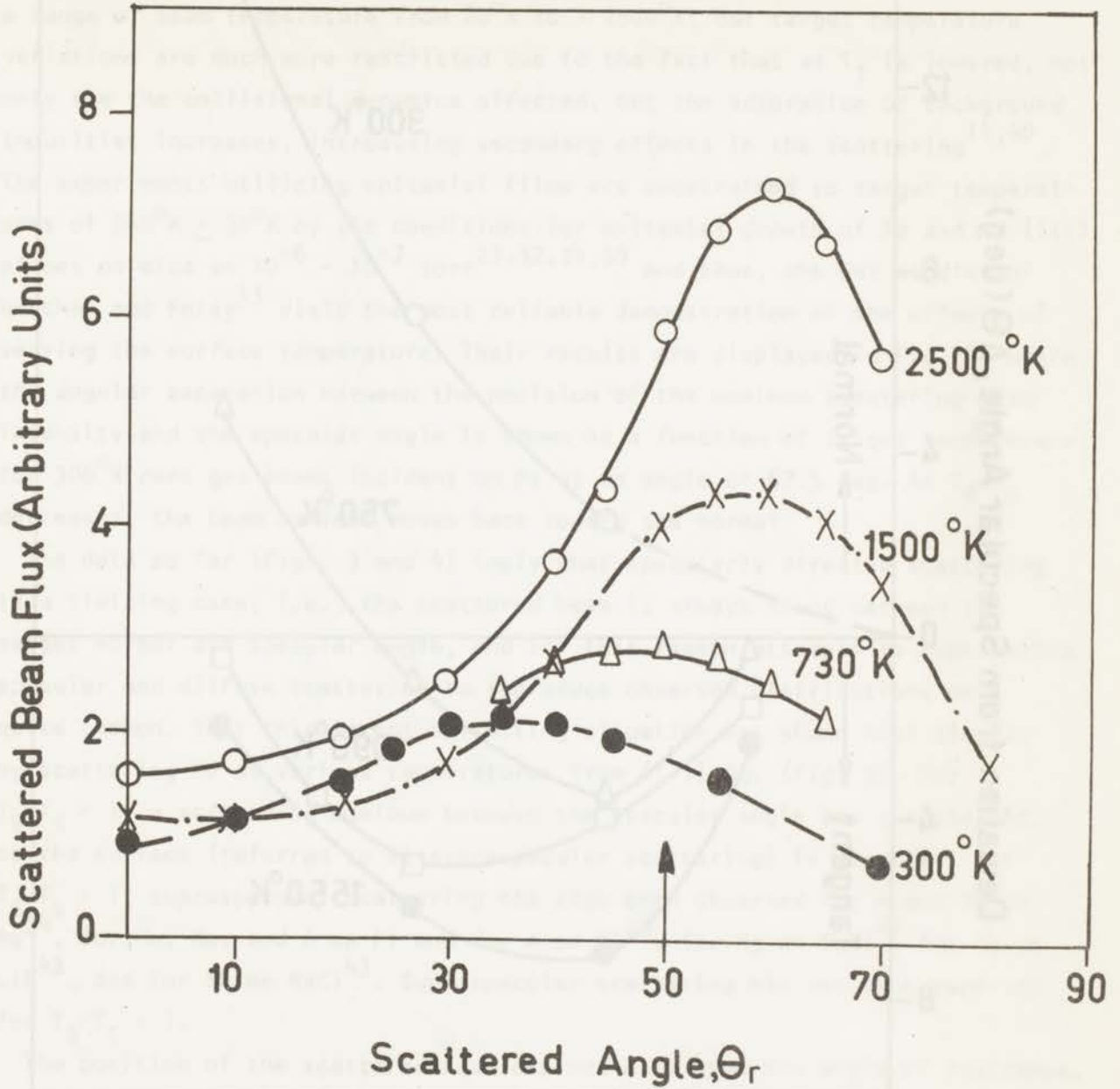
Fig. 5 - Xe scattering from Ag(111) at four beam temperatures $T_T = 560°K$, $\theta_i = 50°$. Ref. 34.
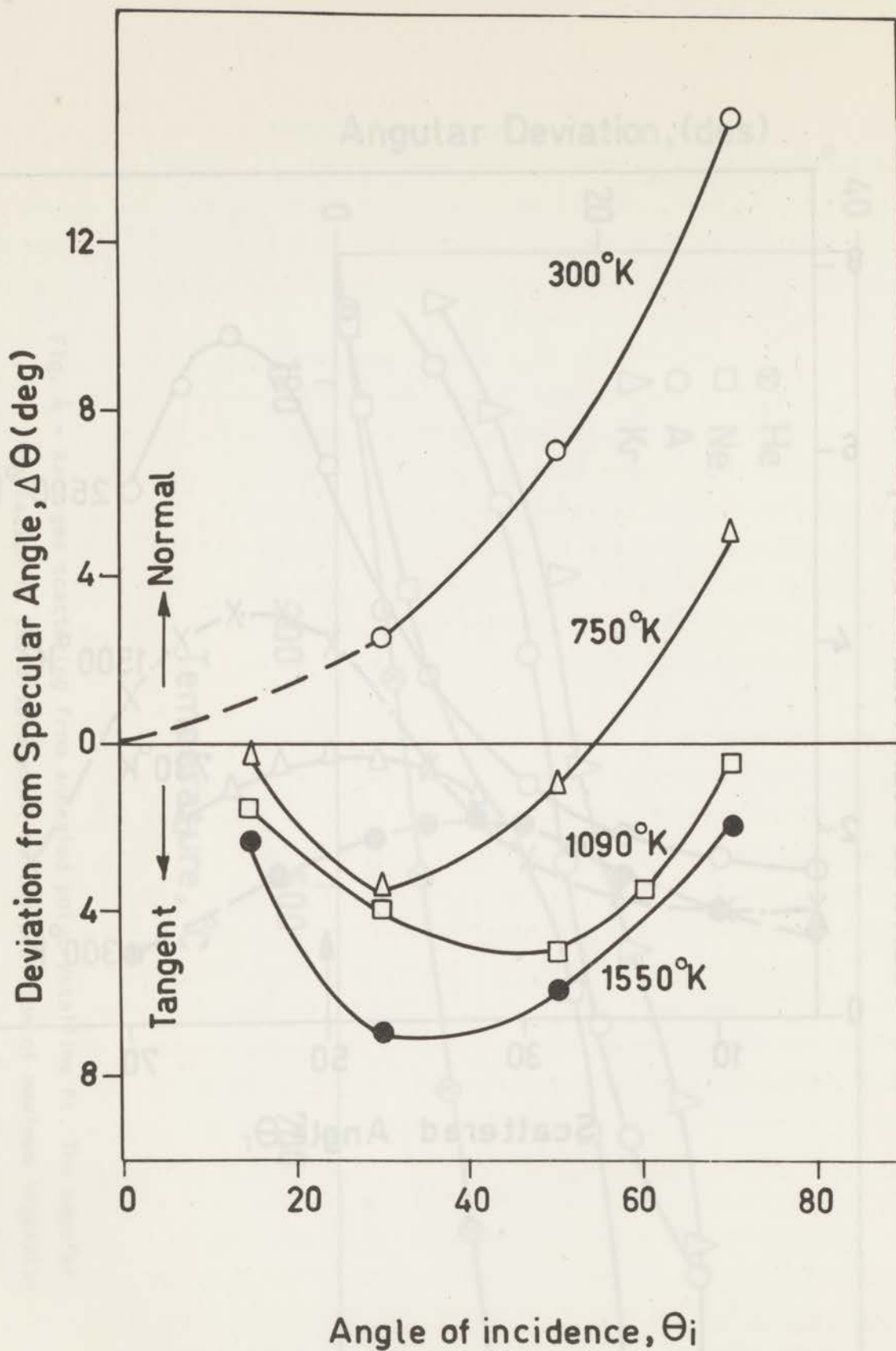
Fig. 6 - Angular deviation of the scattered beam from the specular angle as a function of θ_i at four beam temperatures, for A on Ag(111), $T_T = 560°K$. Ref. 34.

T_B/T_S is increased, the scattered beam moves away from the target normal and the width of the beam decreases (Fig. 3). This observation has been made over a range of beam temperature from $80°K$ to ~ $2500°K$, but target temperature variations are much more restricted due to the fact that as T_T is lowered, not only are the collisional dynamics affected, but the adsorption of background impurities increases, introducing secondary effects in the scattering[11,40]. The experiments utilizing epitaxial films are constrained to target temperatures of $560°K \pm 30°K$ by the conditions for epitaxial growth of Ag and Au (111) planes on mica at $10^{-6} - 10^{-7}$ torr[27,32,34,39] and thus, the UHV studies of Hinchen and Foley[13] yield the most reliable demonstration of the effects of varying the surface temperature. Their results are displayed in Fig. 4, where the angular separation between the position of the maximum scattering beam intensity and the specular angle is shown as a function of target temperature for $300°K$ rare gas beams incident on Pt at an angle of 67.5 deg. As T_B/T_S decreases, the beam maximum moves back toward the normal.

The data so far (Figs. 3 and 4) imply that specularly directed scattering is a limiting case; i.e., the scattered beam is always found between the target normal and specular angle, and for this reason attempts to superimpose specular and diffuse scattering to reproduce observed distributions were quite common. That this is not a limiting situation was shown most clearly by scattering Xe at various temperatures from (111) Ag. (Fig. 5). For $T_B/T_S > 1$, a scattering maximum between the specular angle and the tangent to the surface (referred to as supraspecular scattering) is observed. For $T_B/T_S > 1$, supraspecular scattering has also been observed for A and Ne on Ag^{34}, for He, Ne, and A on Pt and for A on Ni^{28}, for Hg on $NaCl^{41}$ for Hg on LiF^{42}, and for Sb on $NaCl^{43}$. Supraspecular scattering has not been reported for $T_B/T_S < 1$.

The position of the scattered beam depends also upon the angle of incidence, as shown in Fig. 6 for A on Ag. At a beam temperature of $300°K$ ($T_B/T_S = 0.54$), a steadily increasing $\Delta\Theta$ is observed as Θ_i increases. It is also observed that the width of the scattered beam increases as Θ_i increases, with an associated decrease in intensity. For $T_B/T_S > 1$, supraspecular scattering is observed for a range of Θ_i, becoming subspecular at glancing incidence. Intensity variations of the beam are also observed in this latter case but are not simply related to the variations in $\Delta\Theta$. For $\Theta_i > 45°$, A on Pt exhibits behavior that is qualitatively the same as shown in Fig. 6, but for given Θ_i and
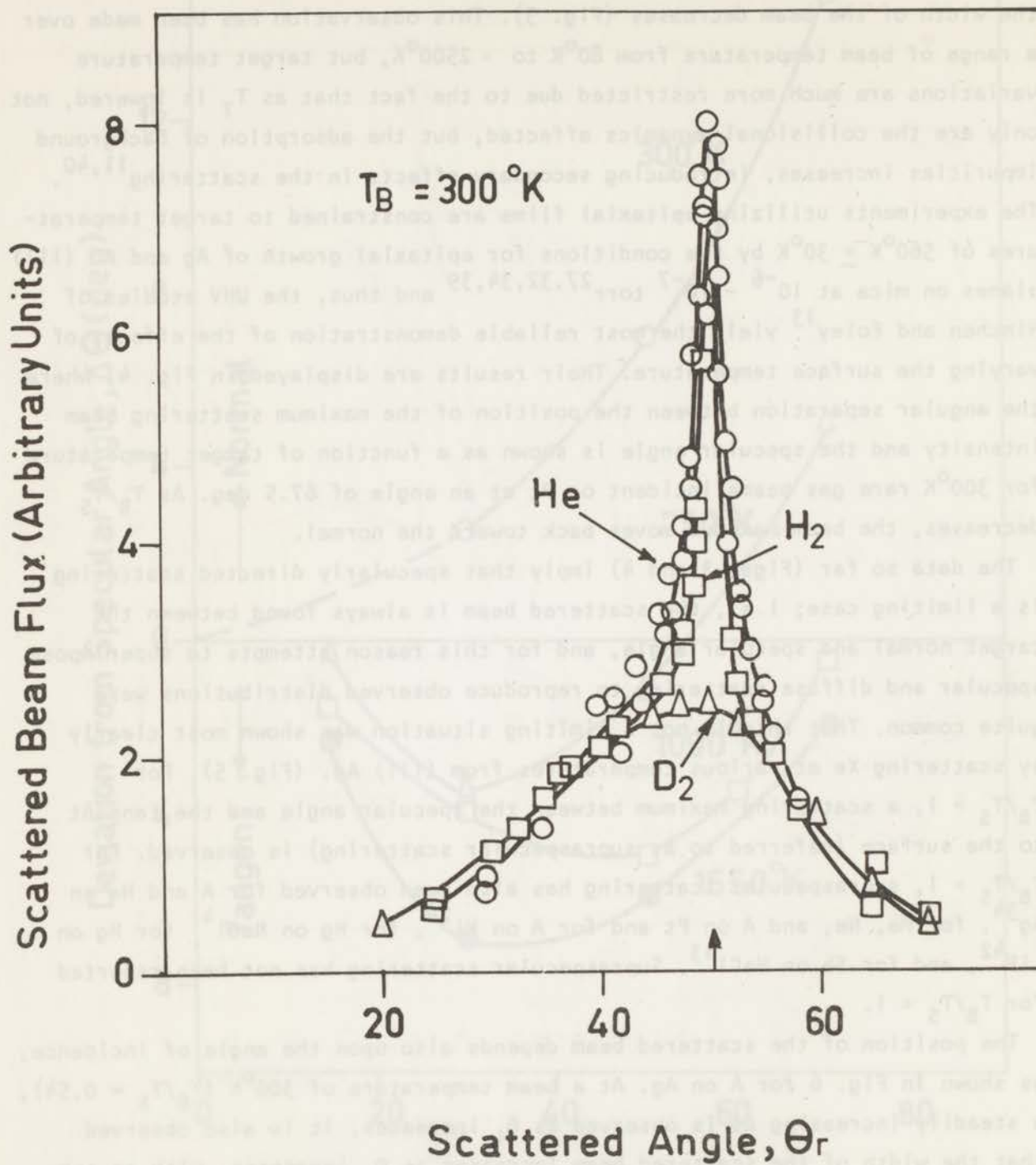
Fig. 7 - Scattering of He, H_2 and D_2 from Ag(111), $T_B = 300°K$, $T_T = 560°K$,
$\theta_i = 50°$. Ref. 32.

T_B/T_S, $\Delta\Theta$ is larger on Pt than on Ag. This type of comparison, however, is subject to the limitations described above.

Though the hard cube model[38] predicts qualitatively the type of behavior shown in Fig. 6. It would also predict that Kr on Au should behave very nearly as does A on Ag. The data (Fig. 4) imply that supraspecular scattering does not occur on Au. This may be due simply to a different surface topography although the fact that all rare gases look alike on Au at high temperatures (with the exception of a diffuse component for Xe) suggests a more fundamental difference between these metals.

The problem of the relative roles of the interaction potential and the gas particle mass has also been approached in the past by studying the scattering of He and D_2 from metal surfaces[40]. More recent work has indicated that this comparison is complicated by the possibility of rotational transitions in D_2[32]. The scattering distributions of He, H_2, and D_2 from the (111) plane of Ag are shown in Fig. 7. Although for He and H_2 the resolvable peak at the specular angle is quite prominent, it accounts for less than 5% of the scattered beam, the remaining 95% being found in the broad portion of the distribution. A search for first-order diffraction peaks of He was unsuccessful and presumably, if they were present, they were obscured by the low intensity of the specular component relative to the specularly directed beam. One might attribute the broadening in D_2 (relative to He) to the increase in ΔH and the difference between D_2 and H_2 to the mass difference, but this would require that a factor 2 in mass offset a factor of approximately 4 in ΔH in order to permit the close correspondence between He and H_2. On the other hand, Ne, which represents a 40% decrease in ΔH and a 5-fold mass increase as compared with D_2, is very nearly indistinguishable from D_2 in terms of scattering behavior. Clearly one must look elsewhere to explain the difference between H_2 and D_2 and it has been argued that rotational state transitions occur most readily in D_2, than in H_2. In support of this assertion, one notes that the energy required for the $J = 0 \to 2$ rotational transition in ortho D_2 corresponds very nearly to the maximum bulk phonon energy available from the Ag lattice whereas the corresponding energy for the H_2 transition is twice as large. Feuer has shown that coupling can occur between rotational and translational modes in collisions if the rotational level spacing is small[44].

Energy Transfer

Compared with experiments in which direct measurements of scattered beam
distributions are made, measurements of, or measurements related to, energy
transfer are quite limited. Ellett, Olson and Zahl[8] studied the scattering of
a thermal (Maxwellian) beam of Cd from NaCl. Using a velocity selector (SDVS)
they determined that Cd atoms scattered at the specular angle were nearly mono-
energetic, with a velocity 60% to 100% greater than the mean velocity of the
incident beam and that the velocity at the specular angle increased as the
angle of incidence increased, for $0.99 < T_B/T_S < 1.5$. Further, 83% of the Cd
scattered from a first NaCl crystal was diffusely reflected; if the specular
component of the scattered beam was then directed at a second NaCl crystal,
at the same angle of incidence, nearly all the Cd atoms were scattered in the
specular direction. Qualitatively similar results were obtained from Zn[45].
Using the Stern-Gerlach effect, Ellett and Cohen[17] examined the velocity
distribution of K scattered by MgO, and observed cosine scattering with a
Maxwellian velocity distribution characteristic of the surface temperature
($\pm$ 5%) in the scattered beam, indicating nearly complete accommodation. Marcus
and McFee[19], using a SDVS, investigated K scattered from Cu, W, MgO and LiF.
Maxwellian distributions characteristic of the surface temperature were observed
in the scattered beam (indicating equilibration) on all but LiF. For K on LiF,
a considerable deviation from a Maxwellian distribution was observed and attri-
buted to incomplete accommodation at the surface. Unfortunately, these measure-
ments did not include the determination of the spatial character of the scatt-
ering. Scott[15] and Hagena[16] using time-of-flight techniques have obtained pre-
liminary results on scattered beam velocity distributions, indicating a de-
creasing mean velocity as one goes toward the target surface for the case
$T_B/T_S > 1$.

Less direct determinations of the energy transfer in the gas-surface collis-
ion have been made by determining the mean velocity, $\bar{v}$, of the scattered beam.
Leonas[46], Hinchen and Foley[13], and Moore, Datz, and Taylor[14] determine beam
transit times (from source to detector) using phase-shift measurements with
modulated beams; Smith[11] and McKinley[12] made simultaneous measurements of the
number density and flux to determine $\bar{v}$. Such techniques require the assumption
of a Maxwellian velocity distribution to relate the scattered beam "temperature"
to the beam energy; the results of the experiments of Ellett, Olson and Zahl,

and of Marcus and McFee, indicate that this may be a poor assumption in many instances. However, the relative values are of interest. For A on Pt, Hinchen and Foley measured an accommodation coefficient (AC) of 0.5 under surface conditions that result in a very wide lobe in the scattered beam, but when the surface is thoroughly outgassed, yielding a relatively narrow scattered beam, the AC drops to 0.1. For A on Ni, Smith[11] observed an angular variation in the AC of a directed beam; AC = 0.8 at the target normal, and fell to 0.2 at the scattered beam maximum. Leonas, using a mono-energetic incident beam, measured AC ≈ 1.0 for A and CO_2 on surfaces of Cu, Fe, Ta and also estimated an adsorption energy from phase lags.

Molecular beam studies of the influence of internal energy modes on energy transfer are even more limited. Ehrhardt, Einhaus, and Engelke[47] have studied vibrational energy transfer in the collision of a propane molecular beam with stainless steel. By examining the ion spectrum produced upon electron impact, the vibrational energy of the parent molecule can be determined and thus a measure of the vibrational energy transfer is obtained. The accommodation coefficient for vibrational energy transfer, $(AC)_{vib}$, is quite insensitive to beam temperature ($100^{\circ}C < T_B < 500^{\circ}C$), but quite sensitive to surface temperature; $(AC)_{vib} = 0.8$ at $T_S = 100^{\circ}C$ and $(AC)_{vib} = 0.4$ at $T_S = 500^{\circ}C$.

Sasaki, Taku, and Kutani[48] reported torsion balance measurements of internal and translational accommodation of N_2 ($31.3^{\circ}C$) on Ni ($518^{\circ}C$) and found $(AC)_{trans} = 0.393$; $(AC)_{int}$ found by conventional thermal studies on the same surface was 0.314. Lack of experimental detail makes it difficult to assess the results.

SUMMARY AND CONCLUSIONS

The scattering of molecular beams from solid surfaces is beginning to yield information on the fundamental processes in the interaction. The geometrical aspects of diffraction are well-established, but a complete QM theory of surface diffraction, including a prediction of diffraction peak intensities, is not yet available. The variety or origins of diffuse scattering makes it less useful in interpretation than directed scattering phenomena. For the latter, the geometrical theory is being developed, but a detailed theoretical treatment still eludes us.

For directed scattering, the phenomenology of the spatial distribution seems well established within some limits: the same general effects due to increasing

T_B/T_S are consistently observed, although there are cases where the details are not the same (e.g. Au surfaces do not exhibit supraspecularity). The structurally sensitive nature of the scattering, however, makes detailed prediction difficult and serves to emphasize the need to do work on carefully prepared crystals so as to approach as closely as possible the idealized theoretically perfect lattice boundary. This is apparent from the observed effects of contamination on energy transfer and scattering and of crystal perfection, particularly for light gas scattering. Further, it is clear that scattering studies will become much more interpretable when velocity and spatial distributions are available simultaneously over the entire 3D space since questions of total scattered beam intensity relative to incident beam intensity cannot yet be answered. It is known that the directed scattered beam distribution is not rotationally symmetric about the maximum intensity axis[28,32] and hence full 3D distributions are required. Although one interprets the spatial distribution in terms of energy transfer, measurements to test the conceptual picture are only now being carried out. Further, the relationship of trapping calculations to beam scattering experiments involves a clear definition of trapping in the theory, but the experimentalist must place a time scale on re-emission to relate it to the theoretical predictions.

The major experimental deficiency at present is the fact that little is known about the response of the "other" collision partner --the surface. Crudely, the contamination and the gross crystal structure play a role, but many qualitative observations are independent of rather wide variations in these properties. The role of point and line defects in scattering is yet to be assessed. In the final analysis, beam scattering will probably be used as a probe to investigate these questions, but only studies from well-characterized surfaces will be useful to assess this proposal. Tools such as LEED[49] and RHEED[50] may provide some answers when coupled with scattering studies. Again, measurement of energy transfer may be important for observation of the relevant phenomena since the spatial distributions could be relatively insensitive to imperfections, but energy transfer will most likely not be insensitive. Scattering from oxygen covered (111) Ag may spatially resemble that from (111) Ag itself, but all the theoretical studies indicate significant effects of adsorbed species on energy transfer.

Another possibility is a study of some property of the solid which would be sensitive to the collision event. The most obvious property is the phonon

spectrum. With appropiately thin films at low enough temperatures, one might be able to see the electron-phonon interaction and its perturbation by surface collisions. Mean displacements of surface atoms may be perturbed by collision and may also be observable.

The use of mono-energetic incident beams to simplify the theoretical analysis has also been proposed, but theoretical studies of the hard cube model imply this simplification is not as great as assumed on an a priori basis and the major effort will have to be directed toward studies of the solid.

Since the ideal experiment is not yet at hand, and there is an increasing amount of research activity in surface scattering, it might be appropriate to adopt some standard reference surface to make the comparison of data somewhat more reliable. We have found that epitaxially grown (111) Ag (on mica) provides a reproducible stable scattering surface whose preparation is relatively simple and straightforward and we would like to urge that such a surface be included in new experiments to provide a correlating standard. We recognize that this surface is perhaps not ideal but it is reproducible and is under intensive investigation by many other techniques designed to reveal its detailed structure. Such a concentrated effort can lead to improved understanding of the scattering phenomena.

REFERENCES

1. W.L. Fite and S. Datz, Annual Rev. of Phys. Chem. 14, 61 (1963).

2. E.L. Knuth, Appl. Mech. Rev. 17, 751 (1964).

3. J.B. French, AIAA Journal, 993 (June 1965); AGARDograph (April 1966).

4. F.M. Devienne, J. Souquet and J.C. Roustan, Rarefied Gas Dynamics, Academic Press, N.Y. (1966), Vol. II, p. 584.

5. J. Boring, private communication, 1966.

6. L. Sodickson, J. Carpenter and G. Davidson, AFCRL report No. AFCRL-65-337 (1965).

7. T.H. Johnson, Phys. Rev. 35, 650 (1930).

8. A. Ellett, H.F. Olson and H.A. Zahl, Phys.Rev. 34, 493 (1965).

9. F.C. Hurlbut, Recent Research in Molecular Beams, Academic Press N.Y. 1959; I. Estermann, ed., p. 145.

10. G.S. Holister, R.T. Brackmann and W.L. Fite, Physical Chemistry in Aerodynamics and Space Flight, Pergamon Press, N.Y. (1960) p. 162.

11. J.N. Smith Jr., J. Chem. Phys. <u>40</u>, 2520 (1964).

12. J.D. McKinley, J. Phys. Chem. <u>66</u>, 554 (1962).

13. J.J. Hinchen and W. Foley, Rarefied Gas Dynamics, Academic Press, N.Y. (1966) Vol. II, p. 505.

14. G.E. Moore, S. Datz and E.H. Taylor, J. Catalysis <u>5</u>, 218 (1966).

15. P.B. Scott, P.H. Bauer, H.Y. Wachman and L. Trilling, Rarefied Gas Dynamics, Academic Press N.Y. (1967) Vol. II, p. 1353.

16. O.F. Hagena, Appl. Phys. Letters <u>9</u>, 385 (1966).

17. A. Ellett and V.W. Cohen, Phys. Rev. <u>52</u>, 509 (1937).

18. J.A. Eldridge, Phys. Rev. <u>30</u>, 931 (1927).

19. P.M. Marcus and J.H. McFee, Recent Research in Molecular Beams, Academic Press N.Y. (1959), p. 43.

20. R.E. Stickney and F.C. Hurlbut, Rarefied Gas Dynamics, Academic Press N.Y. (1963), Vol. I, p. 454.

21. N. Abuaf and D.G.H. Marsden, Rarefied Gas Dynamics, Academic Press N.Y. (1967), Vol. I, p. 199.

22. D. McKeown and M.G. Fox, Rev. Sci. Inst. <u>36</u>, 656 (1965).

23. J.K. Roberts, Proc. Roy. Soc. A<u>135</u>, 192 (1932).

24. J. Estermann and O. Stern, Z. für Physik <u>61</u>, 95 (1930).

25. R.M. Zabel, Phys. Rev. <u>42</u>, 218 (1932).

26. J.C. Crews, J. Chem. Phys. <u>37</u>, 2004 (1962).

27. J.N. Smith Jr. and H. Saltsburg, J. Chem. Phys. <u>40</u>, 3585 (1964).

28. J.J. Hinchen and E.F. Shephard, Rarefied Gas Dynamics, Academic Press N.Y. (1967), Vol. I, p. 239.

29. R.W. Roberts, Brit. J. Appl. Phys. <u>14</u>, 537 (1963).

30. I. Estermann, O. Frisch and O. Stern, Z. für Physik <u>73</u>, 348 (1931).

31. J.C. Crews, Fundamentals of Gas-Surface Interactions, Academic Press Inc. N.Y. (1967) p. 31.

32. H. Saltsburg, J.N. Smith Jr. and R.L. Palmer, Rarefied Gas Dynamics, Academic Press, N.Y. (1967), Vol. I, p. 223.

33. J.E. Lennard-Jones and A.E. Devonshire, Proc. Roy. Soc. A<u>156</u>, 6 (1936).

34. H. Saltsburg and J.N. Smith Jr., J. Chem. Phys. <u>45</u>, 2175 (1966).

35. A.R. Kuhlthau and M.N. Bishara, Rarefied Gas Dynamics, Academic Press N.Y. (1966), Vol. II, p.518.

36. J.A. Alcalay and E.L. Knuth, Rarefied Gas Dynamics, Academic Press N.Y. (1967), Vol. I, p. 253.

37. K. Müller, Z. für Physik, <u>195</u>, 105 (1966).

38. R.M. Logan, J.C. Keck and R.E. Stickney, Rarefied Gas Dynamics, Academic Press N.Y. (1967), Vol. I, p. 49.

39. J.N. Smith Jr. and H. Saltsburg, Rarefied Gas Dynamics, Academic Press, N.Y. (1966), Vol. II, p. 491.

40. S. Datz, G.E. Moore and E.H. Taylor, Rarefied Gas Dynamics, Academic Press N.Y. (1963), Vol. I, p. 347.

41. H.A. Zahl and A. Ellett, Phys. Rev. <u>38</u>, 977 (1931).

42. R.R. Hancox, Phys. Rev. <u>42</u>, 864 (1932).

43. J.M.B. Kellogg, Phys. Rev. <u>41</u>, 635 (1932).

44. P. Feuer, J.Chem. Phys. <u>39</u>, 1311 (1963).

45. H.A. Zahl, Phys. Rev. <u>36</u>, 893 (1930).

46. V.B. Leonas, Pr. k. Nekh. i Tekh. Fiz. <u>2</u>, 84 (1965).

47. H. Ehrhardt, R. Einhaus and H. Engelke, Z. für Physik <u>191</u>, 469 (1966).

48. N. Sasaki, K. Taku and K. Mitani, Memoirs of Coll. of Sci., U. of Kyoto, Series A, <u>2</u>, 75 (1949).

49. J.J. Lander, Progress in Solid State Chemistry, Pergamon Press, Oxford (1965) p. 26.

50. P.B. Sewell and M. Cohen, Appl. Phys. letters <u>7</u>, 32 (1965).

CHAPTER II

Scattering of Velocity-Filtered Atomic Beams of Ar and Xe from the (111) Plane of Silver*

JOE N. SMITH, JR., HOWARD SALTSBURG, AND ROBERT L. PALMER

Gulf General Atomic Incorporated, San Diego, California

(Received 22 March 1968)

The scattering of nearly monoenergetic atomic beams of Ar and Xe from the (111) plane of silver has been studied as a function of the nominal velocity v_0 transmitted by a slotted-disk velocity selector (SDVS) used as a velocity filter on the incident thermal-energy (Maxwellian) beam. The selector has a velocity spread of $\pm 0.19\ v_0$ and studies were carried out over a range of v_0 from 2.2×10^4 to 5.3×10^4 cm/sec. The scattered beam distributions were found to be directed, corresponding closely to those of Maxwellian beams when $v_0 = \bar{v} = \frac{3}{4}(2\pi k T_B/M)^{1/2}$, the average velocity of the corresponding Maxwellian beam of temperature T_B. These results, together with the results of earlier scattering studies, imply that the thermal motion of the lattice is the dominant factor in producing the spatial dispersion as well as the velocity dispersion in the scattered beam that has been observed by other investigators. The most likely origin of these dispersive effects is the languidness of the collision in the sense used by Goodman to describe gas atom–lattice collisions.

I. INTRODUCTION

In most studies of directed scattering of molecular beams from solid surfaces, ideal specular scattering is rarely observed. Even though the maximum scattered intensity may lie at the specular angle, the dispersion of the scattered beam is much broader than that of the incident beam. In fact, it has been found that the probability $P(\theta_r)$ for finding the scattered beam at the reflected angle θ_r is a function of many variables.[1] The variables that have been observed experimentally to be relevant include the incident angle, the beam energy, the surface temperature, the solid and gas masses, and the heat of adsorption. Additionally, in most molecular beam–surface scattering experiments, beams (originat-

ing from Knudsen sources) that have a Maxwellian distribution of velocities have been used. It is natural, therefore, to assume the existence of a conditional probability $P(\theta_r \mid v_i)$ for scattering at θ_r for each incident velocity v_i. The observed dispersion of the scattered beam could then result in part from the averaging of $P(\theta_r \mid v_i)$ over the Maxwellian distribution of v_i in the incident beam and might tend, therefore, to obscure the details of the scattering phenomena. This type of velocity averaging has been proposed previously by several authors.[2,3]

Aerodynamic nozzle-beam sources can yield considerably higher translational energies (~ 1.0 eV) than are available with Knudsen sources (<0.5 eV) but only at the expense of fluid enthalpy, and hence the resulting

---

[1] For ideal specular scattering $P(\theta_r) = 1$ if $\theta_r = \theta_i$ and 0 otherwise. For diffuse scattering, $P(\theta_r) \propto \cos\theta_r$ only, but we shall restrict this discussion to directed scattering.

[2] J. N. Smith, Jr., J. Chem. Phys. **40**, 2520 (1964).
[3] J. J. Hinchen and E. S. Malloy, *Fundamentals of Gas Surface Interactions*, H. Saltsburg, J. N. Smith, Jr., and M. Rogers, Eds. (Academic Press Inc., New York, 1967), p. 448.
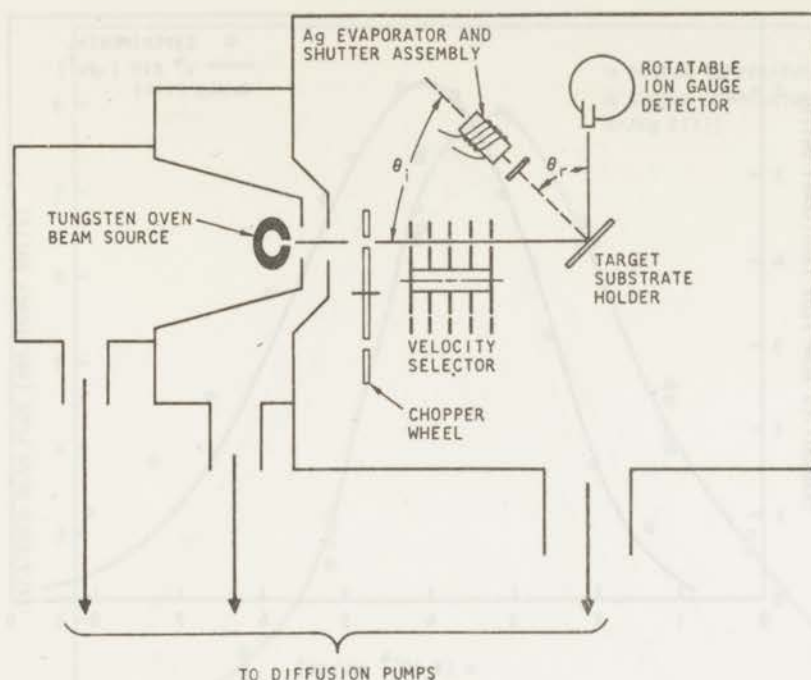
beams have a significantly narrowed distribution of molecular velocities. Recent gas–surface scattering experiments in which these high-energy, "monoenergetic" beams have been used have also resulted in broad scattering distributions.[4-7] It is not clear, however, whether this result demonstrates that velocity averaging is unimportant or that the dispersion in the scattered beam is because of the high incident beam velocity. A direct comparison between the scattering of a Maxwellian beam and a monoenergetic beam, in the electron-volt energy range, has not been obtained.

In contrast to the assumption that velocity averaging has a strong effect on the observed scattering distribution, a recent calculation by Stickney, Logan, Yamamoto, and Keck (SLYK)[8] based on the "hard-cube" model of Logan and Stickney indicates that little difference should be observed between the scattering of a thermal Maxwellian beam and an appropriate mono-energetic beam, exemplified by Ar scattered from Ag. As we shall show, this result of the SLYK analysis is verified by the experimental data given below, but, as discussed in Sec. IV, this agreement between analysis and experiment is not necessarily proof of the correctness of the hard-cube model as a complete description of the atom–lattice collision. The agreement, however,

does emphasize the importance of describing the lattice as a dynamic partner in the collision, having thermal motion prior to collision with the gas atom.

The present experiments were undertaken to investigate explicitly the extent to which velocity averaging affects thermal-energy scattering and therefore the physical description of the scattering mechanism. The principle reason that such experiments have not been undertaken previously is the practical consideration of the loss in beam intensity when a velocity selector is inserted into the path of the incident molecular beam. For the best velocity resolution obtainable the losses are probably still too great. The design of the slotted-disk velocity selector (SDVS) used in the present experiments[9] represents a compromise, between transmission and resolution, that was readily adaptable to the molecular-beam apparatus used in previous molecular beam–surface scattering experiments in this laboratory.[10-14]

The scattering from the (111) plane of Ag of velocity filtered beams of Ar and Xe in the velocity range of 2.2×10^4–5.3×10^4 cm/sec was studied and compared

[4] J. A. Alcalay and E. C. Knuth, *Rarefied Gas Dynamics*, C. L. Brundin, Ed. (Academic Press Inc., New York, 1967), Vol. 1, Suppl. 4, p. 253.

[5] P. B. Scott, Ref. 3, p. 537.

[6] O. F. Hagena, J. E. Scott, Jr., and A. R. Kuhlthau, Ref. 3, p. 538.

[7] R. G. Wilmott, masters thesis, University of Virginia, School of Engineering and Applied Science, August 1967.

[8] R. E. Stickney, R. M. Logan, S. Yamamoto, and J. C. Keck, Ref. 3, p. 422.

[9] A. E. Grosser and R. B. Bernstein, "A Compact Molecular Beam Velocity Selector," USAEC Rept. COO-1328-15, University of Wisconsin, 1 September 1965 (unpublished).

[10] J. N. Smith, Jr., and H. Saltsburg, J. Chem. Phys. 40, 3585 (1964).

[11] J. N. Smith, Jr., and H. Saltsburg, *Rarefied Gas Dynamics*, J. H. de Leeuw, Ed. (Academic Press Inc., New York, 1966), Vol. 2, Suppl. 3, p. 491.

[12] H. Saltsburg and J. N. Smith, Jr., J. Chem. Phys. 45, 2175 (1966).

[13] J. N. Smith, Jr., H. Saltsburg, and R. L. Palmer, Proc. Symp. Rarefied Gas Dynamics 6th, July, 1968 (to be published).

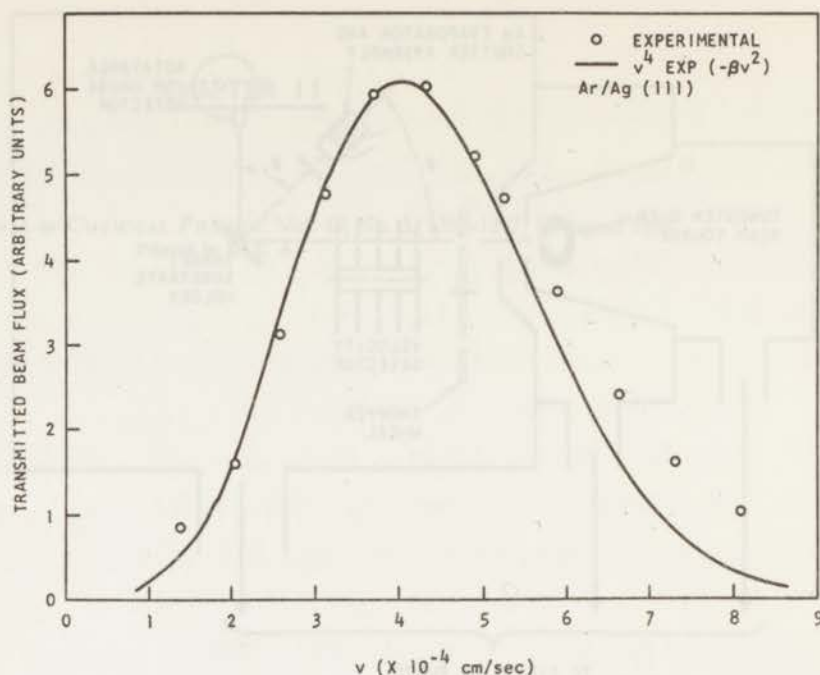[14] H. Saltsburg, J. N. Smith, Jr., and R. L. Palmer, Ref. 4, p. 223.

FIG. 2. Velocity distribution of an incident beam of Ar. Beam temperature=300°K. Experimental points obtained by removing target and measuring transmitted Ar signal, in direct beam, as a function of selector transmission velocity.

with the scattering of appropriate Maxwellian beams. It was observed that the scattering distributions obtained with the velocity filtered beams were quite broad; there were only slight differences between these distributions and those obtained with appropriately related Maxwellian incident beams in the temperature range from 300°–1200°K. These results are discussed in terms of both the physical aspects of the gas–surface collision and the inherent features of the measurements introduced by using a SDVS with a relatively broad resolution.

II. APPARATUS

The apparatus depicted in Fig. 1 differs from that used previously in thermal-beam scattering experiments in only one respect; the SDVS is positioned in the path of the incident beam between the neutral beam chopper and the target. The basic design of the SDVS is that of Grosser and Bernstein,[9] except for the mechanical construction of the disks, which is described elsewhere.[15] In brief, the selector consists of an array of 5 slotted disks (120 slots per disk), each 5 cm in diameter, with an over-all beam path length through the selector (5 disks) of ~2.08 cm. The velocity resolution R for a nominal velocity v_0 is 19%, whereas the transmission is just under 50%.[16] This disk assembly is driven by a variable speed motor controlled by an audio oscillator. The rotational speed of the SDVS is determined by using a

photocell to measure the frequency of a light beam chopped at one of the five disks. The selector has been operated successfully for extended periods at rotational speeds in the range from 9000–27 000 rpm with a corresponding transmission velocity v_0 in the range of 2×10^4–6×10^4 cm/sec. For short periods of operation this range may be extended to 1×10^4–9×10^4 cm/sec. The velocity selector may be lowered out of the path of the incident beam to permit the scattering behavior of the primary Maxwellian beam to be examined.

The remainder of the apparatus has been described elsewhere.[10–14] As before, the target surfaces in these experiments were produced by depositing Ag on a mica substrate maintained at 560°K. The deposition was performed *in situ* in the scattering apparatus and the resulting Ag film was a twinned single crystal with the (111) plane parallel to the surface. The structure and scattering behavior of these films has been described elsewhere.[12,13] All measurements reported here were taken after film deposition, rather than during deposition, as was the case in many of the measurements reported earlier, and are for a fixed incident angle, $\theta_i=50°$ (see Fig. 1).

The calibration of the SDVS was checked against the calculated value by examining the velocity distribution of the incident beam effusing from the oven source, at low-source pressure. The resulting distribution is shown in Fig. 2, which compares the transmitted beam flux with the ideal skewed Maxwellian distribution $[\propto v^4 \exp(-\beta^2 v^2)]$ characteristic of the velocity bias of the selector that is operative on the normal effusive distribution. The calibration factor of 1.33 (m/sec)(rps)$^{-1}$ so determined is 2% higher than that calculated on the basis of the rotor geometry.

[15] A. Kristensen, R. L. Palmer, H. Saltsburg, and J. N. Smith, Jr., Rev. Sci. Instr. 38, 987 (1967).
[16] Throughout this article the quoted velocity filtered beam velocity v_0 is the velocity at the center of the transmitted band of velocities. The shape of the "shutter function" is assumed to be triangular, with a base width of $2Rv_0$, where R is the resolution of the selector.
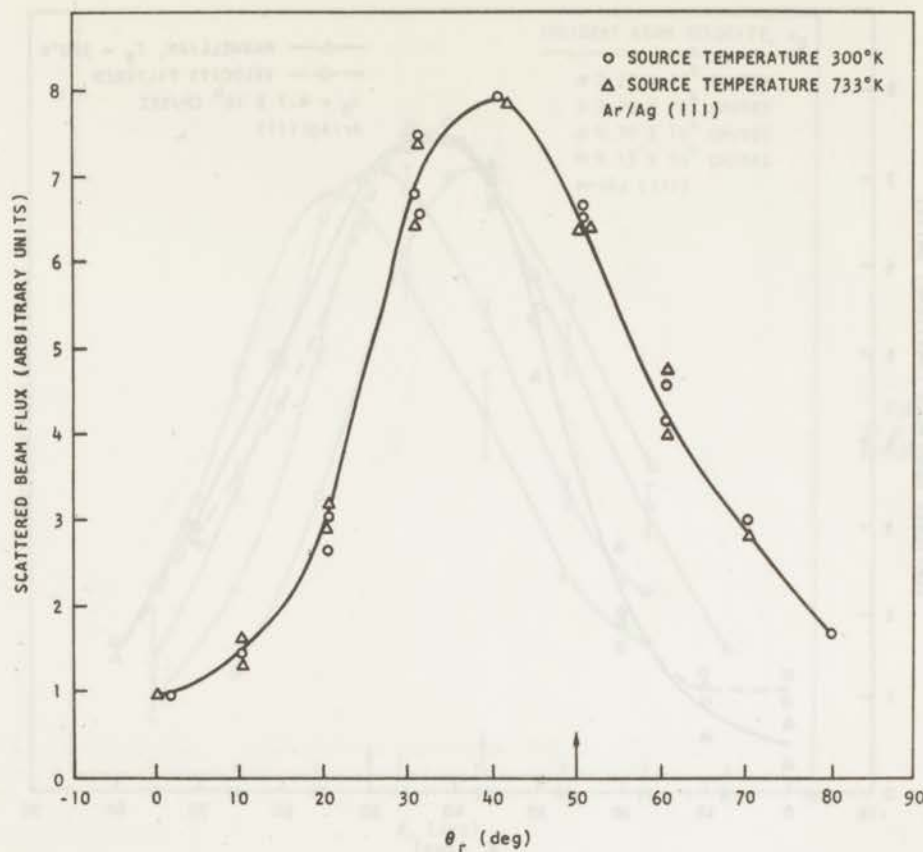
○ SOURCE TEMPERATURE 300°K
△ SOURCE TEMPERATURE 733°K
Ar/Ag (111)

FIG. 3. Scattering of a velocity filtered beam of Ar at two-beam source temperature as indicated; $v_0 = 3.95 \times 10^4$ cm/sec, $\theta_i = 50°$.

One further diagnostic test assured that, for the purposes of the present experiments, the beam velocity was determined by the velocity selector and was independent of that portion of the velocity distribution function of the primary beam that falls within the band pass of the selector. A comparison was made of Ar scattered from Ag with beam-source temperatures of 300° and 733°K, but with the rotational speed of the selector fixed so that the transmitted molecular velocity v_0 was 3.95×10^4 cm/sec in both cases. The result is shown in Fig. 3. For the 300°K beam, the velocity distribution function varies slowly within the band pass of the selector because v_0 is only slightly below the average beam velocity. At 733°K, the velocity distribution function varies more rapidly within the band of transmitted velocities, but the scattered beam distributions for the two cases are indistinguishable experimentally. As will be shown, the angular distribution of the scattered beam is a function of the incident beam velocity, and the fact that the scattering distribution is independent of source temperature for fixed v_0 indicates that the resolution of the velocity selector is adequate for the present studies.

III. RESULTS

For Ar, a direct comparison of the scattering of a Maxwellian beam at a beam temperature T_B of 300°K with a velocity filtered beam of $v_0 = \bar{v}$, where

$$\bar{v} = \tfrac{3}{4}(2\pi k T_B/M)^{1/2} \tag{1}$$

is shown in Fig. 4. The two sets of data are seen to be very nearly indistinguishable except that the filtered beam scattering distribution seems to lie slightly closer to the surface normal and is slightly narrower. Comparison with data obtained earlier under apparently identical conditions[12] shows that the present (Maxwellian) scattering distribution is slightly narrower on the low-angle side $(0 < \theta_r \lesssim 50°)$ and the maximum in the distribution lies some 2° farther from the target normal. These small differences result from an improvement in the angular resolution of the detector and a reduction in the angular divergence of the incident beam in the present experiments. A similar comment applies to the Xe data reported below.

The effect upon the scattering due to a change in the incident beam velocity was studied by inserting the SDVS into the incident beam and measuring the scattered beam distribution for several fixed selector speeds. The results for Ar at four velocities from 2.32×10^4–5.33×10^4 cm/sec are shown in Fig. 5. For comparison with earlier work, if these velocities are taken to be average velocities of Maxwellian beams at the four different source temperatures, by means of Eq. (1), then T_B lies between 74° and 392°K. (For all the data
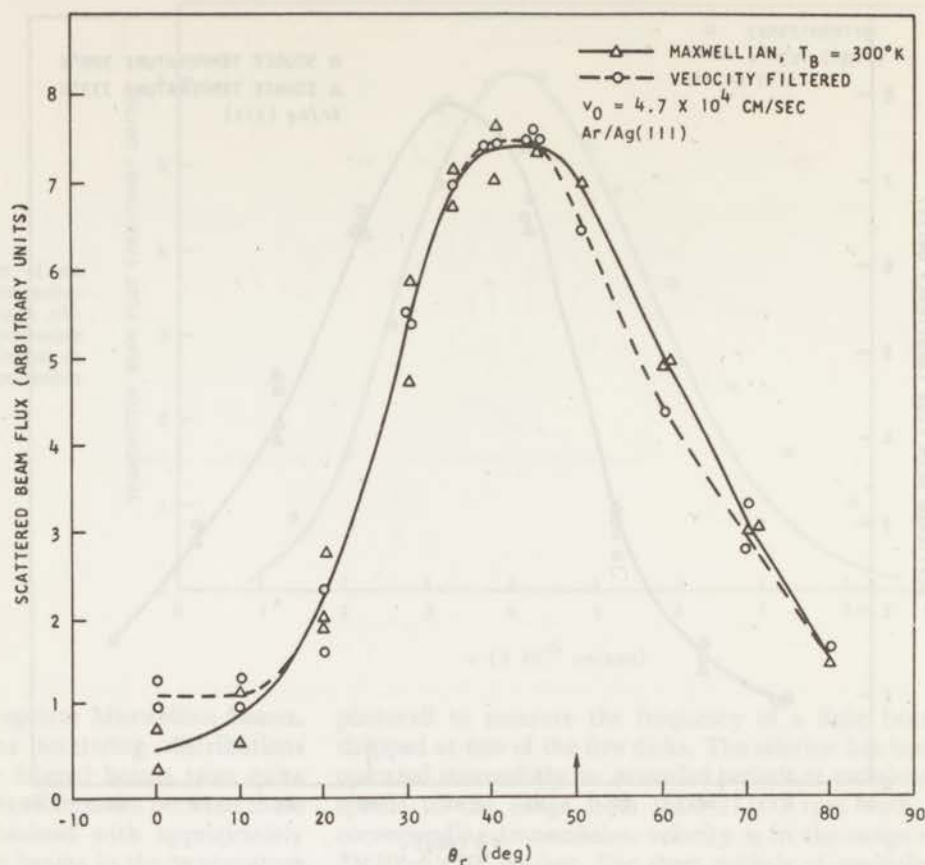
FIG. 4. Comparison of the scattering of a Maxwellian beam at a temperature $T_B = 300°K$ with the scattering of a filtered beam with $v_0 = \bar{v}$, see Eq. (1); data for Ar, $\theta_i = 50°$.

of Fig. 5, the beam oven source was held at 300°K.) The scattered beam is seen to move away from the target normal as the incident beam velocity increases. However, the shape of the scattered beam distribution is virtually unchanged; if the distribution at $v_0 = 2.32 \times 10^4$ cm/sec is simply translated $\sim 18°$ away from the target normal, it nearly coincides with the distribution taken at $v_0 = 5.32 \times 10^4$ cm/sec.

The comparison between the scattering of Maxwellian beams of Xe with that of velocity filtered beams, at $v_0 = \bar{v}$ from Eq. (1), is shown in Figs. 6, 7, and 8. At 300°K ($\bar{v} = 2.54 \times 10^4$ cm/sec) the correspondence between the filtered and Maxwellian scattering distributions is similar to the corresponding data for Ar; the filtered beam scattering distribution tends to lie somewhat closer to the normal than does the Maxwellian beam, and is narrower. As the beam temperature (velocity) is increased, the beam scattering distributions tend to move away from the target normal and the two distributions tend to become identical, except that the contribution near the surface normal (which may be indicative of a diffuse component) remains for the Maxwellian beam and is diminished for the velocity filtered beam. At 1230°K (5.1×10^4 cm/sec) the scattered Xe beam is supraspecular by $\sim 7°$.[12] Note, however, that the scattering distribution for a filtered beam at $v_0 = 5.1 \times 10^4$ cm/sec is significantly narrower

than at $v_0 = 2.23 \times 10^4$ cm/sec, in contrast to the result for Ar in the same velocity range (see Fig. 5).

IV. DISCUSSION

The most striking result of this experiment is that broad scattering distributions are obtained with velocity filtered beams; in fact, thermal (Maxwellian) beam scattering and velocity filtered beam scattering are very nearly the same when v_0 and T_B are related by Eq. (1) (see Figs. 4, and 6–8). There are several factors that could contribute to this result: (1) the actual velocity spread of the incident beam (since the filtered beam is not truly monoenergetic); (2) the effects of surface roughness; and (3) the contribution of the lattice itself, resulting from the fact that it is a dynamical partner in the collision, particularly as characterized by its thermal motion. These possibilities are discussed below. When they are taken together with some recent observations of the velocity distribution in the scattered beam,[6,7,17] it is possible to draw certain conclusions concerning the details of the scattering process and the origin of the broadening.

A. The Velocity Distribution of the Incident Beam

Although data of Figs. 4–8 indicate that there is no striking reduction in the width of the scattered beam

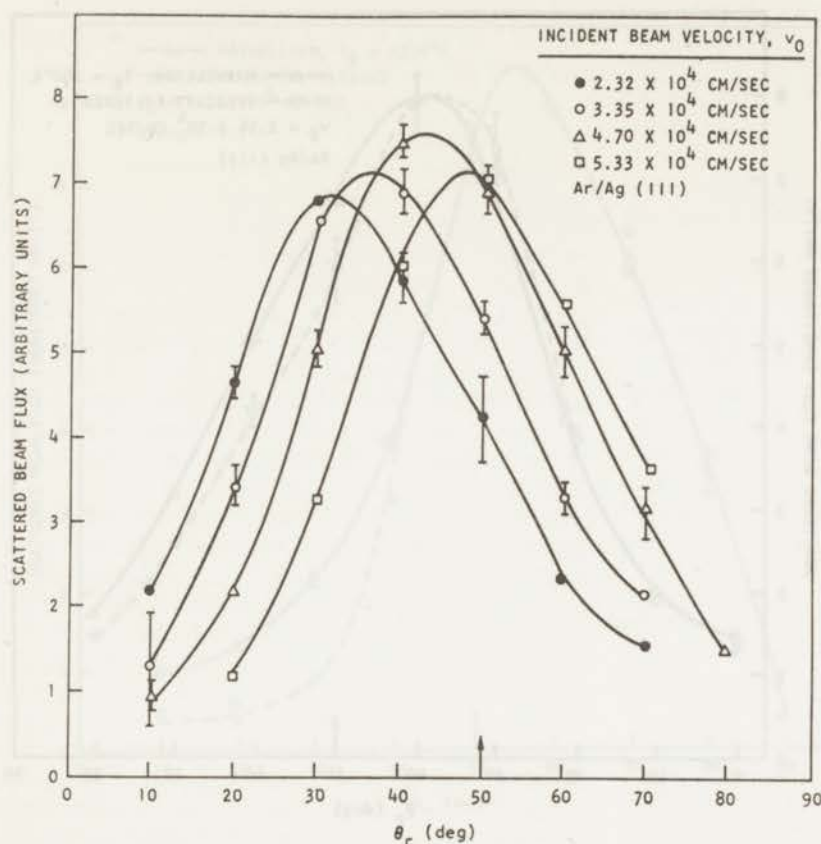[17] J. P. Moran, H. Y. Wachman, and L. Trilling, Ref. 3, p. 461.

FIG. 5. Scattering of a filtered Ar beam as a function of incident velocity, v_0; $\theta_i = 50°$.

when the velocity spread of the incident beam is limited to $\Delta v = \pm 0.19\ v_0$, the question remains as to what would result in the limit of a truly monoenergetic beam. It is to be noted that even with the present SDVS ~80% of the incident atoms possess velocities outside of the band pass of the selector and do not, therefore, contribute to the filtered-beam scattering distribution. That this great reduction in the velocity spread of the beam has so small an effect on the scattering distribution implies that even a truly monoenergetic beam would yield broad scattering distributions, although small differences might be observed when a comparison is made with the corresponding Maxwellian beam scattering.

The only relatively comparable data involve studies of the scattering of N_2 and Ar from polycrystalline Ni in which an aerodynamic nozzle beam was employed.[7] Although the incident beam velocity was substantially greater than that used in the present work, the nozzle beam has a narrow spread in velocity, even relative to the 300°K thermal beam. Scattering patterns were observed which were quite broad, again indicating that velocity averaging was not involved. Although this dispersion could be caused by the high beam energy, as a result of some significant distortion of the lattice occurring during the collision (which would not occur in the corresponding thermal energy monoenergetic case), there is close agreement (in terms of beamwidth)

between the scattering distributions obtained with the aerodynamic beam and earlier data on the same gas/metal system using thermal Maxwellian beams.[2] This implies that additional processes occurring at the higher energies do not affect the spatial distributions, barring any unsuspected compensatory effects.

To demonstrate the internal consistency of the present data, the filtered beam data of Fig. 5 were superimposed and compared with the corresponding Maxwellian beam scattering data. The four distributions of Fig. 5 were normalized to the same unfiltered incident beam flux and corrected for the velocity bias of the SDVS (by dividing each distribution by the corresponding v_0), which in effect should reproduce the scattering distribution that would result from a Maxwellian incident beam. The comparison is shown in Fig. 9, and close agreement between the two is obtained as expected.

From these results, one can conclude that the finite spread of velocities in the filtered beams does not affect the nature of the scattering distributions which are observed.

B. Surface Roughness

We have observed previously the sensitivity of the scattering to polycrystallinity and to impurity.[10] Consequently, the scattering distributions of unfiltered (Maxwellian) beams of He were measured for each Ag target that was employed in the Ar and Xe scattering

FIG. 6. Comparison of Maxwellian and filtered beam scattering for Xe; T_B and $v_0 = \bar{v}$ related by Eq. (1); $\theta_i = 50°$, $T_B = 300°K$, $v_0 = 2.54 \times 10^4$ cm/sec.

FIG. 7. Comparison of Maxwellian and filtered beam scattering for Xe; T_B and $v_0 = \bar{v}$ related by Eq. (1); $\theta_i = 50°$, $T_B = 885°K$, $v_0 = 4.42 \times 10^4$ cm/sec.
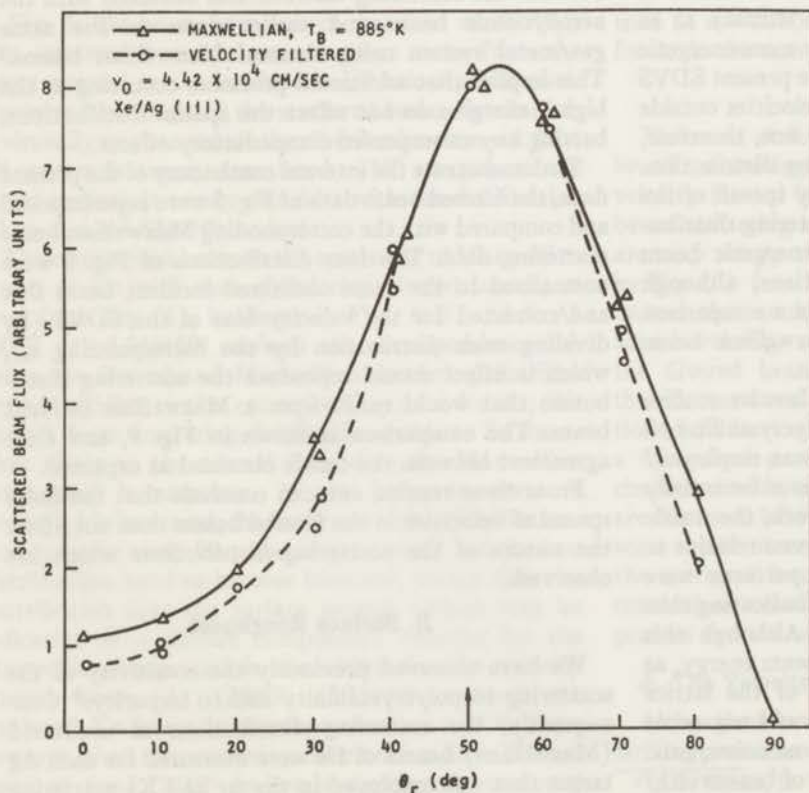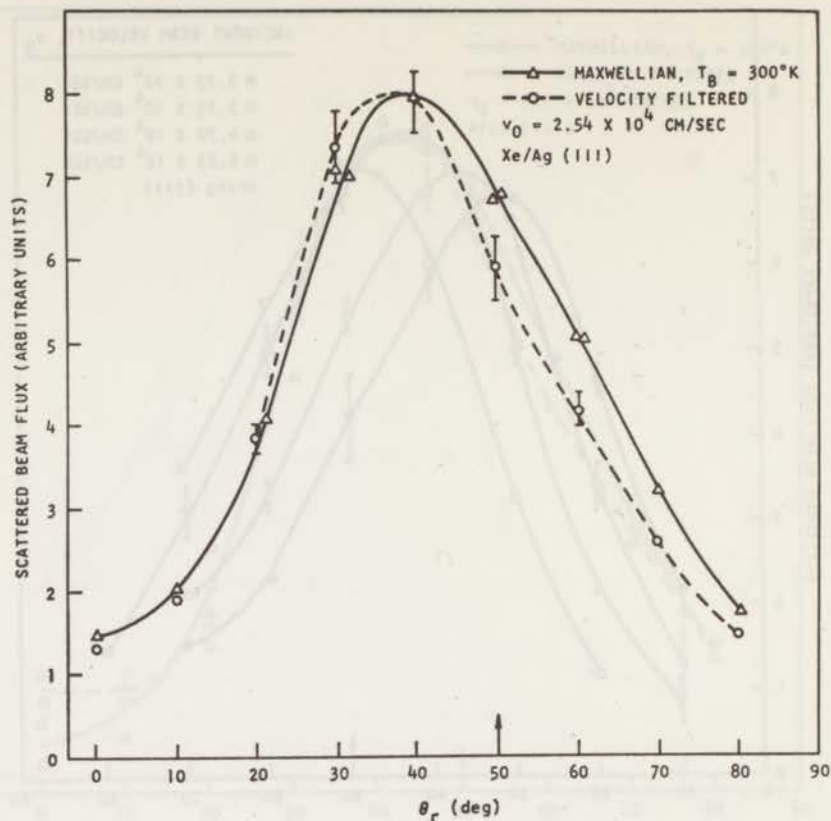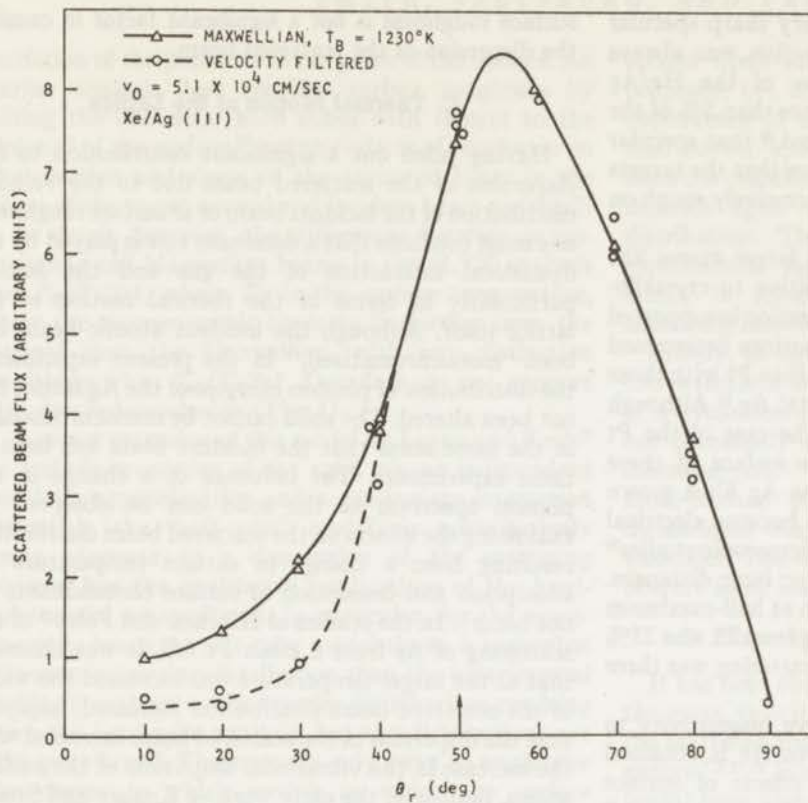
FIG. 8. Comparison of Maxwellian and filtered beam scattering for Xe; T_B and $v_0 = \bar{v}$ related by Eq. (1); $\theta_i = 50°$, $T_B = 1230°K$, $v_0 = 5.1 \times 10^4$ cm/sec.
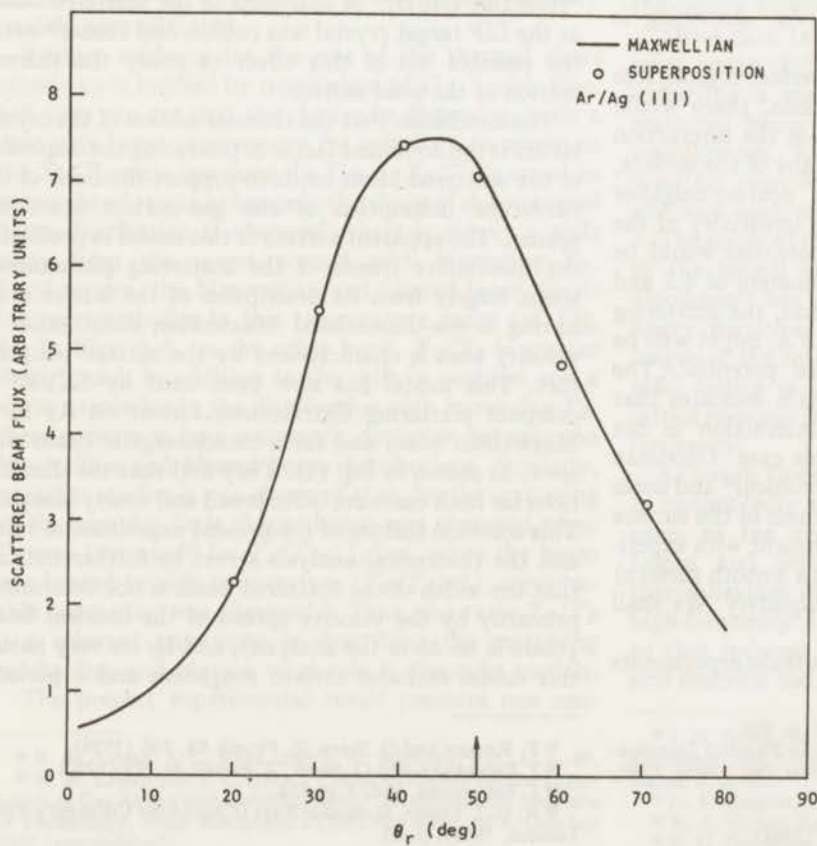

FIG. 9. Comparison between the scattering distribution of a Maxwellian Ar beam (solid line) and a superposition of the filtered beam scattering data of Fig. 5; see text.

studies reported here. With He, a very sharp specular component in the scattering distribution was always obtained. Although previous studies of the He/Ag scattering system showed that not more than 5% of the incident beam was specularly scattered,[14] that specular scattering was observed at all indicates that the targets used in the current study were not excessively rough on the atomic scale.

Further, it is to be expected that larger atoms like Ar and Xe would be even less sensitive to crystallographic roughness than He. This contention is supported by a comparison of scattering distributions determined by Hinchen and Foley[18] on polycrystalline Pt with those of the present authors on single-crystal Ag.[12] Although considerable annealing occurred in the case of the Pt foil targets, it is probable that the surface of these targets was rougher than that of the Ag films grown epitaxially on a mica cleavage plane because electrical conductivity studies[19] and electron-microscopic studies[20] show that the Ag films are smooth over large distances. When the width of the scattered beam at half-maximum was taken as a criterion, Ar scattering from Pt was 25% broader than from Ag, whereas He scattering was three times broader.

Additional evidence for the relative insensitivity to surface imperfection of Ar relative to He is obtained by a comparison of the observed effects of surface contamination on the scattering of these two gases.[10] Upon contamination of an Au target, He scattering is broadened considerably, whereas Ar scattering is affected only slightly.

Even if the Ag target film were a perfect crystal, free of dislocations and other imperfections, there would still be an effective roughness because the interaction potential varies periodically in the plane of the surface, with a period of $d = 2.88$ Å, the nearest-neighbor distance in the Ag (111) plane. The sensitivity of the incident atom to this variation in potential would be low for Xe and Ar, with atomic diameters of 4.2 and 3.5 Å, respectively. On the other hand, the scattering of He, with an atomic diameter of 1.8 Å, might well be affected by the variation in suface potential. The specularity of He scattering once again indicates that this feature of the atom/surface interaction is not dominant even in this most favorable case. Goodman has recently discussed this potential problem[21] and notes the effective potential-induced roughness of the surface gives results which exhibit poor agreement with experiment, whereas the hard-cube model (a smooth surface) seems to describe the data more adequately. We shall return to this point later.

We can conclude, therefore, that in these experiments surface roughness is not a significant factor in causing the dispersion of the scattered beam.

C. Thermal Motion of the Lattice

Having ruled out a significant contribution to the dispersion of the scattered beam due to the velocity distribution of the incident beam or to surface roughness, one must conclude that a dominant role is played by the dynamical interaction of the gas and the lattice, particularly in terms of the thermal motion of the lattice itself. Although the incident atomic beam has been "monochromatized," in the present experiments the distribution of phonon energies of the Ag lattice has not been altered. The solid cannot be monochromatized in the same sense that the incident beam has been in these experiments. The influence of a change in the phonon spectrum of the solid can be observed by examining the effects on the scattered beam distribution resulting from a change in surface temperature (if adsorption and desorption of surface contaminants do not occur). In the studies of Hinchen and Foley[18] of the scattering of Ar from a clean Pt foil, it was observed that as the target temperature was increased the width of the scattered beam distribution increased, implying that the dispersion in the scattered beam increased with the increase in the vibrational amplitude of the surface atoms. Similarly, the early work of Knauer and Stern[22] and of Estermann and Stern[23,24] showed an increased "reflecting power," or sharpness of the scattered beam, as the LiF target crystal was cooled, and Fraser[25] noted the possible use of this effect to study the thermal motion of the solid surface.

The conclusion that the thermal motion of the crystal lattice is the dominant factor in producing the dispersion of the scattered beam tends to support the basis of the hard-cube description of the gas–surface scattering system. The apparent success of this model in predicting the qualitative trends of the scattering phenomenon stems largely from its description of the lattice atom having a one-dimensional Maxwellian distribution in velocity that is characterized by the surface temperature. This model has now been used by SLYK[8] to compute scattering distributions for Ar on Ag for a Maxwellian beam and for a monoenergetic beam with $v_0 = \bar{v}$, as shown in Eq. (1). They find that the distributions for both cases are quite broad and nearly identical. This common feature of the present experimental result and the theoretical analysis serves to further indicate that the width of the scattered beam is not determined primarily by the velocity spread of the incident beam (there is no Δv in the analysis), and by its very nature this model excludes surface roughness and a periodic

[18] J. J. Hinchen and W. T. Foley, Ref. 11, p. 505.
[19] D. S. Campbell, *The Use of Thin Films in Physical Investigations*, J. C. Anderson, Ed. (Academic Press Inc., New York, 1966), p. 299.
[20] M. J. Stowell, Ref. 19, p. 131.
[21] F. O. Goodman, Phys. Rev. **164**, 1113 (1967).

[22] F. Knauer and O. Stern, Z. Physik **53**, 766 (1929).
[23] I. Estermann and O. Stern, Z. Physik **61**, 95 (1930).
[24] I. Estermann, Ref. 3, p. 534.
[25] R. G. J. Fraser, *Molecular Rays* (Cambridge University Press, London, 1931), p. 85.

variation of the potential in the plane of the surface. An earlier analysis does consider surface roughness by tilting the elemental hard cubes with respect to the "plane" of the surface,[26] but the effects of roughness on the position and shape of the scattered beam in the plane of the target normal and incident beam are small.

In detail, however, the differences between mono-energetic and Maxwellian beams in the SLYK analysis for $T_S/T_B \gg 1$, where T_S is the surface temperature, show the monoenergetic beam to lie farther from the normal than the Maxwellian, with any distinction vanishing when $T_B/T_S \gg 1$. Our data do not support this detailed conclusion (Fig. 4).

A recent extension of this model by Logan and Keck[27] to include properties of the solid via an independent oscillator approximation and a gas–surface interaction potential (the "soft-cube" model) is quantitatively more adequate as a description of the scattering process, but the qualitative implications of the hard-cube model are unaltered. In particular, for the mono-energetic beam the soft-cube model shows a somewhat narrower scattering distribution than the experimental result, in contrast to the broader distributions resulting from the hard-cube analysis, but the distributions are still quite broad. These results only serve to emphasize the degree to which models in which the surface temperature is included are successful even though the lattice nature of the solid is either ignored or very crudely approximated.

Further evidence for the role of the thermal characteristics is implied by comparison of Fig. 5 with Figs. 6–8. One can see that the change in dispersion, with a change in beam temperature (or velocity), increases as the T_B/T_S ratio increases. In Fig. 5, T_B/T_S is equal to or less than 1, and no change in the shape of the scattered beam distribution is observed; there is simply a shift away from the target normal with increasing T_B. Furthermore, the Maxwellian and filtered beam distributions are similar in this temperature range (cf. Fig. 4). In Figs. 6–8, on the other hand, T_B/T_S is greater than 1, and, in addition to the shift in position and a slight narrowing in the distribution with increasing T_B, there appears to be a systematic deviation between the Maxwellian and filtered beam distributions. Similarly, in earlier studies it was observed that, for the scattering of Ne from Ag, little shape change was observed when T_B was increased[12] for $T_B/T_S < 1$, but, when the beam was heated to high temperature ($T_B/T_S > 1$), considerable narrowing was observed.[13] Thus, the ratio T_B/T_S is a relevant parameter in describing the scattering mechanism and plays a vital role in the cube models.

The present experimental result removes one con-straint upon any interaction model that might be proposed, i.e., it is no longer necessary that a strong dependence of the shape of the scattered beam flux distribution upon the incident beam velocity result from the calculation. The location of the maximum flux depends upon velocity but not upon the velocity distribution. The need to incorporate simultaneous experimental measurements of the response of the lattice in future scattering experiments is clearly indicated, however.

Finally, in terms of its ability to predict the qualitative features of the scattering phenomenon, the choice of a dynamical description of the lattice, is, of course, not necessarily unique. In the particular case of the monoenergetic "cube" models, the results of a single atom–surface collision are averaged over the one-dimensional Maxwellian distribution of surface atom velocities. This averaging process might be expected to obscure some inadequacies of the model.

D. Dispersive Effects in the Scattered Beam

It has been observed that in thermal beam scattering the mean velocity of the scattered beam v_r varies with the scattered angle for a fixed incident angle and beam energy.[2,3,17,28] Studies at higher energies (using a nozzle beam) have also shown that $v_r = f(\theta_r)$, and, in addition to this broadening in velocity, a spatial divergence of the nearly monoenergetic beam is also observed.[6,7,29,30]

These data taken together with those of the present work imply that the solid must act as a "scrambler," imparting a spatial and velocity divergence to the scattered beam without, however, achieving thermal equilibration. We would expect, therefore, to observe $v_r = f(\theta_r)$ even for the monoenergetic thermal beams, although such measurements have not yet been made.

The origin of this scrambling effect lies most probably in the length of the collision time for the process. Goodman[31] has shown in detail that, particularly for heavy particles, the collisions are "languid," i.e., the length of the interaction time of the gas atom and the solid lattice is long with respect to a characteristic lattice response frequency, which is related to the Debye frequency.

Although Goodman considers a 0°K lattice (and this is undoubtedly a bad assumption for scattering processes, as the success of the much less sophisticated Logan and Stickney theory seems to imply), the thermalization of the lattice really introduces another high-frequency motion to the lattice, which is similar to that induced by the collision, and hence one may still describe the collision with a hot lattice as languid.

[26] R. M. Logan, J. C. Keck, and R. E. Stickney, Ref. 4, p. 49.
[27] R. M. Logan and J. C. Keck, "Classical Theory for the Interaction of Gas Atoms with Solid Surfaces," Massachusetts Institute of Technology, Fluid Mechanics Laboratory Rept. 67-8, October 1967 (unpublished).

[28] J. N. Smith, Jr., and W. L. Fite, *Rarefied Gas Dynamics*, J. A. Laurmann, Ed. (Academic Press Inc., New York, 1966), Vol. 1, Suppl. 2, p. 430.
[29] O. F. Hagena, Ref. 3, p. 531.
[30] R. A. Oman, Ref. 3, p. 532.
[31] F. O. Goodman, Ref. 11, p. 366.

Consideration of the magnitude of typical thermal accommodation coefficients of heavy gas atoms at low temperatures shows that for the solid to exchange energy either one multiphonon process or repetitive single-phonon processes must occur. It is reasonable to favor one-step single-phonon processes over a one-step multiphonon process, and a languid type of collision allows one to repetitively pump energy to or from the lattice in single-phonon steps. This process allows partial thermalization and development of observed divergences. On this basis, an increase in velocity (shorter collision time) would be expected to yield narrower scattering distributions. For light gases at 300°K and for heavier gases at elevated temperatures, this result has been observed experimentally.

Further, the languid collision allows one to consider that the thermal oscillations of the lattice could result in a time-averaged potential which may be smoother than that which the calculation of the variations of surface potential of a static lattice would lead one to expect. Thus, a more planar surface would result during the collision, and one of the significant simplifications of the cube models may be less unrealistic than it first appears. This smoothing will be particularly important in the repulsive region where most of the energy transfer seems to occur.[31]

E. The Choice of $v_0 = \bar{v}$

From the discussion above regarding the scrambling effects of the collision, it appears that the close correspondence between the Maxwellian scattering distribution and the filtered-beam scattering distribution is not unique in terms of the particular choice of $v_0 = \bar{v}$ [see Eq. (1)], except to the extent that this places v_0 near the probable velocity in the incident beam. If the velocity distribution of the incident beam were not relatively symmetric in the vicinity of the most probable velocity within the velocity range of interest (cf. Fig. 2), and if a monotonic increase in displacement away from the target normal with increasing velocity (with little or no change in shape) was not a property of the system under study (cf. Fig. 5), then the close correspondence between the Maxwellian scattering and the filtered scattering for $v_0 = \bar{v}$ would not be expected.

V. CONCLUSIONS

The present study shows that the dispersion in the scattered beam observed in typical gas–surface molecular beam scattering studies does not result from the distribution of velocities in the incident beam or from surface roughness. The dispersion results from the dynamical nature of the lattice involved in the collision. It appears further that the specific nature of the involvement is related to the collision time of the interaction and that the scrambling of the incident beam, leading to dispersions in space and velocity of the scattered beam, is because of the languidness of the collision. Theoretical models of the scattering must then show little dependence on the velocity distribution of the incident beam when comparison with experiment is attempted. The cube models of Logan, Keck, and Stickney[26] and Logan and Keck[27] seem to show this behavior correctly, and the successful application of such simple models may result from time averaging during the languid collision. The need for a dynamical rather than a purely geometrical model of scattering is clearly emphasized by these studies.

Rare-Gas Scattering from LiF: Correlation with Lattice Properties. II*

Joe N. Smith, Jr., D. R. O'Keefe, and R. L. Palmer

Gulf General Atomic Incorporated, San Diego, California 92112

(Received 11 July 1969)

The scattering of thermal energy atomic beams of Ne, Ar, Kr, and Xe from the (001) face of LiF has been studied. Two dominant peaks in the scattering distributions in the plane of incidence are observed: one peak remains fixed with respect to the crystal whereas the position of the other displays a strong dependence on angle of incidence, incident energy, and azimuthal orientation of the target. The former peak is associated with the normal modes of the lattice, in particular with dipole–induced dipole attractive forces produced by longitudinal optical modes in next-nearest-neighbor unlike ion directions. The latter peak is discussed in terms of the surface properties of the crystal, e.g., interaction potential and elastic properties, the latter acting on the transfer of tangential momentum. For Ne, additional peaks occur which arise from diffraction effects. The present results provide additional insight into the phenomenon of preferential scattering reported earlier and strongly emphasize the inadequacies of existing theoretical descriptions of thermal energy atomic and molecular (TEAM) scattering from surfaces, especially when applied to the surfaces of ionic crystals.

I. INTRODUCTION

In a previous paper, a study of the scattering of Ar from LiF was reported in which bimodal scattering distributions were observed in the plane of incidence.[1] One peak was seen to be fixed[2] with respect to the axes of the crystal and it was suggested that it resulted from dipole–induced-dipole attractive forces in directions aligned with rows of second-nearest-neighbor unlike ion chains emerging from the surface of the crystal; longitudinal optical (LO) modes in these preferred directions giving rise to the dipole moment. An inelastic peak was also observed which showed an incident angle and beam temperature dependence reminiscent of earlier inelastic lobular patterns obtained with metal targets, except that here it was possible to demonstrate unequivocally a significant influence of tangential momentum transfer upon the scattering.

The present study is an extension of this earlier work to include Ne, Kr, and Xe in order to further study the influence of surface and bulk properties on the scattering of thermal energy atomic and molecular (TEAM) beams. In general terms, the present results bear out the earlier conclusions based solely on the Ar/LiF system; however, new details are brought to light. Among these are the appearance of specular reflection and diffraction in Ne and the possible existence of a critical value for the normal component of incident momentum for exact alignment of the fixed peak with the LO direction, and some degree of correlation between the behavior of the inelastic peak with the predictions of various hyperthermal model calculations. This later correlation is

discussed in terms of "structure" scattering as introduced by Oman.[3] However, when all the present data are considered it becomes clear that no single theoretical calculation to date includes all of the parameters that are demonstrated to be important in the case of rare-gas scattering from the surface of an ionic crystal.

II. EXPERIMENTAL TECHNIQUE

The geometry of the beam-target-detector coordinate system is shown in Fig. 1. All other experimental details are identical with those described in Ref. 1, with the exception of reporting the present scattered beam data in terms of the quantity ψ/N_0 sr^{-1}; i.e., the ratio of the number of scattered atoms per steradian per second to the incident flow expressed in atoms per second. This measurement is obtained by measuring the total incident flux upstream from the target and calibrating this signal against the response of the scattered beam flux detector, when located in the incident beam (with the target removed). In this way a geometric factor C is obtained such that $\psi/N_0 = C(S_{\text{reflected}}/S_{\text{direct}})$, where S is the corresponding detector signal. The uncertainty in the value of C is $\pm 30\%$. However, the uncertainty in $S_{\text{reflected}}/S_{\text{direct}}$ is less than $\pm 5\%$. Therefore, although the absolute value of ψ/N_0 may be in error by as much as 35%, the major portion of this error is due to the value of C, but this value is the same for all gases, and comparisons *between* any data shown below is accurate to within ~5%. More complete details of this method of expressing the data will appear elsewhere.[4]

III. RESULTS

Figure 2 displays the behavior of Ne scattering as a function of incident beam temperature T_B for $\theta_i = 51°$ and with the plane of incidence intersecting the surface

* Supported by the U.S. Air Force Office of Scientific Research under Contract F 44620-69-C-0034.

[1] J. N. Smith, Jr., D. R. O'Keefe, H. Saltsburg, and R. L. Palmer, J. Chem. Phys. **50**, 4667 (1969).

[2] Throughout this paper the term "fixed" peak is used to denote the major peak in the scattering distribution that lies closest to the target surface. The term "inelastic" peak in used to denote the major peak that lies closest to the target normal. This choice of terminology is subjective and is used primarily for identification of the peaks and clarity of discussion, although the motivation for this assignment of terms will become clear in the subsequent discussion.

[3] R. A. Oman, J. Chem. Phys. **48**, 3919 (1968).

[4] D. R. O'Keefe, H. Saltsburg, R. L. Palmer, and J. N. Smith, Jr. (unpublished).
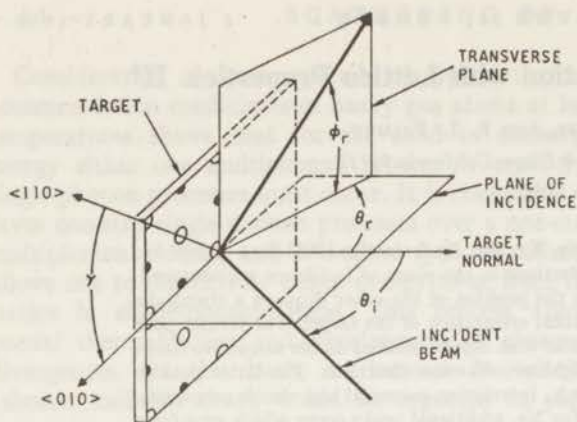
FIG. 1. Schematic of the scattering geometry. The position of the scattered beam flux detector is defined by the angles ϕ_r and θ_r as indicated, and θ_i and γ define the orientation of the incident beam with respect to the LiF crystal.

in the $\langle 010 \rangle$ azimuth. Among the observations to be made from an examination of this figure are the following: First, the position of the inelastic peak moves toward the surface and increases in intensity as T_B is increased whereas the fixed peak increases in intensity also but its location is virtually stationary. (A slight shift of $\lesssim 3°$ away from the surface with increasing T_B may be inferred from the data.) These data are in qualitative agreement with previously published data for Ar[1] with one notable exception: the position of this latter fixed peak in Ne is approximately 5° closer to the surface than the corresponding Ar peak. Second, specular scattering is clearly resolved in the distribution for $T_B = 300°K$ and vestiges of the specular peak remain at the higher temperatures. Further, for $T_B = 300°K$, a fourth peak in the distribution is resolvable in the vicinity of the expected position of a $(-1, -1)$ diffraction peak, calculated on the basis of the most probable wavelength of the Maxwellian beam and a like ion spacing of $d = 2.84$ Å.

Figure 3 shows the behavior of Ne scattering, again in the $\langle 010 \rangle$ azimuth, as a function of θ_i with $T_B = 573°K$. Note that both major peaks in these distributions move toward the surface with increasing θ_i, although the motion of the fixed peak ($\lesssim 7°$) is much less than that of the inelastic peak ($> 30°$). There are only vestiges of specular peaks in these distributions, although additional peaks are resolvable for $\theta_i = 30°$ and 40°, i.e., at $\theta_i = 30$, slight peaks occur at the $(-2, -2)$, $(+1, +1)$, and near the $(+2, +2)$ diffraction peak positions (calculated as described in connection with Fig. 2). At $\theta_i = 40°$ peaks occur at the $(\pm 1, \pm 1)$ diffraction locations, similarly calculated.

Figures 4 and 5 compare the scattering of Ne, Ar, Kr, and Xe ($\theta_i = 40°$, $T_B = 573°K$); the data in Fig. 4 were taken in the $\langle 010 \rangle$ azimuth and the data of Fig. 5 in the $\langle 110 \rangle$ azimuth. Perhaps the most prominent feature of these comparisons is the observation that the location of the inelastic peak moves toward the surface in the

order Ne:Ar:Kr:Xe, a trend which is opposite to that observed in the single lobe patterns obtained with metal targets.[5] However, for any given gas, e.g., Ne, this peak lies closer to the normal in the $\langle 010 \rangle$ azimuth than in the $\langle 110 \rangle$ azimuth, again in accord with the earlier results for the Ar/LiF system.[1]

With regard to the fixed peak, there seems to be a trend for the lighter gas to lie closer to the surface. However, this trend may be exaggerated by the fact that, especially for Kr and Xe, the influence of the inelastic peak in the distribution would be to move the *apparent* peak position of the fixed peak toward the normal. A similar caveat must be invoked when attempting to compare the intensities of the fixed peak for the various gases.

From a comparison of the distributions of Fig. 4 with those of Fig. 5 it becomes evident that for each gas, more particles are scattered into the plane of incidence in the $\langle 010 \rangle$ azimuth than in the $\langle 110 \rangle$ azimuth. In either azimuth, with the exception of Ne, the total integrated in-plane intensity increases as the mass of the scattered atom increases; Ne lies intermediate
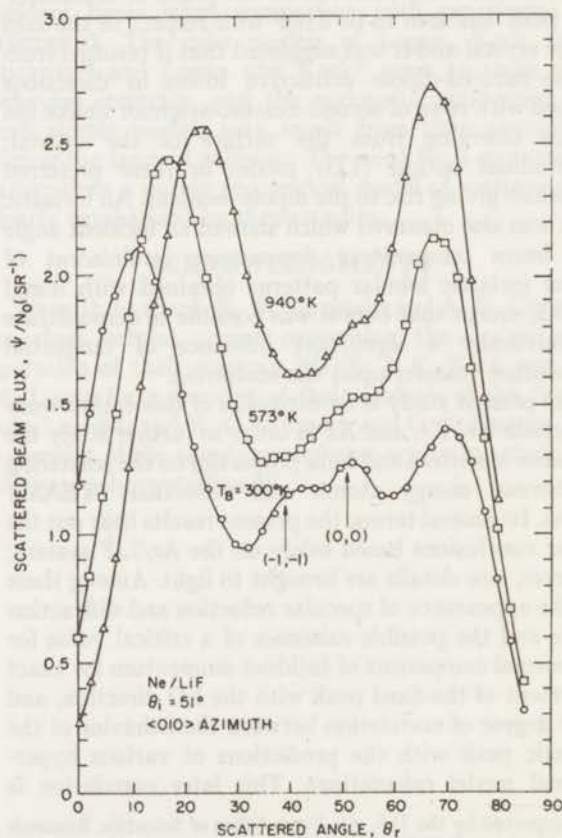

FIG. 2. Ne scattering from LiF in the $\langle 010 \rangle$ azimuth, as a function of incident beam temperature, T_B. $\theta_i = 51°$, $T_S = 300°K$, $\phi_r = 0$. For $T_B = 300°K$, the predicted location of the $(-1, -1)$ diffraction peak is indicated.

[5] J. N. Smith, Jr. and H. Saltsburg, in *Fundamentals of Gas Surface Interactions* (Academic Press Inc., New York, 1967), p. 370.

between Xe and Kr in total in-plane intensity in both azimuths although the difference between Ne and Xe is small.

Two additional observations were made which are not indicated in the figures. First, as the temperature T_S of the LiF target is increased, the location of the inelastic peak moves away from the normal, again a trend opposite to that observed for thermal energy scattering from metals.[5] The location of the fixed peak is relatively insensitive to variations in T_S. Second, as with Ar,[1] fixed peaks were also observed on either side of the plane of incidence ($\phi_r \neq 0$). However, for Ne, these out-of-plane fixed peaks correspond even more closely with the directions of rows of next-nearest-neighbor unlike ions than do the analogous in-plane Ne peaks, or the previously reported out-of-plane peaks for Ar.

IV. DISCUSSION

A. Diffraction in Ne

For 50° incidence, first-order diffraction maxima are resolved and are located in good agreement with the predicted locations, using the same value of lattice
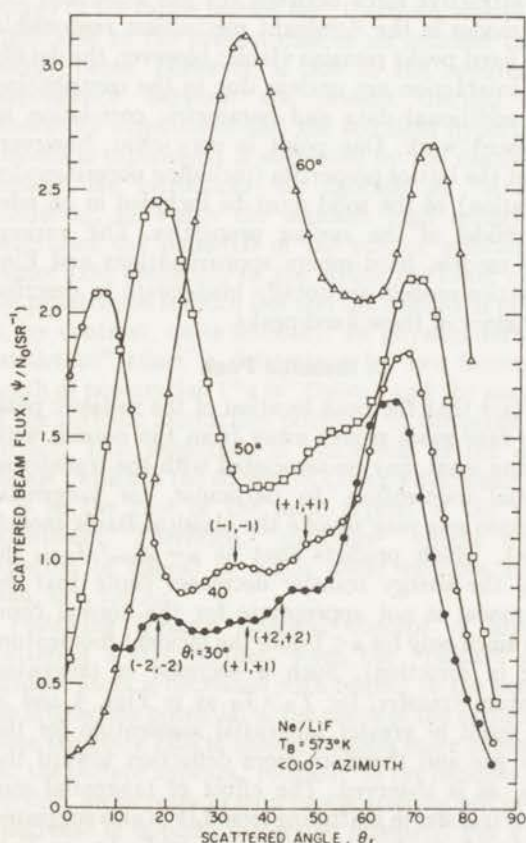

FIG. 3. Ne Scattering from LiF in the ⟨010⟩ azimuth, as a function of angle of incidence, θ_i. $T_B = 573°$K, $T_S = 300°$K, $\phi_r = 0$. Predicted locations of diffraction peaks are indicated on the curves for $\theta_i = 30°$ and $\theta_i = 40°$.

FIG. 4. Scattering of rare gases from LiF in the ⟨010⟩ azimuth. $T_B = 573°$K, $\theta_i = 40°$, $T_S = 300°$K $\phi_r = 0$. Note that the Xe data is plotted half-scale.

spacing d determined from He diffraction experiments on these same crystals.[4] Zabel noted structure in both Ne and Ar scattering from NaCl but from the location of the peaks was forced to accept a different value of d for each of the gases He, Ne, and Ar.[6] In the Ne distribution for $\theta_i = 30°$ (Fig. 3), the existence of ($\pm 2, \pm 2$) diffraction peaks may also be inferred (in He diffraction there is also a trend for these second-order peaks to become more prominent as θ_i decreases).[4] From Fig. 2 it appears that the intensity of the specular, or (0, 0), peak in Ne decreases with increasing T_B but even this qualitative statement, as well as similar statements about the θ_i dependence of the specular component, are in considerable doubt due to the strong influence of the major peaks in the total scattering distribution.

B. Fixed Peaks

The directions corresponding to rows of second-nearest-neighbor unlike ion chains emerging from the surface of the crystal, in the plane of incidence, are located at $\theta_r = 63.5°$ in the ⟨010⟩ azimuth and at $\theta_r = 54.8°$ in the ⟨110⟩ azimuth. Of the four rare gases studied, the fixed peaks in Ar are observed to coincide most closely with these preferred directions. Although there are differences of as much as 12° in the location of these peaks between the various gases (for the same θ_i

[6] R. M. Zabel, Phys. Rev. **42**, 218 (1932).
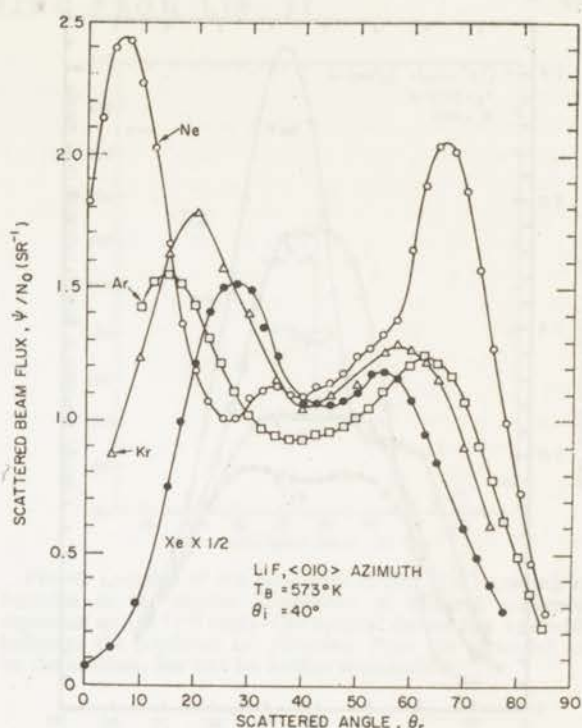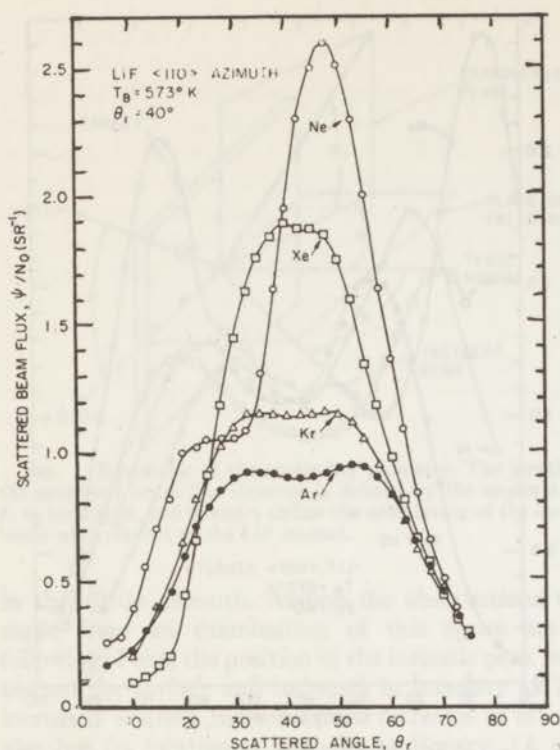
FIG. 5. Scattering of rare gases from LiF in the $\langle 110 \rangle$ azimuth. $T_B = 573°K$, $\theta_i = 40°$, $T_S = 300°K$ $\phi_r = 0$.

and T_B) for any given gas, their position is relatively insensitive to variations in θ_i or T_B (c.f. Figs. 2 and 3 and also Ref. 1). The small variations that are observed may be summarized by stating that as T_B increases or θ_i decreases, the peak tends to move away from the surface.

These latter trends suggest a correlation between the normal component of incident momentum and the location of the fixed peak. To explore this possibility, in Fig. 6 are plotted the locations of the fixed peak as a function of the normal component of incident momentum for all the data of the present paper and also of Ref. 1. The points themselves are the peak locations taken from the experimental distributions. In those cases where the actual fixed-peak location may be influenced by the inelastic peak, the corresponding data point is labeled with an arrow that indicates the direction in which the peak would move if a correction for this influence was made (the magnitude of such a shift would probably be less than about 2°). The trend indicated in Fig. 6 is for the fixed peak to move away from the surface with increasing normal momentum, with a critical normal momentum for exact alignment with the predicted LO direction. This is seen also by comparing the data for 570°K Ar at $\theta_i = 40°$ (Fig. 4), 573°K Ne at $\theta_i = 30°$ (Fig. 3), and 300°K Kr at $\theta_i = 40°$ (data not shown), i.e., at approximately the same normal component of incident momentum, the fixed peak lies very nearly at 63.5°, in the $\langle 010 \rangle$ azimuth.

These points are signified by the closed circles labeled 1 (two points, one from Ref. 1), 2, and 3, respectively, in Fig. 6. A similar comparison is not possible in the $\langle 110 \rangle$ azimuth due to the fact that the peaks are not clearly resolved.

Although the fixed-peak locations may correlate with incident momentum, the peak intensities do not, viz., for the three comparisons mentioned above, ψ/N_0 varies from approximately 2.72 sr^{-1} for Ne to roughly 0.8 for Ar and Kr (after compensating the raw data of Fig. 4 for the influence of the "tail" of the inelastic peak). On the other hand, a crude correlation between collision time, taken as the product of the Lennard-Jones range parameter and the inverse thermal velocity of the incident atom, can be made. Making due allowance for the uncertainty in determining the absolute fixed peak intensity, the observed trend is for a decrease in intensity to occur with increase in collision time, between the extremes of 940°K Ne and 573°K Xe. This same trend is seen more explicitly, of course, in the Ne data of Fig. 2 and in the Ar data of Ref. 1 and was previously attributed to an increase in energy loss with increasing collision time thereby giving rise to a decrease in directionally preferred re-emission.[1]

To summarize, the suggestion that a dipole–induced dipole attractive force between the gas atom and LO lattice modes is the dominant mechanism responsible for the fixed peaks remains viable; however, the details of this interaction are unclear due to the contribution of the additional data and parametric correlation in the present work. One point is very clear, however, i.e., that the lattice properties (including normal modes of vibration) of the solid must be included in an adequate model of the *surface* properties. The various "cube" models, hard-sphere approximations and Einstein lattice models are totally inadequate to describe the behavior of these fixed peaks.

C. Inelastic Peak

The fact that the peak location of the inelastic peak for the rare gases moves away from the normal with increasing mass may be associated with the transfer of tangential momentum. In particular, for tangential momentum one may invoke the classical Baule model, for $\mu > 1$, which predicts that as $\mu = M_{gas}/M_{solid}$ increases, the energy transfer decreases (note that the Baule model is not appropriate for the normal component since only for $\mu < 1$ does the incident momentum reverse in direction). Such a decrease in tangential momentum transfer, for $T_B > T_S$ as in Figs. 4 and 5, would result in greater tangential momentum for the heavier gas and therefore more deflection toward the surface, as is observed. The effect of tangential momentum transfer in scattering from LiF is also suggested by the trends produced by variations in T_S, i.e., as T_S is increased the principal effect is to increase the tangential momentum of the scattered particle, thereby moving the peak toward the surface.

In the case of the inelastic peak, it is quite clear that the intensity decreases in the order Xe:Ne:Kr:Ar in the ⟨010⟩ aximuth and for the ⟨110⟩ azimuth Xe is certainly the most intense, but the subsequent ordering Kr:Ne:Ar is questionable due to the influence of the adjacent fixed peak (Fig. 5). On this basis, Ne seems to display an anomalous behavior when compared with the other gases, but it should be remembered that only for Ne are vestiges of purely elastic events observed (specular reflection and diffraction) and it is suggested that, in general, Ne scattering is much more nearly elastic than for the heavier gases, leading to a more intense in-plane peak than would be expected on the basis of the heavier gas trend. A similar argument could apply to the total integrated in-plane intensity for the various gases, i.e., Ne is intermediate between Xe and Kr in both azimuths.

Similar trends in peak location (but not peak intensity) follow from the hard sphere approximations of Goodman[7] and of Jackson and French[8] and also from the "independent oscillator lattice" model of Oman.[3] All of these models are designed to be appropriate to "hyperthermal" scattering, i.e., where the kinetic energy of the incident atom greatly exceeds the phonon energy of the target lattice, and, therefore, should not be applicable to the present case of an incident thermal-energy beam. However, a clue to the apparent correspondence between the present thermal energy laboratory experiment and the so-called hyperthermal numerical experiment is suggested by the discussion of Oman.[8] He introduces the concept of "structure" scattering, in which the incident high energy atom penetrates the potential of the surface sufficiently to "sense" the periodicty of the lattice (at lower energies the penetration is much less and the collisional potential is, by contrast, quite smooth). In physical terms this "structure" effect is determined by two factors—the depth of penetration ("a la" Oman) and the amplitude of the periodic interaction potential in the plane of the surface. This amplitude is much less in the case of metals (which is the subject of Oman's discussion) than it is in the case of the ionic crystal of the present experiment. Therefore, "structure" effects may be expected to appear at much lower energies for LiF than, say, for Ag.

Following Oman's classical concept of structure scattering a step further, when the "radius" of the incident atom is decreased with respect to the period of the interaction potential in the plane of the surface then these structure effects should become more prominent, i.e., the surface appears "rougher" to the incident atom. Further, an increase in structure scattering will produce a decrease in in-plane integrated intensity. For a cubic lattice such as LiF, this classical idea implies that more in-plane scattering should occur in the ⟨010⟩ azimuth
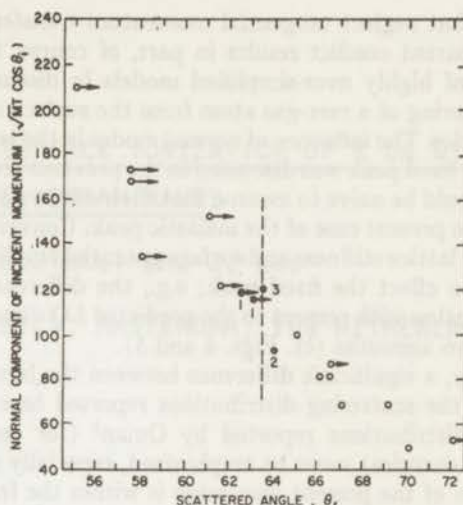

FIG. 6. Location of the fixed peak in the ⟨010⟩ azimuth as a function of the normal component of incident momentum, expressed as $(MT)^{1/2} \cos\theta_i$. The vertical dotted line at $\theta = 63.5°$ indicates the predicted LO direction. Note the expanded scale on the abscissa. See text for further explanation.

than in the ⟨110⟩ azimuth due to the ~20% decrease in effective "aperture" as seen by the incident atom in the former azimuth, and therefore less sensitivity to the amplitude of the periodic potential in the plane of the surface. From Figs. 4 and 5 such an increase in in-plane flux is indeed observed in the ⟨010⟩ aximuth as compared with the ⟨110⟩ azimuth.

The influence of this periodic variation in the surface potential is further suggested in a recent experiment by the present authors in which diffraction of He was not observed from a (001) Ag film grown epitaxially (in situ) upon a diffracting (001) LiF surface; however, there was a sevenfold increase in specular scattering from the Ag surface as compared with the LiF.[9] In other words, it is suggested that the relative "potential smoothness" of Ag and the lack of deep penetration of thermal energy He into the surface potential combined in such a way as to make the Ag surface appear more mirrorlike and less like a diffraction grating to the incident He atom.

For a given gas, two trends are observed which do not follow directly from the various hyperthermal models: (1) as T_B is increased, the inelastic peak moves toward the surface (Fig. 2), and (2) the inelastic peak lies closer to the surface in the ⟨110⟩ azimuth (Fig. 5) than in the ⟨010⟩ azimuth (Fig. 4). The latter trend has been previously interpreted[1] as resulting from the fact that the LiF lattice is stiffer in the ⟨110⟩ direction,[10] resulting in less transfer of tangential momentum. The former trend is analogous to that observed in scattering from metals[5] and which is reproduced in the "cube"

[7] F. O. Goodman, Surface Sci. 7, 391 (1967).
[8] D. P. Jackson and J. B. French. Proc. Intern. Symp. Rarefied Gas Dyn. 6th 1968, 2, 1119 (1969).

[9] R. L. Palmer, H. Saltsburg, D. R. O'Keefe, and J. N. Smith, Jr. (unpublished).
[10] C. V. Briscoe and C. F. Squire, Phys. Rev. 106, 1175 (1957).

models that neglect tangential momentum transfer.[11,12] This apparent conflict results in part, of course, from the use of highly over-simplified models in discussing the scattering of a rare-gas atom from the surface of an ionic lattice. The influence of normal modes in the lattice upon the fixed peak was discussed in the previous section and it would be naive to assume that their effect was not felt in the present case of the inelastic peak. Conversely, effects of lattice stiffness and surface potential amplitude must also effect the fixed peak; e.g., the difference in peak location with respect to the predicted LO direction in the two azimuths (cf. Figs. 4 and 5).

Finally, a significant difference between the bimodal form of the scattering distributions reported here and similar distributions reported by Oman[3] (for certain incident energies) must be emphasized, especially since a portion of the present discussion is within the framework of "structure scattering" as put forth by Oman. We find one peak relatively fixed with respect to the major axes of the crystal and correlate it with lattice properties—Oman reports no such fixed peaks, nor is his independent oscillator lattice model able to predict such a phenomenon. Structure scattering, as discussed here, and by Oman, is concerned with the ability of the incident atom to sense the periodicity of the lattice and does not necessarily imply structure in the scattering distribution.

V. SUMMARY AND CONCLUSIONS

First-order (and possibly second-order) diffraction maxima are resolved for Ne in the present experiments. To the authors' knowledge this represents the first clear evidence for diffraction for atoms heavier than He. The appearance of completely elastic scattering (i.e., diffraction and specular reflection) in Ne may be related to the apparent analomous behavior of Ne, when compared with the heavier rare gas atoms, in terms of the intensity of the inelastic peak and total in-plane flux.

Coupling between the incident (polarizable) atom and the dipole moment associated with LO modes in second-nearest-neighbor unlike ion directions is still suggested as the dominant mechanism responsible for the fixed peaks. However, a detailed comparison between the rare gases suggests that other factors are also important; e.g., there seems to be evidence for a "critical" normal component of incident momentum for near perfect alignment with the preferred LO directions.

Other contributing factors are suggested by a study of the behavior of the inelastic peak in the distribution, e.g., for the inelastic peak, the trends observed for the rare gases and the trend, for a given gas, produced by a change in azimuth imply the strong influence of tangential momentum transfer. Some correspondence between these trends are consistent with the so-called hyperthermal model calculations[3,7,8] and that his correspondence should not be too surprising is suggested by the fact that the amplitude of the interaction potential, in the plane of the surface, is much greater for the present ionic lattice than for metal crystals (the subject of these model calculations). The result if this is that a thermal-energy rare-gas atom may "sense" the potential structure of the LiF surface, thereby vitiating the assumption of a smooth surface ("a la" the cube models).[11,12]

In summary then, the discussion of the fixed peaks emphasizes the role played by normal modes in the lattice whereas the discussion of the inelastic peak emphasizes the surface properties, e.g., stiffness (or surface Debye temperature) and interaction potential. But this separation of properties is, at best, artificial, and is done simply because the gross behavior of these two peaks is quite different. All properties of the system must be taken into account for a complete description of the observed phenomena. In short, these data demonstrate the necessity for a theoretical description of TEAM scattering that includes the lattice properties of the solid as well as surface properties and the true atomic character of the incident particle (e.g., polarizability). All existing theories fail on one or more of the foregoing considerations.

Note added in proof: A recent classical calculation by McClure [J. Chem. Phys. **51**, 1687 (1969)] yields bimodal scattering distributions such as reported here. In particular, one of the two peaks remains fixed throughout the incident energy range 0.039–9.477 eV. McClure attributes this structure in the scattering distribution to the periodicity of the interaction potential in the plane of the surface and the consequent limiting values of θ_r as the impact parameter varies over the unit cell, in analogy with rainbow scattering effects in binary collisions. The present authors wish to acknowledge the possibility that this effect may also explain the structure observed in the rare-gas/LiF system.

[11] R. M. Logan, J. C. Keck, and R. E. Stickney, Proc. Intern. Symp. Rarefied Gas Dyn. 5th 1966 **1**, 49 (1967).
[12] R. M. Logan and J. C. Keck, J. Chem. Phys. **49**, 860 (1968).

CHAPTER IV

RESIDENCE TIME MEASUREMENTS FOR THE SURFACE IONIZATION OF K ON W:

THE EFFECTS OF SURFACE CONTAMINANTS

Joe N. Smith Jr.[*], J. Wolleswinkel and J. Los

FOM-INSTITUTE FOR ATOMIC AND MOLECULAR PHYSICS, AMSTERDAM, THE NETHERLANDS

ABSTRACT

The surface residence time, τ, for K^+ on W is measured and the values of
τ_o and Q_i, defined by the relation $\tau = \tau_o \exp Q_i/kT$ are derived. The effect
on τ_o and Q_i produced by contamination by carbon, oxygen, nitrogen and
hydrogen are reported. A critical analysis of these results as compared
with earlier work is presented. In addition, a discussion is presented
which relates the present results to previous physical interpretations of
τ_o and Q_i. The present results suggest that strongly bound contaminants lead
to small or negligible changes in these parameters while loosely bound
(mobile) gaseous contaminants lead to a decrease in Q_i and an increase in τ_o.
These results are also related to contamination effects observed in the
scattering of thermal energy atomic beams from surfaces.

[*] Currently on leave of absence from Gulf General Atomic Inc., San Diego, Calif.

INTRODUCTION

The temperature dependence of the surface residence time, τ, for alkali ions produced in the surface ionization of alkali atoms on heated refractory metals has been studied extensively in the past, using a variety of experimental techniques[1-10]. From these measurements the values of τ_0 and Q_i, defined by the relation $\tau = \tau_0 \exp Q_i/kT$, are reported; however, there is, in general, considerable disagreement in the values obtained by different authors. Such divergent results may be due to unknown surface contamination, surface structure, experimental method and analysis, or a combination of these factors.

With one exception[7], these earlier results were taken with polycrystalline targets and, in all cases, the degree of surface contamination is either unspecified or simply infered from indirect observations.

The present experiments were undertaken to study explicitly the effects of surface contamination on τ in order to partially resolve the earlier discrepancies and also to investigate the factors that determine the values of τ_0 and Q_i. For this study, the potassium-tungsten system was chosen and changes produced by contamination by carbon, oxygen, nitrogen and hydrogen was examined. For the cleanest surface conditions obtainable in the present experiment, the value of $Q_i = 2.36 \pm .06$ eV was obtained, which is in agreement with Kaminsky[6] and Evans[1]. However, the values of τ_0 obtained by these later workers is substantially lower than that reported in the present work, where it is shown that a surface carbon impurity reduces τ_0 without changing Q_i.

To summarize the present results, it may be stated that surface impurities which are strongly bound to the surface (e.g. carbon and oxygen) produce little change in Q_i but effect τ_0 whereas more mobile adsorbed layers (e.g. nitrogen and hydrogen) tend to decrease Q_i and drastically increase τ_0. These results are discussed in terms of the identification of Q_i with the electrostatic image potential and the statistical mechanical derivation of τ_0 due to Kruyer[11].

Finally, some comparison is made between the present results and the earlier observations of contamination effects on the scattering of rare gas atoms from solid surfaces (cf. refs. 33 - 35) and it is shown that the present results re-inforce the inferences made in the earlier work.

EXPERIMENTAL TECHNIQUE

A schematic block diagram of the apparatus used in these experiments is shown in figure 1 and has been described in detail elsewhere[12]. For the present purposes it is sufficient to state that the incident K atom beam had an energy of $.66 \pm .13$ eV, obtained by velocity-filtering a beam of atoms produced by Ar^+ sputtering of a solid K target. The resultant incident atom flux was on the order of 10^7 atoms per sec per cm^2. The tungsten target was a polycrystalline ribbon which was heated ohmically and could be flashed at temperatures up to $3000°K$. Ribbon temperatures were measured with an optical pyrometer which was calibrated against a standard filament. The base pressure in the chamber containing the tungsten target and detector was 2×10^{-9} torr and measurements of τ could be made within minutes after flashing, assuring that the surface was substantially free of adsorbed contaminants. Contaminant gases (CH_4, O_2, N_2 and H_2) were introduced into this chamber via a variable leak valve. The surface coverage of potassium may be estimated from the relation $\Theta = n\tau$, where n is the incident flux ($\approx 10^7$ atoms sec^{-1} cm^{-2}) and τ is the mean residence time. Since, at the temperatures involved in these experiments, it may be assumed that potassium exists mainly as K^+ on the surface[1], and since the present measurements yield values of τ for K^+ on the order of 10^{-3} sec, the resulting coverage of potassium may be estimated to be $\sim 10^4$ cm^{-2}. Thus one may neglect mutual interactions in the interpretation of the present data.

Values of τ may be obtained by observing the exponential time decay of the desorbing ion current after exposing the target to a short pulse of atoms[3]. In the present experiments this time response, h(t), is obtained by using correlation techniques as described elsewhere[13]. Briefly, the Ar^+ ion beam is modulated electrostatically by a function x(t), giving rise to a neutral atom beam with the same modulation. The cross-correlation function, ϕ_{xy}, between this modulation and the desorbing ion signal, y(t), is electronically computed. It is shown in ref. 13 that

$$\phi_{xy}(t) = \int_0^\infty d\lambda h(\lambda) \phi_{xx}(t-\lambda)$$

where ϕ_{xx} is the autocorrelation function of x(t) and λ is a variable of integration. If, as in the present case, x(t) is broad band random noise, $\phi_{xx}(t-\lambda) \approx \delta(t-\lambda)$ and

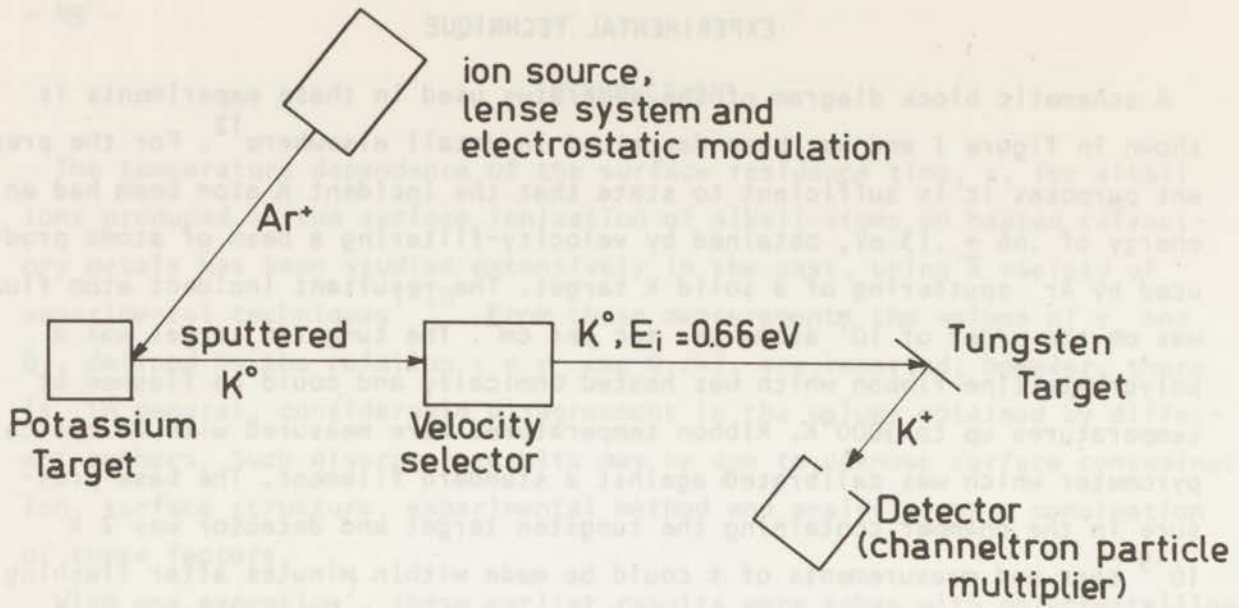$$\phi_{xy}(t) \approx h(t) .$$

Fig. 1 - Schematic diagram of the experimental apparatus.

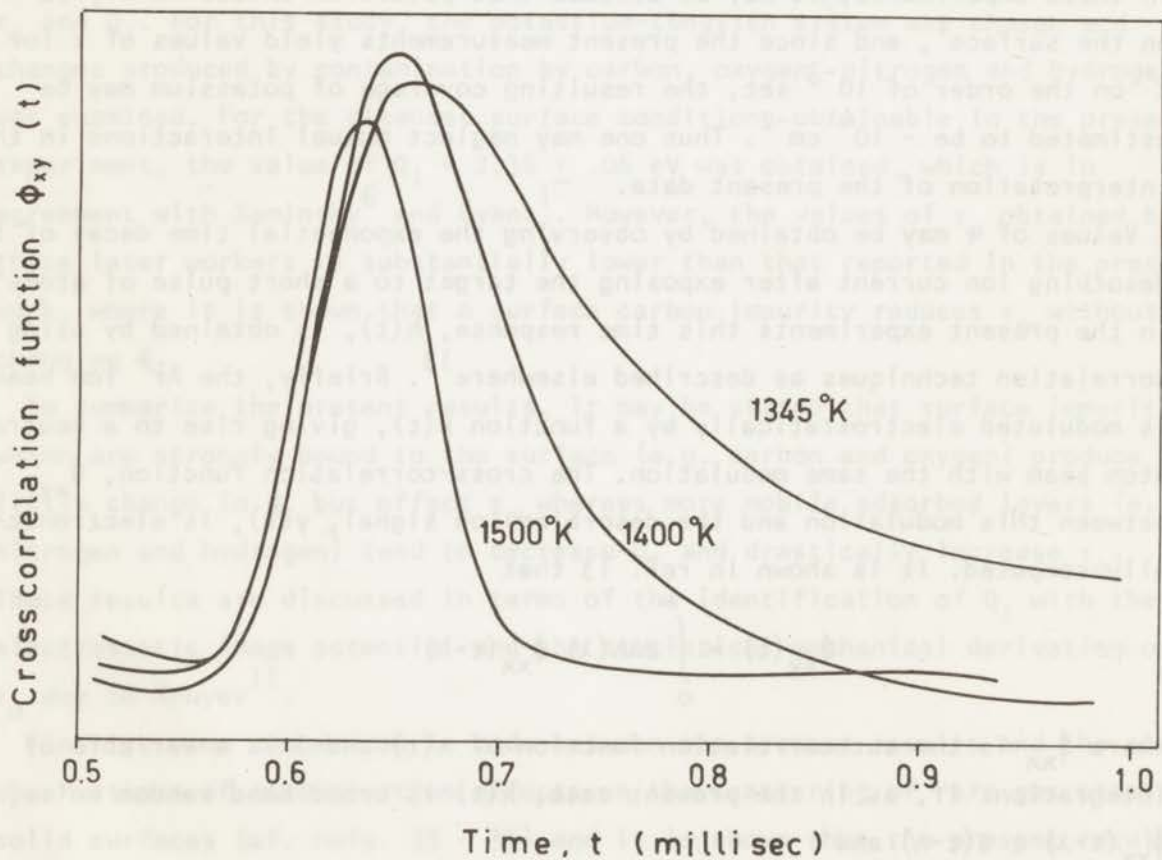Fig. 2 - Cross correlation function for K^+ desorbing from W at three target
temperatures.

V(r)

$V_a(r)$

$V_i(r)$

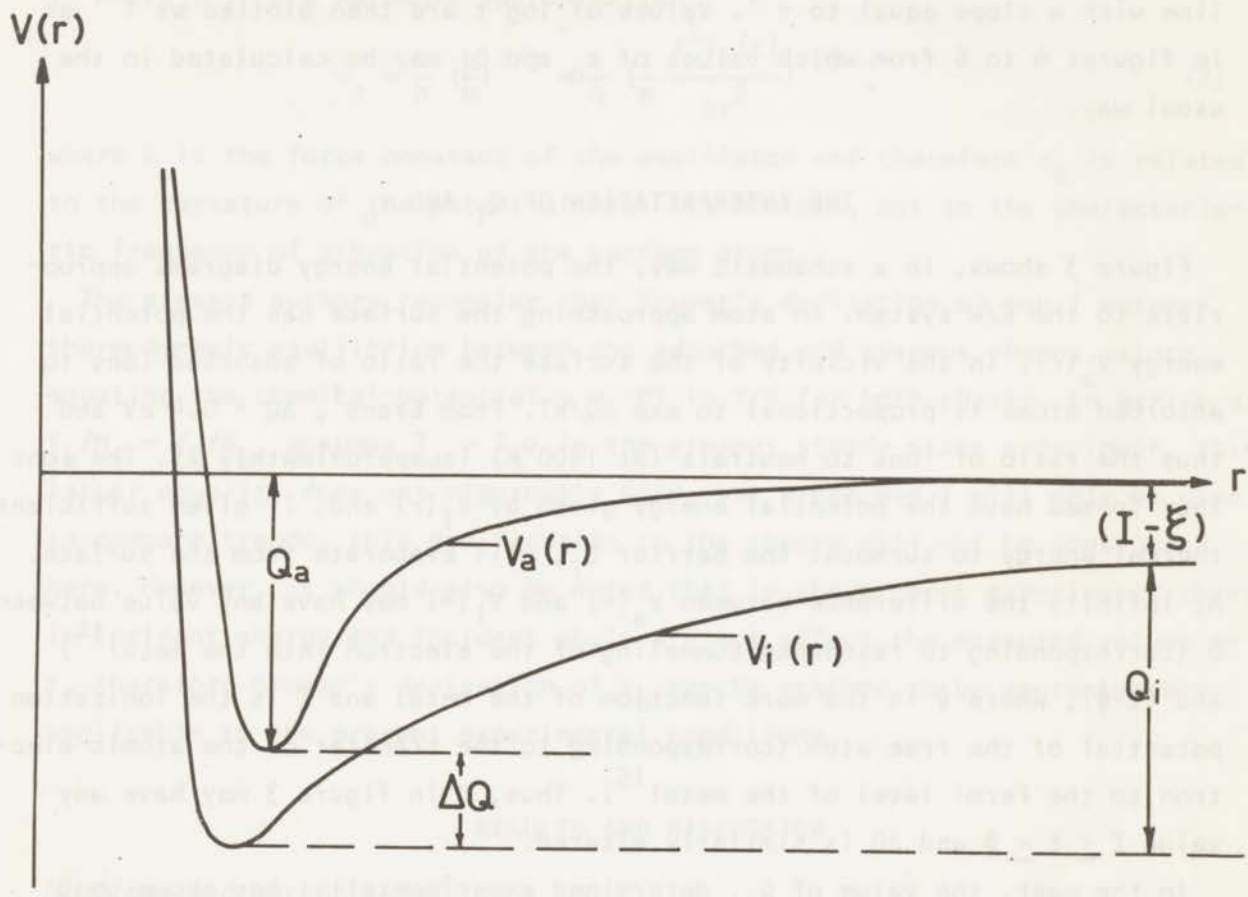Q_a

Q_i

ΔQ

$(I - \xi)$

r

Fig. 3 - Schematic representation of potential energy diagram for the K-W
system. See text for discussion of symbols.

In figure 2 are shown x-y recordings of $\phi_{xy}(t)$ for three target temperatures. At 1500°K, the residence time τ is too short to be measurable and the resultant $\phi_{xy}(t)$ differs from $\phi_{xx}(t)$ only due to transit time and resolution effects in the incident beam. At the lower temperatures, the logarithm of the trailing edge of $\phi_{xy}(t) = h(t)$ is plotted vs t, yielding a straight line with a slope equal to τ^{-1}. Values of log τ are then plotted vs T^{-1} as in figures 4 to 6 from which values of τ_o and Q_i may be calculated in the usual way.

THE INTERPRETATION OF Q_i AND τ_o

Figure 3 shows, in a schematic way, the potential energy diagrams appropriate to the K/W system. An atom approaching the surface has the potential energy $V_a(r)$. In the vicinity of the surface the ratio of adsorbed ions to adsorbed atoms is proportional to exp $\Delta Q/kT$. From Evans[1], $\Delta Q \approx 0.4$ eV and thus the ratio of ions to neutrals (at 1400°K) is approximately 25. The ions thus formed have the potential energy given by $V_i(r)$ and, if given sufficient thermal energy to surmount the barrier Q_i, will evaporate from the surface. At infinity the difference between $V_a(\infty)$ and $V_i(\infty)$ may have any value between 0 (corresponding to resonance tunneling of the electron into the metal[14]) and $(I-\phi)$, where ϕ is the work function of the metal and I is the ionization potential of the free atom (corresponding to the transfer of the atomic electron to the Fermi level of the metal[15]). Thus, ξ in figure 3 may have any value $I \leq \xi \leq \phi$ and ΔQ is similarly altered.

In the past, the value of Q_i, determined experimentally, has shown good agreement with the value of the electrostatic image potential, $e^2/4r$, with r taken to be the ionic radius of the alkali ion[1,3,5]. The experimentally observed reduction in Q_i upon gaseous contamination is then attributed to a screening effect due to the adsorbed gas layer, i.e. $Q_i \rightarrow e^2/4\epsilon r'$, where $r' > r$ is the new equilibrium distance from the surface and $\epsilon > 1$ is the "dielectric constant" of the gas layer.

The value of τ_o, in the relation $\tau = \tau_o$ exp Q_i/kT, was derived by Frenkel as $\tau_o = 1/\nu_z$, where ν_z is the frequency of vibration of the ad-ion normal to the surface[16]. More recently Kruyer[11] has shown this to be a special case of the more general equation

$$\tau_o = \frac{h}{kT} \frac{f^a_{tr}}{f^a_{free\ tr}} f_z \qquad (1)$$

where f^a_{tr}, $f^a_{free\ tr}$ are the partition functions for hindered and free transl-
ation of the ad-ion along the surface respectively and f_z is the partition
function for vibration normal to the surface. If the bonding normal to the
surface is assumed to be harmonic and $h\nu_z << kT$, then $f_z \to kT/h\nu_z$ and thus
if motion in the plane of the surface is unhindered ($f^a_{tr} = f^a_{free\ tr}$),
$\tau_o \to 1/\nu_z$. In the harmonic approximation

$$\nu_z = \frac{1}{h}(\frac{k}{m})^{1/2} = \frac{1}{h}(\frac{1}{m}\frac{\partial^2 V_i(r)}{\partial r^2})^{1/2},\qquad(2)$$

where k is the force constant of the oscillator and therefore τ_o is related
to the curvature of the potential near its minimum, not to the characteris-
tic frequency of vibration of the surface atoms.

The present authors recognize that Kruyer's derivation of eqn 1 assumes
thermodynamic equilibrium between the adsorbed and gaseous phases, since
equating the chemical potential $\mu = -RT \ln f/N$ for both phases, to arrive at
$f_a/N_a = f_g/N_g$, assumes $T_a = T_g$. In the present steady state experiment, this
latter equality does not rigorously hold, but since eqn 1 will only be used
to compare trends, this modification to the theory will not be considered
here. However, it should also be noted that in the present experiments changes
in incident energy and incident angle did not affect the measured values of
τ, therefore Kruyer's derivation of τ_o may be assumed to be approximately
applicable to the present experimental conditions.

RESULTS AND DISCUSSION

A) Clean and carbonized W

Figure 4 shows data taken at a base pressure of 2×10^{-9} torr and contains
results obtained after four specific pretreatments of the W ribbon and which
fall into two categories: points lying along curve A correspond to the clean-
est surface conditions obtainable and points on curve B were obtained when
a carbon contamination was present on the surface.

The first series of data points (labeled by the symbol $\otimes$ in figure 4) were
obtained after flashing an otherwise "virgin" ribbon at 2300°K. Secondly, the
well known decarbonizing procedure was employed to remove surface carbon im-
purities arising from diffusion to the surface of the usual bulk carbon im-
purity present in tungsten, viz the ribbon was heated extensively in an O_2
atmosphere, then flashed at 3000°K in ultimate vacuum[17]. Subsequent to this
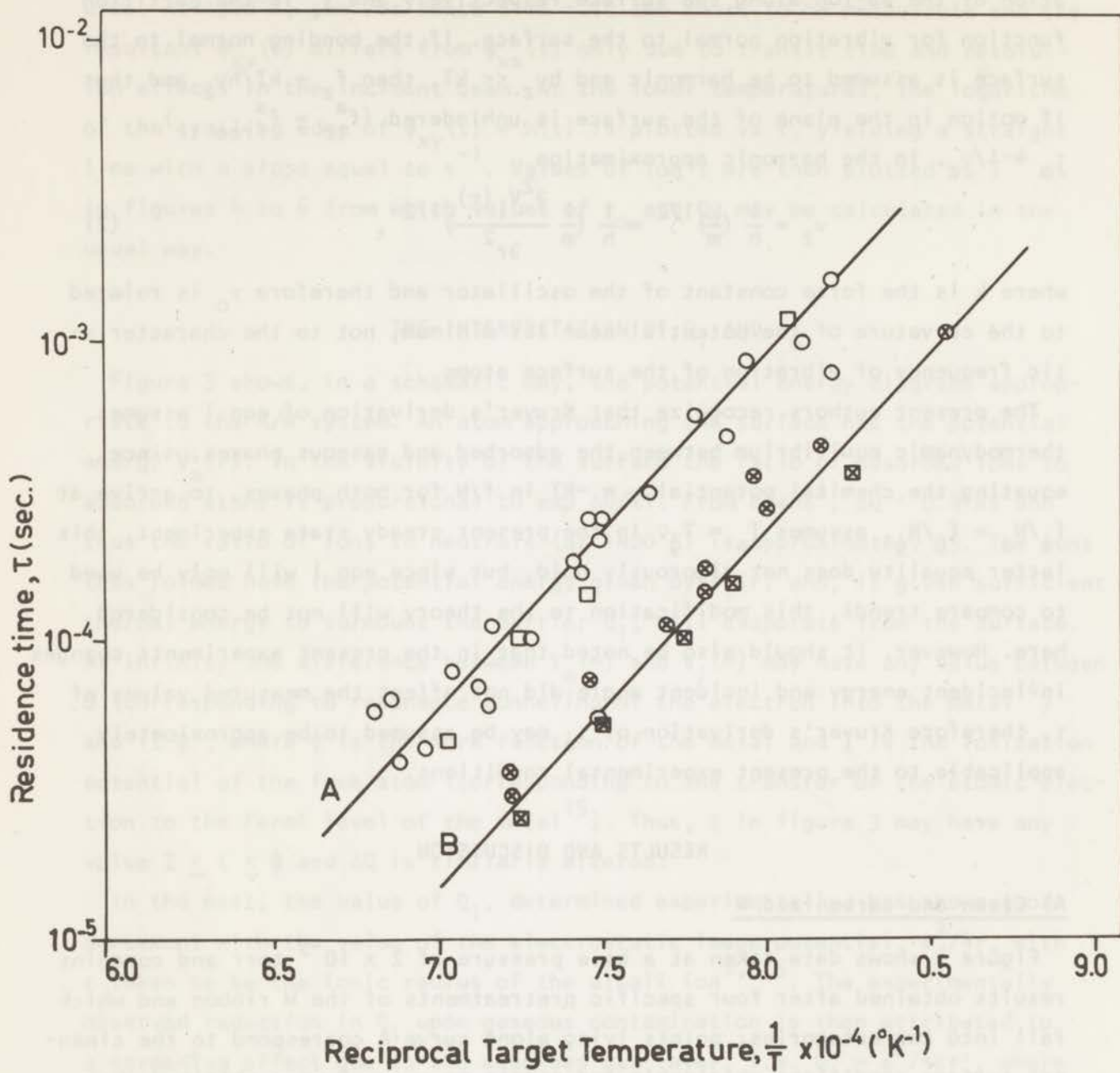
Fig. 4 - Residence time versus reciprocal target temperature for K$^+$ desorption from W. For curve A, the target was decarbonized; for curve B, a carbon impurity was present.

treatment, the second series of data points were obtained (labeled ○ in figure 4). It is seen that the resultant values of τ are about a factor 4 larger than those obtained prior to the O_2 treatment.

In order to further establish that this change in τ was indeed due to a surface carbon impurity, the ribbon was next heated to $2300°K$ in a CH_4 background, following the experiments of Boudart and Ollis[18]. The third set of data were then obtained (labeled ⊠ in figure 4) and it is seen that this intentional carbonization of the ribbon did indeed restore the original values of τ.

Finally this carbonized ribbon was again subjected to an O_2 treatment as before and the resulting τ values (labeled □) of the "clean" surface were again obtained. The values of Q_i and τ_o for the clean and carbonized surface, derived from figure 4, are summarized in table I and compared with earlier results.

Within experimental error, the value of Q_i is unaffected by carbonization and further, agrees with the values reported by Kaminsky[6] and by Evans[1]. On the other hand, in the present work, the value of τ_o is decreased by a factor of 4 for the carbonized surface and this lower value is in much better agreement with the values reported by Kaminsky and Evans for a "clean" surface. From this comparison, it may be surmised that in the earlier work, although the surface may have been free of adsorbed gases, a carbon impurity was present. It should also be noted that Hughes and Levinstein report a lowering of τ_o by a factor of 3 upon exposing their tungsten surface to oil vapor[7].

Even for a clean W surface, one would expect $f_{tr}^a < f_{free\ tr}^a$ in eqn 1 since translations will be hindered not only by the periodic variation of the potential in the plane of the surface ("hopping" atoms) but also, to a larger extent, by defect sites present on the surface. Therefore τ_o, in the harmonic approximation, can be expected to be less than ν_z^{-1}. Since the decomposition of CH_4 on W is known to produce an ordered array, with a cell larger than that of the W (but smaller than a "unit cell" composed of defect sites)[18], one would expect translations to be further hindered by carbonization, leading to a decrease in f_{tr}^a, and therefore τ_o, as compared with the value for clean W.

The fact that Q_i is apparently unaffected by the presence of carbon can

also be rationalized on the grounds that carbon forms a stable, relatively open structure on the surface of W. Thus, if Q_i is associated with the electrostatic image potential, relatively little "screening" would be expected to result from the formation of such an ordered array. Similarly, little perturbation of the curvature of $V_i(r)$ in the region of its minimum would be expected so that this contribution to a decrease in τ_o can most probably be ignored in comparison to the decrease in f^a_{tr} mentioned above.

B) Continuously oxygenated W

Four runs were made (over a period of two months) in the presence of a partial pressure of 2 to 3×10^{-8} torr of O_2. These results are shown in figure 5. Two runs were made with a de-carbonized ribbon (symbol □) and two runs were made with a carbon impurity present (○). Although the scatter in the data at temperatures below about $1450^\circ K$ is somewhat greater than that of figure 4, several distinct features of the data are to be noted. First there are no large differences between the data for carbonized and de-carbonized targets, in contrast to the same conditions in the absence of O_2 (figure 4). This result is not unexpected, as the presence of O_2 would tend to remove the carbon impurity from the surface, if it were present.

Secondly, there seems to be three distinct temperature regimes in which $\log \tau(1/T)$ may be approximated by straight lines, indicating the possibility of three distinct binding states for K^+ on oxygenated W. Assuming that it is valid to assign values of τ_o and Q_i to these three temperature regimes, the approximate values of these quantities are tabulated in table II. Below $1250^\circ K$, Q_i and τ_o are within the range reported in table I, while above $1450^\circ K$ Q_i is about 18% smaller. The values of Q_i and τ_o reported at intermediate temperatures must be considered highly speculative, as an examination of figure 5 will indicate.

The complicated nature of the present oxygenated tungsten results, may be correlated, in a qualitative way, with earlier LEED, work function and mass spectrometric studies of the complex O_2/W system. Using LEED, Taylor[19] observes three separate stable structures, resulting from the adsorption of O_2 on W, with the appearance of these structures depending (in an ill-defined way) on both the extent of O_2 exposure and the subsequent flashing temperature (on the order of $1400^\circ K$ or greater). Also using LEED, Germer and May[20] report highly complex diffraction patterns when a (110) W crystal
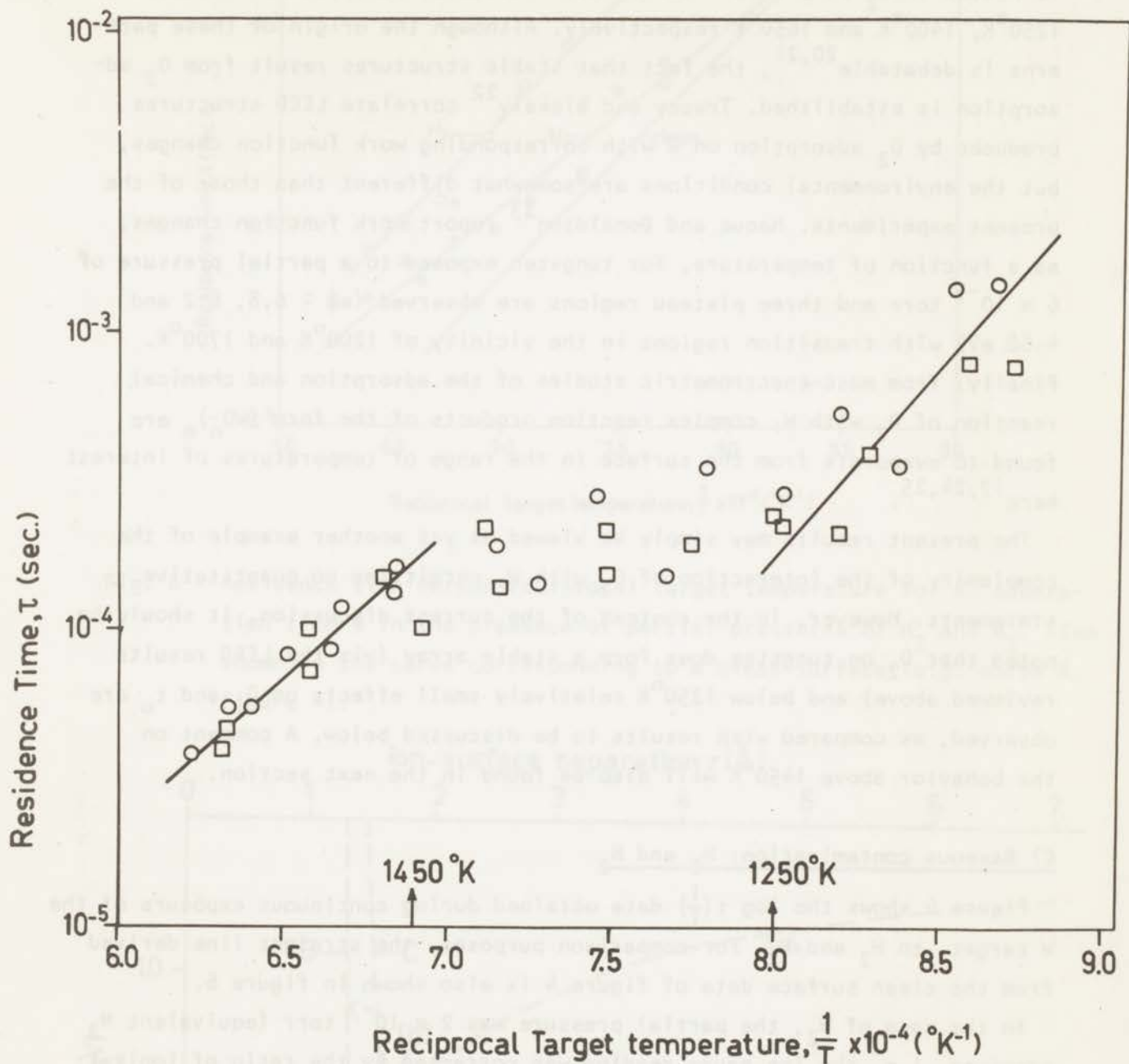
Fig. 5 - Residence time versus reciprocal target temperature for K⁺ desorp-
tion from continuously oxygenated W.

is heated in O_2 at 5×10^{-3} torr. Three different patterns are observed at 1250°K, 1400°K and 1650°K respectively. Although the origin of these patterns is debatable[20,21], the fact that stable structures result from O_2 adsorption is established. Tracey and Blakely[22] correlate LEED structures produced by O_2 adsorption on W with corresponding work function changes, but the environmental conditions are somewhat different than those of the present experiments. Haque and Donaldson[23] report work function changes, as a function of temperature, for tungsten exposed to a partial pressure of 6×10^{-7} torr and three plateau regions are observed (e$\phi \approx 6.8$, 6.2 and 4.68 eV) with transition regions in the vicinity of 1200°K and 1700°K. Finally, from mass-spectrometric studies of the adsorption and chemical reaction of O_2 with W, complex reaction products of the form $(WO_n)_m$ are found to evaporate from the surface in the range of temperatures of interest here[17,24,25].

The present results may simply be viewed as yet another example of the complexity of the interaction of O_2 with W, permitting no quantitative statements. However, in the context of the current discussion, it should be noted that O_2 on tungsten does form a stable array (viz the LEED results reviewed above) and below 1250°K relatively small effects on Q_i and τ_o are observed, as compared with results to be discussed below. A comment on the behavior above 1450°K will also be found in the next section.

C) Gaseous contamination: H_2 and N_2

Figure 6 shows the log $\tau(\frac{1}{T})$ data obtained during continuous exposure of the W target to H_2 and N_2. For comparison purposes, the straight line derived from the clean surface data of figure 4 is also shown in figure 6.

In the case of H_2, the partial pressure was 2×10^{-7} torr (equivalent N_2 pressure, i.e. the ion gauge reading was corrected by the ratio of ionization cross sections for H_2 and N_2[26]). From the results of Hickmott[27], the H_2 coverage at $\sim 1400^\circ$K, for this pressure, may be estimated as approximately 10^{-4} monolayers.

In the case of N_2, the partial pressure was 3×10^{-7} torr. Although no high temperature data for the N_2/W system are known to the present authors, a crude estimate of the N_2 coverage may be made if one assumes that the adsorption to be in the "β-state" with a desorption energy of ~ 75 K cal/mole[28]
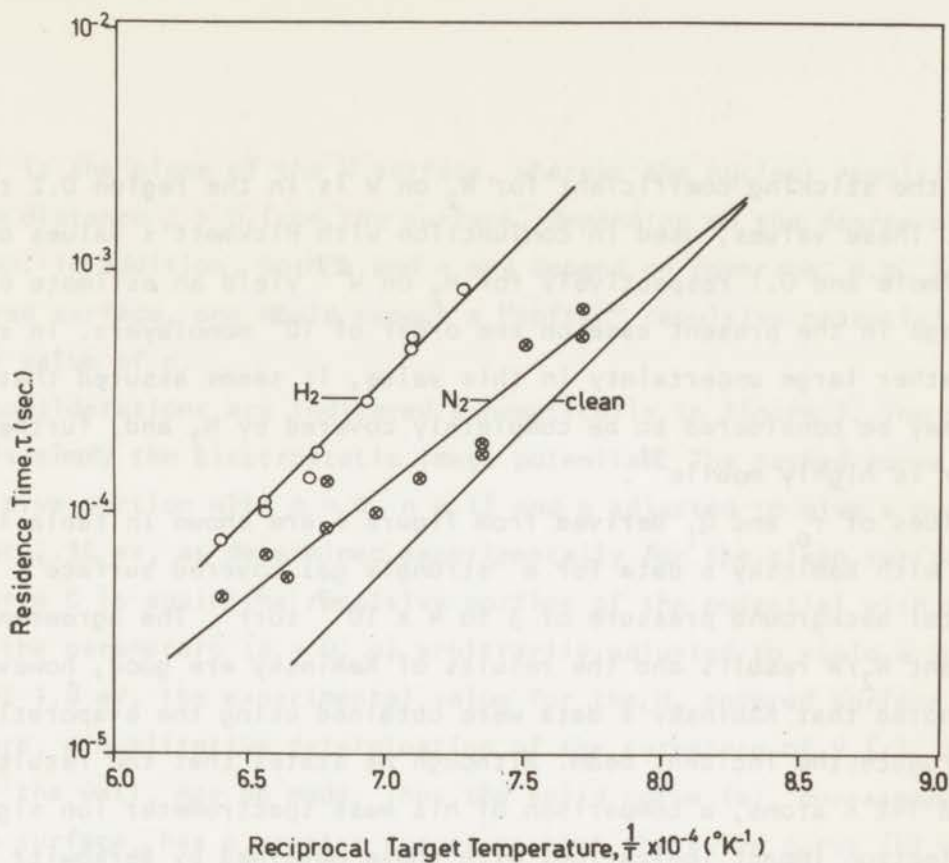
Fig. 6 - Residence time versus reciprocal target temperature for K^+ desorption from W in the presence of partial pressures of H_2 and N_2. Also shown is the curve corresponding to a clean surface (e.g. curve A, figure 4).
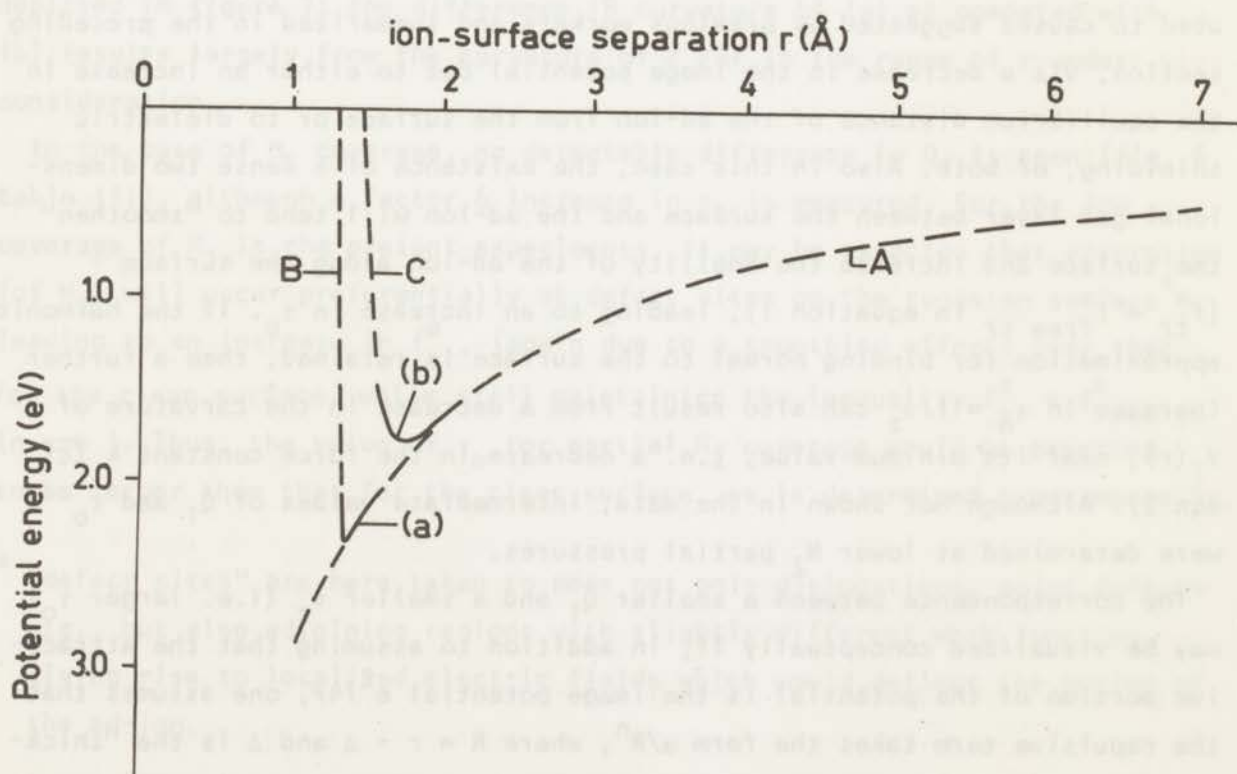

Fig. 7 - Potential energy diagram of the K^+-W system which illustrates qualitatively the effect of gaseous contamination on τ_o (see text).

and that the sticking coefficient for N_2 on W is in the region 0.2 to o.6[29,30]. These values, used in conjunction with Hickmott's values of 31 K cal/mole and 0.1 respectively for H_2 on W[27] yield an estimate of the N_2 coverage in the present case on the order of 10^2 monolayers. In spite of the rather large uncertainty in this value, it seems assured that the surface may be considered to be completely covered by N_2 and, further, this gas layer is highly mobile[31].

The values of τ_o and Q_i derived from figure 6 are shown in table III and compared with Kaminsky's data for a "strongly gas covered surface", i.e. for a total background pressure of 3 to 4 x 10^{-7} torr[5]. The agreement between the present N_2/W results and the results of Kaminsky are good, however it must be noted that Kaminsky's data were obtained using the evaporation of KCl to produce the incident beam. Although he states that the resultant beam contained 74% K atoms, a comparison of his mass spectrometer ion signals (using electron impact ionization) with those obtained by Berkowitz and Chupka[32] tends to discredit this assertion in as much as the latter workers conclude that the K^+ ion signal results from the process $KCl + e^- \rightarrow K^+ + Cl + 2e^-$ and the evaporating species consist mainly of KCl with a small amount of $(KCl)_2$, and with K atoms absent.

For the case of high gas coverage (N_2) the reduction in Q_i may be attributed to causes suggested by previous workers and summarized in the preceding section, viz a decrease in the image potential due to either an increase in the equilibrium distance of the ad-ion from the surface or to dielectric shielding, or both. Also in this case, the existence of a dense two dimensional gas layer between the surface and the ad-ion will tend to "smoothen" the surface and increase the mobility of the ad-ion along the surface ($f_{tr}^a \rightarrow f_{free\ tr}^a$ in equation 1), leading to an increase in τ_o. If the harmonic approximation for binding normal to the surface is retained, then a further increase in $\tau_o = 1/\nu_z$ can also result from a decrease in the curvature of $V_i(r)$, near its minimum value, i.e. a decrease in the force constant k (cf. eqn 2). Although not shown in the data, intermediate values of Q_i and τ_o were determined at lower N_2 partial pressures.

The correspondence between a smaller Q_i and a smaller ν_z (i.e. larger τ_o) may be visualized conceptually if, in addition to assuming that the attractive portion of the potential is the image potential $e^2/4r$, one assumes that the repulsive term takes the form α/R^n, where $R = r - \Delta$ and Δ is the "thickness" of the gas layer. In other words, the plane of symmetry for the image

potential is the plane of the W surface, whereas the nucleur repulsion oc-
curs at a distance $\Delta \geq 0$ from the surface, depending on the degree of con-
tamination. In addition, both α and n may depend on coverage, e.g. for a
gas covered surface, one would expect a "softer" repulsive potential, thus
a smaller value of n.

These considerations are indicated schematically in figure 7. The dashed
curve A is simply the electrostatic image potential. The dashed curve B is
the repulsive portion with $\Delta = 0$, $n = 12$ and α adjusted to give a potential
minimum at 2.36 eV, as determined experimentally for the clean surface. The
dashed curve C is again the repulsive portion of the potential with $n < 12$
and with the parameters $(\Delta \geq 0, \alpha)$ arbitrarily adjusted to yield a potential
minimum at 1.8 eV, the experimental value for the N_2 covered surface. From
this figure, a qualitative determination of the curvature of $V_i(r)$, at the
bottom of the well, may be made. Thus the solid curve (a), corresponding to
the clean surface, has a greater curvature than the solid curve (b) which
corresponds to the N_2 covered surface, i.e. ν_z is larger (and therefore τ_o
smaller) in the well (a) than in the well (b). This trend, viz a larger Q_i
and smaller τ_o for the clean surface, is in accord with the experimental
findings as reported in tables I and III. Note also that the arbitrary choice
of $n < 12$ for the N_2 covered surface does not effect the qualitative changes
depicted in figure 7: the difference in curvature of (a) as compared with
(b) results largely from the curvature of $e^2/4r$ in the range of r under
consideration.

In the case of H_2 coverage, no detectable difference in Q_i is seen (fig. 6,
table III), although a factor 6 increase in τ_o is measured. For the low
coverage of H_2 in the present experiments, it may be expected that adsorption
(of H_2) will occur preferentially at defect sites on the tungsten surface[*],
leading to an increase in f^a_{tr}, (again due to a smoothing effect) over that
for the clean surface, while still maintaining the inequality $f^a_{tr} < f^a_{free\ tr}$
in eqn 1. Thus, the value of τ_o for partial H_2 coverage would be expected
to be larger than that for the clean surface, as is determined experimentally.

---

[*] "defect sites" are here taken to mean not only dislocations, point defects
etc., but also adjoining regions with slightly different work function,
giving rise to localized electric fields which would deflect the motion of
the ad-ion.

It is difficult to imagine that such low coverages of H_2 would produce significant changes in the curvature of $V_i(r)$ and, therefore, changes in f_z can probably be ignored in this case as compared with the increase in the surface mobility of the ad-ion.

Comparing the clean surface data with the H_2 data (low contaminant coverage) and with the N_2 data (intermediate to high coverage), there emerges a trend: low coverages tend to increase τ_o; as the coverage increases, decreases in Q_i become observable and more drastic increases in τ_o occur. A physical interpretation of these observations is suggested in the preceding paragraphs.

Returning briefly to the data of figure 5 and table II, the discussion of the present section would suggest that O_2 on W begins to become mobile at temperatures above $\sim1450^{\circ}$K, viz the decrease in Q_i and drastic increase in τ_o reported in table II for $T \geq 1450^{\circ}$K as compared with the values reported for $T \leq 1250^{\circ}$K. In support of this inference, the mass spectrometer data show that evaporation of tungsten oxides becomes most prominent at temperatures $\geq 1400^{\circ}$K[24,25].

SUMMARY AND CONCLUSIONS

The present results indicate quite clearly that surface contaminants can drastically alter the observed values of the binding energy Q_i, and the pre-exponential factor, τ_o, as related to the mean residence time for K^+ on tungsten, through the relation $\tau = \tau_o \exp Q_i/kT$. It is suggested that earlier studies of the K/W system[1,5] were obtained with tungsten surfaces containing a carbon impurity, which serves to effect τ_o but not Q_i. It may be deduced that the nature of the bonding of the contaminant to the surface is important: strong bonding (ordered arrays) tend to produce relatively small changes in τ_o and little or no effect on Q_i. Surface contamination in the form of a two-dimensional gas produces a large decrease in Q_i due to screening effects, and an increase in τ_o due principally to increased surface mobility of the adsorbed K^+ ion. These interpretations are consistent with the existing interpretations of the physical origin of Q_i and τ_o[1,3,4,5,11].

It is instructive to compare these conclusions with those derived from experiments concerned with the scattering of rare gases from metal single crystals and LiF[33-36]. In these latter studies it is found that adsorbed contaminants on Au have a strong effect on the scattering behavior, while for Ag and LiF the effect is greatly reduced. In as much as the bonding of contaminants to Au is much weaker than for the more reactive Ag surface (or

the ionic crystal), it was argued that in the latter cases (Ag and LiF) contamination tended to produce a "reproduction" of the underlying lattice. Further, the angular distribution of the scattered atomic beam can be related to the degree of energy transfer, via the interaction time of the atom with the surface[37,38]. Thus, the present experiments, which demonstrate striking increases in τ for mobile (weak) contaminant adsorption, corroborate the previous inferences made in the case of non-reactive scattering, i.e. a mobile adsorbed contaminant tends to increase τ and, therefore, increase the amount of energy transfer (by allowing multiple collisions), leading to a greater dispersion in the scattered beam.

Finally, it is suggested that the present type of experiment may prove to provide additional information on the "dimensions" of surface structures for strongly bound contaminants, in conjunction with LEED, RHEED, ion neutralization spectroscopy[39] etc, because of the relation between $f^a_{tr}/f^a_{free\ tr}$ and τ_o as given in eqn 1. To this end, experiments are continuing in this laboratory using other alkali metals, having different ionic radii.

ACKNOWLEDGEMENTS

REFERENCES

1) R.C. Evans, Proc.Roy.Soc. A139, 604 (1933).

2) J.B. Taylor and I. Langmuir, Phys.Rev. 44, 423 (1933).

3) M.D. Scheer and J. Fine, J.Chem.Phys. 37, 107 (1962).

4) M.D. Scheer and J. Fine, J.Chem.Phys. 38, 307 (1963).

5) M. Kaminsky, Ann.der Physik 18, 53 (1966).

6) M. Kaminsky, Bull.Am.Phys.Soc. 12, 379 (1967).

7) F.L. Hughes and H. Levinstein, Phys.Rev. 113, 1029 (1959).

8) F. Knauer, Z.Physik 125, 278 (1948).

TK

- 65 -

9) S.V. Starodubtsev, J.Exper.Theor.Phys. (USSR), 19, 215 (1949).

10) J. Perel, R.H. Vernon and H.L. Daley, J.Appl.Phys. 36, 2157 (1965).

11) S. Kruyer, Koninkl.Ned.Akad.Wetenschap Proc., B58, 73 (1955);see also:
J.H. de Boer, Adv. in Catal. VIII, Academic Press (NY) 1956, p.17.

12) J. Politiek, P.K. Rol, J. Los and P. Ikelaar, Rev.Sci.Inst. 39, 1147
(1968).

13) C.A. Visser, J. Wolleswinkel and J. Los, Submitted for publication.

14) L.J. Varnerin Jr., Phys.Rev. 91, 859 (1953).

15) E.Ya. Zandberg and N.I. Ionov, Sov.Phys. Uspehki, 67, 255 (1959).

16) J. Frenkel, Z.Physik, 26, 117 (1924).

17) J.A. Becker, E.J. Becker and R.G. Brandes, J.Appl.Phys. 32, 411 (1961).

18) M. Boudart and D.F. Ollis, The Structure and Chemistry of Solid Surfaces,
John Wiley and Son (NY), 1969, 863-1.

19) N.J. Taylor, Surf.Sci. 2, 544 (1964).

20) L.G. Germer and J.W. May, Surf.Sci. 4, 452 (1966).

21) C.W. Tucker Jr., Surf.Sci. 6, 124 (1967).

22) J.C. Tracey and J.M. Blakely, ref. 18, p.65-1.

23) C.A. Haque and E.E. Donaldson, Rev.Sci.Instr. 34, 409 (1963).

24) B. McCarrol, J.Chem.Phys. 46, 863 (1967).

25) Yu.G. Ptushinskii and B.A. Chuikov, Surf.Sci. 6, 42 (1967).

26) H.S.W. Massey and E.H.S. Burhop, Electronic and Ionic Impact Phenomena,
Oxford Clarendon Press 1952.

27) T.W. Hickmott, J.Chem.Phys. 32, 810 (1960).

28) T.A. Delchar and G. Ehrlich, J.Chem.Phys. 42, 2686 (1965).

29) J.A. Becker and C.D. Hartman, J.Chem.Phys. 47, 156 (1953).

30) T.W. Hickmott and G. Ehrlich, J.Phys.Chem.Solids 5, 66 (1958).

31) R. Gomer, Fundamentals of Gas-Surface Interactions, Academic Press (NY)
1967, p.182.

32) J. Berkowitz and W.A. Chupka, J.Chem.Phys. 29, 653 (1958).

33) J.N. Smith Jr. and H. Saltsburg, J.Chem.Phys. 40, 3585 (1964).

34) H. Saltsburg and J.N. Smith Jr., J.Chem.Phys. 45, 2175 (1966).

35) D.R. O'Keefe, J.N. Smith Jr., R.L. Palmer and H. Saltsburg,
Surf.Sci., in press.

36) J.N. Smith Jr. and H. Saltsburg, ref. 31, p.370.

37) J.N. Smith Jr., H. Saltsburg and R.L. Palmer, J.Chem.Phys. 49, 1287
(1968).

- 66 -

38) F.O. Goodman, Rarefied Gas Dynamics, vol. 2, suppl. 3, Academic Press, N.Y. 1966, p.366.

39) H. Hagstrum and G.E. Becker, Phys.Rev. Letters, 22, 1054 (1969).

TABLE I

	This work[1]	This work[2]	Kaminsky[3]	Evans[4]
Q_i (eV)	$2.36 \pm .06$	$2.36 \pm .06$	$2.41 \pm .03$	2.43
τ_o (sec.)	$2.4 \pm 0.9 \times 10^{-13}$	$.6 \times 10^{-13}$	$.59 \pm 01 \times 10^{-13}$	1.26×10^{-13}

1) decarbonized tungsten

2) carbonized tungsten

3) "atomically clean" tungsten, ref. 6

4) vacuum conditions unspecified, but flashing temperatures between 2700°K and 3000°K employed, ref. 1.

TABLE II [1]

	$T \leq 1250°K$	$1250°K \leq T \leq 1450°K$	$1450°K \leq T$
Q_i (eV)	2.4	$.45$	2.0
τ_o (sec.)	$.5 \times 10^{-13}$	3×10^{-6}	2×10^{-11}

1) approximate values for continuously oxygenated W surface. See text for discussion.

TABLE III

	This work[1]	This work[2]	Kaminsky[3]
Q_i (eV)	1.8	2.36	$1.71 \pm .02$
τ_o (sec.)	6×10^{-11}	1.4×10^{-12}	$4.1 \pm 0.4 \times 10^{-11}$

1) Background pressure of $N_2 \approx 3 \times 10^{-7}$ torr

2) Background pressure of $H_2 \approx 2 \times 10^{-7}$ torr

3) "strongly gas covered", using the evaporation of KCl to produce incident beam, ref. 5.

CHAPTER V

ION RESIDENCE TIME MEASUREMENTS FOR THE SURFACE IONIZATION OF Na ON
CARBONIZED AND DE-CARBONIZED W: PRELIMINARY RESULTS

INTRODUCTION

This final chapter presents preliminary measurements made for the residence time of Na ionized on W. Due to time restrictions, it was not possible to complete these experiments. On the other hand, from the data that was obtained, certain inferences concerning the interaction of Na with carbonized and de-carbonized W may be made and suggestions for future experiments to further explore these inferences are proposed.

At the outset, it should be noted that the Na-W interaction represents a much more complex system than the K-W interaction reported in the previous chapter. This is due to the fact that here (except for strongly oxygenated W) $I > \phi$, where I and ϕ are the ionization potential of the alkali-atom and the work function of the metal respectively. Thus, the potential energy diagram for the system Na-W is, schematically, as shown in figure 1 (compare with figure 3 of chapter 4). From figure 1 it is seen that, since $V_i(\infty)$ lies above $V_a(\infty)$ by an amount equal to or greater than $(I - \phi)$, "curve crossing" may occur. Since the experimental signal is derived from ions leaving the surface, it may not be possible to determine unambiguously whether the derived values of Q correspond to Q_i or $(Q_a)_i$ as indicated in figure 1. In other words, some undetermined fraction of the ions leaving the surface may, due to curve crossing, originate from adsorbed atoms thereby yielding derived values of $(Q_a)_i < Q_i$. This possibly is explored more fully in the discussion section of the present chapter.

It is known that the energy level of the valence electron of the free alkali-atom shifts and the level itself becomes broadened into a band as the distance between the atom and the surface decreases[1]. For the K-W system, $\phi > I$, and the effect of this level shift and broadening is presumably un-important. However, for the Na-W system, with $\phi < I$, this effect may indeed be significant in determining the ionization efficiency.

Thus, a priori, one might expect significant differences in the surface ionization of Na, as compared with K. Indeed several striking differences were noted experimentally. Among them were a long (ca 30 min) "induction" period prior to attainment of a steady state value of τ. No such induction period was
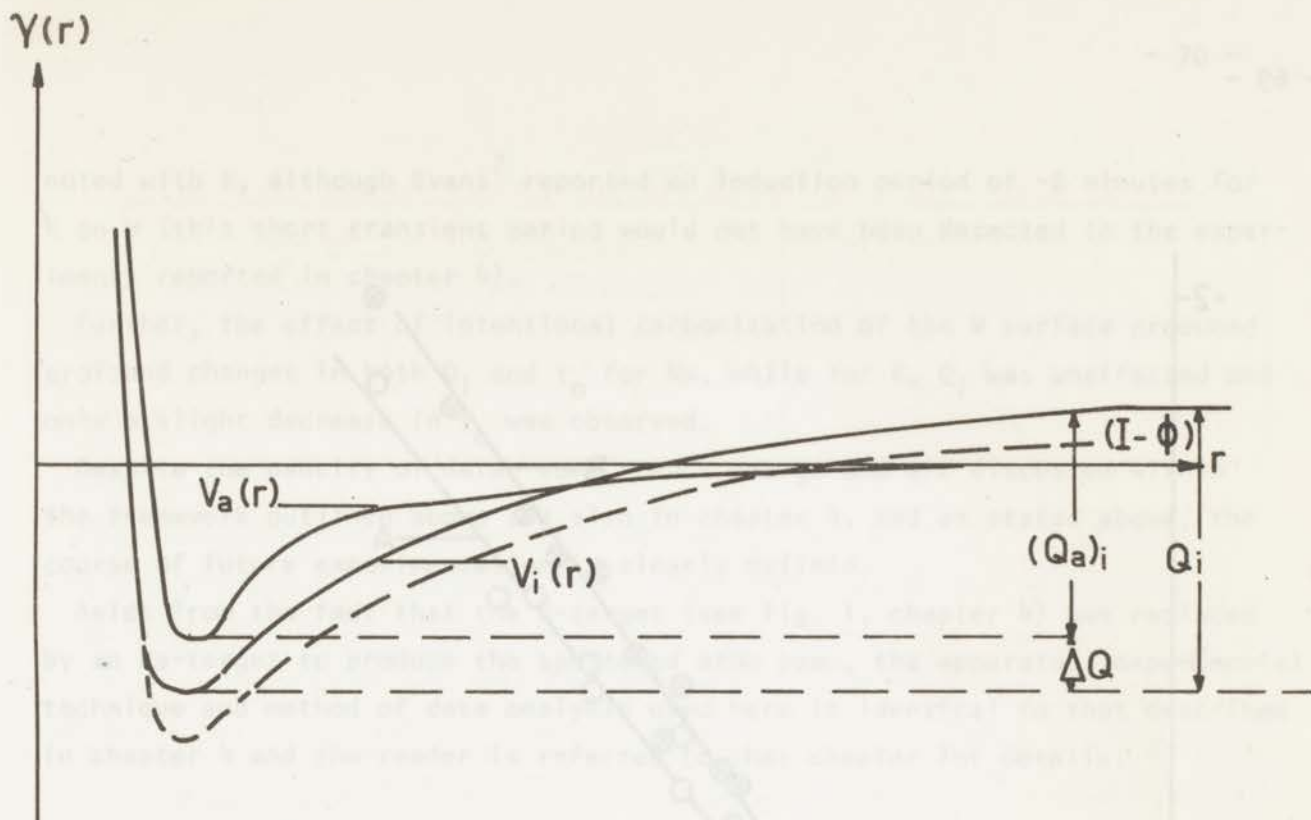
Fig. 1 - Schematic representation of the potential energy diagram for the Na-W system. See text for discussion of symbols.
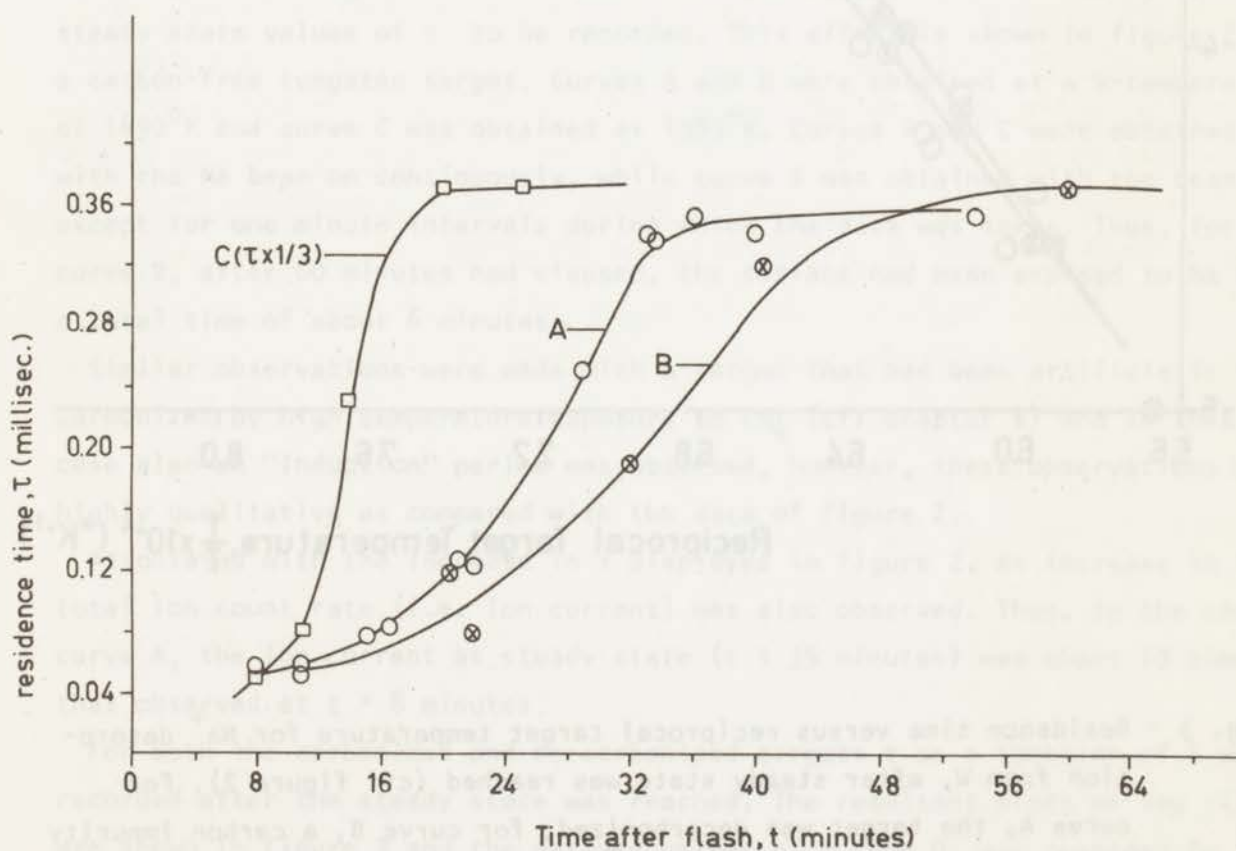
Fig. 2 - Residence time versus time after flash for Na$^+$ desorption from de-carbonized W. Note reduce scale for curve C. See text for further details.

Residence time, τ (sec.)

B

A

Reciprocal Target Temperature, $\frac{1}{T} \times 10^{-4}$ (°K^{-1})
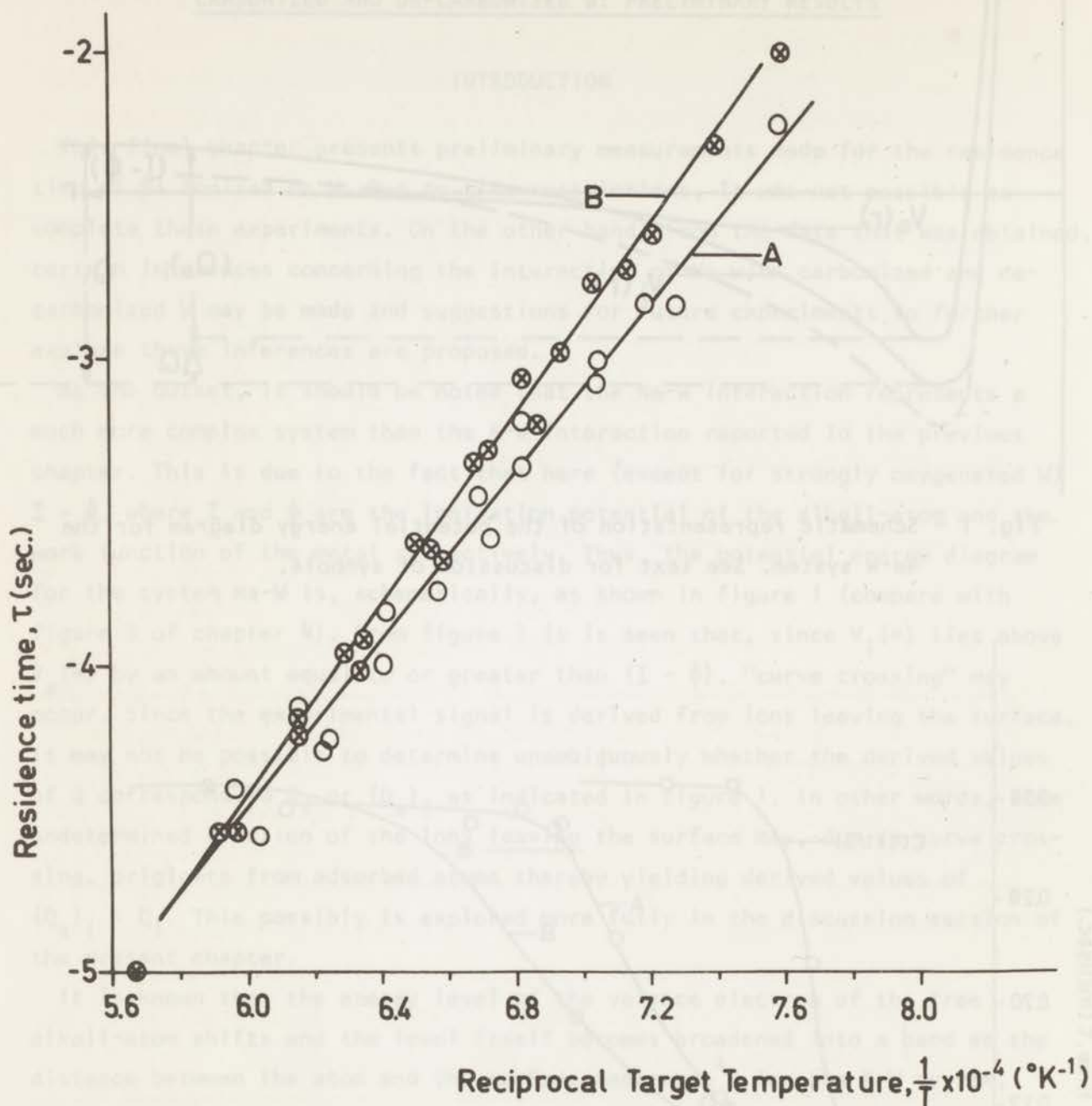
Fig. 3 - Residence time versus reciprocal target temperature for Na$^+$ desorp-
tion from W, after steady state was reached (cf. figure 2). For
curve A, the target was decarbonized; for curve B, a carbon impurity
was present.

noted with K, although Evans[2] reported an induction period of ~2 minutes for K on W (this short transient period would not have been detected in the experiments reported in chapter 4).

Further, the effect of intentional carbonization of the W surface produced profound changes in both Q_i and τ_o for Na, while for K, Q_i was uneffected and only a slight decrease in τ_o was observed.

Despite the paucity of data, some trends emerge and are discussed within the framework outlined above and also in chapter 4, and as stated above, the course of future experimentation is clearly defined.

Aside from the fact that the K-target (see fig. 1, chapter 4) was replaced by an Na-target to produce the sputtered atom beam, the apparatus, experimental technique and method of data analysis used here is identical to that described in chapter 4 and the reader is referred to that chapter for details.

RESULTS

At the outset, it was noted that a long period of time was required, after flashing the W-target to about 2700°K at a pressure of 2×10^{-9} torr, for steady state values of τ to be recorded. This effect is shown in figure 2 for a carbon-free tungsten target. Curves A and B were obtained at a W-temperature of 1490°K and curve C was obtained at 1385°K. Curves A and C were obtained with the Na beam on continuously, while curve B was obtained with the beam off except for one minute intervals during which the data was taken. Thus, for curve B, after 60 minutes had elapsed, the surface had been exposed to Na for a total time of about 6 minutes.

Similar observations were made with a target that had been artificially carbonized by high temperature exposure to CH_4 (cf. chapter 4) and in this case also an "induction" period was observed, however, these observations were highly qualitative as compared with the data of figure 2.

Associated with the increase in τ displayed in figure 2, an increase in the total ion count rate (i.e. ion current) was also observed. Thus, in the case of curve A, the ion current at steady state ($t \approx 35$ minutes) was about 10 times that observed at $t \approx 8$ minutes.

For both the carbonized and de-carbonized targets τ as a function of T was recorded after the steady state was reached. The resultant plots of $\log \tau(1/T)$ are shown in figure 3 and the derived values of τ_o and Q_i are recorded in table I and compared with the "atomically clean surface" data of Kaminsky[3].

TABLE I

	this work (de-carbonized surface)	this work (carbonized surface)	Kaminsky[3]
Q_i (eV)	2.71	3.2	2.69 ± 0.03
τ_o (sec)	2×10^{-13}	6×10^{-15}	$0.85 \pm 0.15 \times 10^{-13}$

From table I it is seen that Q_i for the de-carbonized surface agrees very well with Kaminsky's value, while the present value of τ_o is about twice as large as that reported by Kaminsky. The present results for the carbonized surface are markedly different, when compared with the de-carbonized surface data, than was found for K (cf. chapter 4, table I). Here τ_o is decreased by nearly 2 orders of magnitude and Q_i is increased by almost 20%.

DISCUSSION

If one assumes that the observed "induction" period depicted in figure 2 is due solely to adsorption of a contaminant from the residual background gas ($p \sim 2 \times 10^{-9}$ torr), then from curves obtained at different surface temperatures (e.g. curves A and C) one may estimate the heat of adsorption, ΔH, of that contaminant and, thereby, tentatively identify the particular contaminant responsible. Thus if n is the surface concentration of contaminant and f is the incident flux of that contaminant, one may write

$$\dot{n} = f - n\nu_d \tag{1}$$

where ν_d is a frequency factor for desorption and has the form $\nu_d = \nu \exp \Delta H/kT$. Equation (1) further assumes that the adsorbed species and desorbing species are the same, i.e. no dissociative chemisorption is involved. Equation (1) integrates readily to yield

$$n = \frac{f}{\nu_d} [1 - \exp(-\nu_d t)] \tag{2}$$

The steady state concentration, n(T), will be reached when $\nu_d t \gg 1$. Alternatively, one may write the steady state condition as

$$\nu_d(T_1)t_1 = \nu_d(T_2)t_2 \tag{3}$$

where t_i is the time required to reach steady state at temperature T_i. Assuming that the pre-exponential frequency factor, ν, in the expression for ν_d is temperature independent, one may re-write eqn (3) as

$$t_1/t_2 = \exp \frac{\Delta H}{k} \left(\frac{1}{T_2} - \frac{1}{T_1}\right) \tag{4}$$

Using the values of (t_i, T_i) from curves A and C of figure 2, equation (4) yields a value of $\Delta H \sim 1.0$ eV. This result would seem to rule out O_2 as the contaminating species, since ΔH for O_2 on W is known to be greater than 4 eV[4]. A more likely contender would seem to be CO, which is more abundant as a background contaminant and has a smaller heat of adsorption on W than oxygen.

The increase in total ion signal, during the induction period, may be associated with an increase in ϕ, due to the adsorption of contaminants, via the Saha-Langmuir equation:

$$\alpha = \frac{1}{2} \exp(\phi - I)/kT \tag{5}$$

where α is the ratio of ions to neutrals evaporating from the surface. Since, in the present experiments, the incident beam intensity is constant, eqn (5) may be re-written in terms of the quantity β, the fraction of the incident beam that is ionized, and

$$\beta = \frac{\alpha}{1 + \alpha} \tag{6}$$

From the experimental observation that β increases by a factor of 10 during the induction period, one can estimate from eqn (6) that ϕ increases by ~0.3 eV, a value not incompatible with known work function changes produced by CO adsorption on W .

Next, one may ask whether changes in τ as depicted in figure 2 are due to changes in τ_o or Q_i. Since the ratio of τ_s, at steady state, to τ_{in}, obtained shortly after flash, appears to depend on temperature (cf. curves A vs C, fig. 2), it is tempting to attribute the changes in τ to changes in Q. Indeed if one defines the ratio $R = \tau_s/\tau_{in}$ then, assuming the constancy of τ_o, one arrives at the expression

$$\log \frac{R(T_1)}{R(T_2)} = 0.435 \left(\frac{Q_s - Q_{in}}{k}\right)\left(\frac{1}{T_1} - \frac{1}{T_2}\right) \tag{7}$$

which, from the data of fig. 2, yields a value of $Q_s \cong Q_{in} + 0.2$ eV.

A possible way to correlate this latter result with the estimated change in ϕ from eqn (6) may be visualized with the aid of the potential energy diagram of figure 1. Thus, as ϕ increases, the potential $V_i(r)$ will drop, as indicated schematically by the dashed curve of figure 1. Two features of the potential diagram are altered in this way: ΔQ is increased in the "cross over" point

moves further from the surface. Both factors tend to decrease the number of atoms that are desorbed as ions; an increase in ΔQ decreases the ratio of adsorbed atoms to adsorbed ions and the increase in distance of the cross over point decreases the probability of a transition from an adsorbed atomic state to a gas phase ion state. In other words, one may tentatively identify Q_{in} with $(Q_a)_i$ and Q_s with Q_i, where these factors are identified in eqn (7) and figure 1, and which yields a value of $\Delta Q \approx 0.2$ eV, in general agreement with earlier results[2].

Although the numbers derived via equations (6) and (7) do not refute the above interpretation, they can hardly be construed as conclusive proof that the proposed physical picture is correct. Obviously, a much more detailed study of τ and ϕ, as a function of time after flash, is needed.

A further puzzling aspect concerning the induction period is noted by comparing curves A and B of figure 2. Thus, it appears that the presence of Na promotes the attainment of steady state values of τ. It must be emphasized that the induction period is not entirely due to Na adsorption since, if this were the case, the values of τ obtained at $t = 60$ minutes for curve B and $t = 8$ minutes for curve A would be nearly equal, since the total exposure to Na is approximately the same in both cases. Rather, the data of figure 2 seem to suggest some sort of catalytic effect on the adsorption of background contaminants (e.g. CO). Following this interpretation, the work of Evans would indicate that K was an even "stronger" catalyst, since he observed steady state in less than 2 minutes. One might then infer that the effect of Li on the induction period would be even less than depicted in figure 2 for Na, thus suggesting another future experiment.

Turning now to the Na results for the carbonized W target, as shown in figure 3 and table I, one notes drastic differences as compared with the corresponding K results (cf. chapter 4). It is felt that the following line of reasoning may serve as a qualitative explanation for these results.

As noted in chapter 4, carbon on W forms an ordered array on the surface, with cell dimensions somewhat greater than the underlying W lattice. The principal effect of this carbon structure on K was to hinder the latteral motion of the ad-ion, i.e. reduce f^a_{tr} in Kruyer's expression

$$\tau_o = \frac{h}{kT} \frac{f^a_{tr}}{f^a_{free\ tr}} \times f_z \tag{8}$$

The ionic radius of Na^+ is ~30% smaller than that of K^+, which may permit Na^+ to become "trapped" in the unit cell produced by the carbon array. In this latter case of localized adsorption, an alternative expression for τ_o must be employed (as also derived by Kruyer),

$$\tau_o = \frac{h}{kT} \frac{h^2}{2\pi mkT} \frac{N_S}{0} f_x f_y f_z = 0.375 \times 10^{-15} \frac{N_S}{0} f_x f_y f_z \qquad (9)$$

where $N_S/0$ expresses the number of adsorption sites per $\AA^2$ and the f_i are the partition functions for vibration about the adsorption site in the x, y and z directions. If indeed the carbon structure is only slightly larger than the parent W lattice, then $N_S/0$ will be of the order of 10^{-1}. If one assumes that the binding is harmonic and, further, that $f_x = f_y = f_z = f = kT/h\nu$ then, using $\tau_o = 6 \times 10^{-15}$ sec from table I, eqn (9) yields a value of $\nu = 6 \times 10^{12}$ sec^{-1}, or a value of $\nu^{-1} = 2 \times 10^{-13}$ sec which, perhaps fortuitously, compares well with the decarbonized value of τ_o in table I.

That this postulated localized adsorption would also lead to an increase in Q_i can be rationalized by noting that when the Na ion is in a two-dimensional "box" (the carbon array), it interacts not only with the W, via the image potential as before, but also with the edges (or sides) of the box, thereby increasing its bonding to the surface.

The foregoing argument can be visualized conceptually by imagining the carbonized W surface to consist of a flat surface having an ordered array of circular depressions with fixed radii embossed upon it. Then imagine the ad-ion to be a ball rolling along such a surface. The larger the radius of the ball with respect to the radius of the circular depressions, the smaller will be the perturbations on the motion of the ball produced by these depressions. Conversely, if the radius of the ball is small, its motion will be strongly affected and indeed it may become trapped in the depressions, leading to localized adsorption. Such a model would, in a heuristic fashion, account for the observed differences between the behavior of K and Na on carbonized W.

One major discrepancy with regard to the carbonized W data remains: In chapter 4 it was argued that the K data of Kaminsky and of Evans was obtained using W targets with a carbon impurity. At first glance, the same argument cannot be carried through in the present case of the Na-W system; from table I, the present decarbonized surface values for Q_i and τ_o are in good agreement with Kaminsky, whereas the carbonized values are greatly different. Before one can reject the arguments of chapter 4 relating to the surfaces used by Kaminsky

and Evans, on the basis of the present Na results, one must note that Kaminsky took his data within 45 sec after flashing the W. On the other hand the data of figure 3 were taken after steady state was reached. As stated earlier, the induction period for the carbonized W has not been adequately studied in the present work and until such experiments have been performed, the question of the nature of the surface employed by Kaminsky for the Na-W measurements will have to remain unanswered.

SUMMARY AND CONCLUSIONS

From the residence time measurements for the Na-W system performed to data, it is quite clear that a much more complex interaction is extant here, as compared with the K-W system. Several reasons for this added complexity are discussed in the preceding sections of this chapter.

Decarbonized surface values of both τ and Q_i agree very well with data reported by Kaminsky for an "atomically clean" surface. In the present work, an induction period to reach steady state is observed and from the data some inferences may be made regarding the contaminant species responsible for the induction period and also regarding changes in work function and, possibly, in Q_i. The present results on carbonized W are quite different than those obtained for K and it is suggested that this is due primarily to the fact that the ionic radius of Na is smaller than that of K with the result that localized adsorption on the carbonized surface may occur in the former case.

In the main, however, the present results raise more (interesting) questions than they answer. But, in the process, the course of future experiments, designed to explore these questions, is clearly delineated. Among these future experiments are the following:

1) a detailed study of $\tau(T)$ as a function of time after flash for a decarbon-
   ized W ribbon. These results would permit a more accurate assessment of
   the heat of adsorption of the contaminant gas and also, when combined with
   work function change measurements, enable one to resolve the question as
   to whether or not the value of Q_i is changing during the induction period
   and, if so, add more physical insight into the reason for the change.
2) A similar study to 1), but for a carbonized W surface, in order to resolve
   the possible contradiction between the inferences drawn in chapter 4 re-
   garding the state of Kaminsky's "atomically clean" surface and similar in-
   ferences drawn for the present (preliminary) data.

- 76 -

3) In order to investigate the possible "catalytic" effect of the alkali
   atom on induction period, two experiments are suggested: As mentioned
   earlier, τ vs t measurements for Li would be of interest since, if the K
   results of Evans and the present Na results represent a trend, then the
   catalytic effect of Li might be expected to be negligible. Alternatively
   one might study the induction phenomena for Na by utilizing a second Na
   beam produced by a Knudsen cell, with proper collimation, placed directly
   in the experimental chamber. This procedure would have the advantage of
   permitting a much wider range of incidence fluxes to be obtained, but
   would have the disadvantage of decreasing the signal-to-noise ratio, since
   Na$^+$ ions arising from the second source would be uncorrelated and contribute
   only to the noise signal.

4) Li measurements on carbonized W would also be of interest, because of an
   even smaller ionic radius. Such data would serve to permit more quantitative
   statements to be made about localized adsorption than can be inferred from
   the present Na results.

Finally, as stated in the introduction to this chapter, the Na-W measurements
were terminated at the present state due to the time deadlines imposed by the
need to type, print, bind and distribute this thesis in time to permit the
promotion of the author in May 1970. However, the author does hope to be able
to complete some of the additional experiments outlined above prior to his
departure from the Netherlands in August 1970.

REFERENCES

1. J.W. Gadzuk, Surf.Sci. <u>6</u>, 133 (1967).
2. R.C. Evans, Proc.Roy.Soc. <u>A139</u>, 604 (1933).
3. M. Kaminsky, Bull.Am.Phys.Soc. <u>12</u>, 379 (1967).
4. I. Langmuir, J.Am.Chem.Soc. <u>34</u>, 1310 (1912).

SUMMARY

From the earlier results of rare gas scattering from metal single crystals, as summarized in chapter I, the principle inference to be drawn, within the overall theme of this thesis, concerns the effects of surface contamination on the observed angular distribution of scattered atoms. Generally, it may be stated that surface contaminants that are strongly bound to the surface produce little effect on the observed scattering distributions, while loosely bound contaminants can produce major perturbations in these distributions. These inferences are drawn from studies using epitaxially grown targets of Au and Ag, wherein contamination effects can be observed upon the cessation of metal deposition. Strong degradation of the scattering distributions are thus observed in the case of Au, but in the case of Ag, no changes are noted even after several hours of exposure to a background pressure of 10^{-7} Torr. From the known heats of adsorption of typical vacuum contaminants (e.g. H_2O, CO, N_2, etc.) on these two metals, it is strongly suggested that, in the case of Au, the contamination exists as a loosely bound, mobile species on the surface. On the other hand, the relatively strong binding of these same gases to the Ag surface tends to produce a tightly bound layer which displays many of the properties of the substrate, to the extent that these properties effect the scattering of gas atoms. Further supporting evidence is found in the case of scattering of rare gases from LiF (cf. chapter 3) in which the LiF targets were cleaved in air, at atmospheric pressure, and no subsequent cleaning techniques were employed. Even so, from such surfaces, diffraction phenomena and other structure in the scattering distribution of rare gases were observed. In this latter case it is known that H_2O bonds very strongly to the LiF surface. Indeed a comparison of He diffraction experiments, using a wide variety of crystal preparation techniques including crystal cleavage in U.H.V., yields no striking differences, indicating a minimal effect of strong adsorption.

The experiments of chapter 2 were undertaken to explore the extent to which the Maxwellian velocity distribution of an incident thermal beam of rare gas atoms effected the dispersion of the scattered beam. It was found that the scattering distributions of Maxwellian beams were virtually indistinguishable from those of velocity filtered beams. From these results it was inferred that an important parameter in determining the degree of energy transfer, and therefore the spatial dispersion of the scattered beam, was the ratio of the atom-surface interaction time to the characteristic vibration period of the surface.

Thus, as this ratio increased, the energy transfer increased since more single-phonon energy transfer processes could occur during the interaction of the atom with the surface.

In chapter 3, the scattering of rare gases from LiF was studied and from the results (in addition to the effects of contamination mentioned above) it was shown that thermal energy atomic scattering from surfaces was quite sensitive to the periodicity and amplitude of the interaction potential in the plane of the surface, to anisotropies in the elastic properties of the crystal, and it was also suggested that strong coupling of the interacting gas atom with normal modes of vibration in the crystal occurred. In the latter case, inferences about the interaction time were quite important, but, due to the nature of the experiments, they had to remain inferences.

Chapters 4 and 5 report direct measurements of the interaction time, τ, in the surface ionization of K and Na on W, with particular emphasis on the effects of surface impurities. In general, these results tend to support the earlier inferences drawn from rare gas scattering (cf. chapter 1) regarding the importance of considering the nature of the bonding of the contaminants to the surface. Thus, for K^+ desorption from W (cf. chapter 4), τ tends to decrease for strongly bound contaminants and to increase for weakly bound contaminants.

Further, by expressing the mean residence time, τ, as $\tau = \tau_o \exp Q_i/kT$, and using the statistical mechanical derivation of τ_o due to Kruyer, the results of chapters 4 and 5 seem to demonstrate a definite trend from localized adsorption (Na^+ on carbonized W, chapter 5) to completely free translational motion of the ad-ion in the plane of the surface (K^+ on N_2 covered W, chapter 4). Additionally, some physical correlation between observed changes in τ_o and Q_i emerges as a result of the data of chapters 4 and 5.

Finally, a fundamental difference between the types of measurements reported in chapters 1 - 3 and those reported in chapters 4 and 5 is to be noted. For the rare gas interaction, the mean residence time is orders of magnitude smaller than that for alkali ion desorption. Further, in the latter case energy transfer between the incident atom and the surface is complete, i.e. the ad-ion is in thermal equilibrium with the surface, while in the case of rare gas scattering, the energy transfer can approach zero (cf. He on LiF). Nevertheless, appealing once again to the need to perform differential type experiments in the study of gas-surface interactions (as discussed in the introduction), it is felt that a qualitative comparison between the results of the surface ionization experiments

of chapters 4 and 5 with the non-reactive scattering experiments of chapters
1-3 is very instructive in expanding the understanding of the microscopic details
of the atom-surface interaction.

SAMENVATTING

Hoofdstuk 1 geeft een samenvatting van verstrooiingsmetingen van edelgas-
atomen aan metaal-éénkristallen. De belangrijkste conclusie die hieruit volgt
heeft betrekking op de invloed van oppervlakte-verontreinigingen op de hoekver-
deling van de verstrooide atomen. In het algemeen hebben sterk aan het opper-
vlak gebonden verontreinigingen weinig invloed op de verstrooiingsverdelingen,
terwijl zwak gebonden verontreinigingen grote veranderingen in deze verdelingen
kunnen veroorzaken. De hier bedoelde metingen zijn gedaan aan epitaxiaal ge-
groeide Au en Ag kristallen; door de verdamping van Au of Ag te stoppen kan men
de invloeden van de verontreiniging waarnemen. In het geval van Au ontstaan op
deze manier grote verschillen, maar in het geval van Ag is zelfs na verscheidene
uren blootstelling aan een achtergronddruk van 10^{-7} Torr geen verandering waar
te nemen. De adsorptie-energieën van typische restgascomponenten (bijv. H_2O, CO,
N_2 etc.) op deze twee metalen suggereren, dat in geval van Au de verontreiniging
zwak gebonden en beweeglijk is. Op het Ag-oppervlak daarentegen zal tengevolge
van de relatief sterke binding van deze gassen de gevormde oppervlaktelaag vele
eigenschappen van het substraat vertonen, voorzover het de verstrooiing van gas-
atomen betreft. Dit wordt bevestigd door de verstrooiingsexperimenten van edel-
gassen aan LiF (vergelijk hoofdstuk 3), waarbij de LiF kristallen in de lucht ge-
spleten werden, zonder naderhand het oppervlak te bewerken. Niettemin werden aan
deze oppervlakken diffraktieverschijnselen en andere strukturen in de verstrooi-
ingsverdeling van edelgassen waargenomen; het is bekend, dat de binding van H_2O
aan LiF zeer sterk is. Bij herhaling van de metingen met He, waarbij het kristal
op vele manieren behandeld werd, waaronder splijting onder UHV condities, werden
geen grote verschillen waargenomen, hetgeen de kleine invloed van sterk gebonden
verontreinigingen bevestigt.

De experimenten van hoofdstuk 2 werden gedaan om te onderzoeken in welke mate
de Maxwellse snelheidsverdeling van de invallende thermische bundel edelgasatomen
de dispersie van de verstrooide bundel beinvloedt. Gevonden werd dat de verstrooi-
ingsverdelingen van bundels met deze Maxwellse snelheidsverdeling niet te onder-
scheiden zijn van die van snelheidsgeselecteerde bundels. Uit deze resultaten
werd geconcludeerd dat een belangrijke parameter voor de bepaling van de energie-
overdracht, en dientengevolge voor de ruimtelijke dispersie van de verstrooide

bundel, de verhouding is van de atoom-oppervlakte interactietijd en de karakte-
ristieke vibratietijd van het oppervlak. Naarmate deze verhouding groter wordt
neemt de energie-overdracht toe, aangezien gedurende de interactie van het atoom
met het oppervlak meermalen overdracht van een fonon plaats kan vinden.

In hoofdstuk 3 wordt de verstrooiing van edelgassen aan LiF besproken. De re-
sultaten tonen eveneens aan dat atomaire verstrooiing aan oppervlakken in het
thermische energie-gebied erg gevoelig is voor de periodiciteit en de amplitude
van de wisselwerkingspotentiaal langs het oppervlak. Hetzelfde geldt voor aniso-
tropieën in de elastische eigenschappen van het kristal. Bovendien wordt gesugge-
reerd, dat er een sterke vibratiekoppeling is van het gasatoom loodrecht op het
kristaloppervlak. Voor deze koppeling is een schatting van de interaktietijd van
veel belang. Evenwel, door de aard van het experiment moet het bij een schatting
blijven.

In de hoofdstukken 4 en 5 worden de verblijftijdmetingen besproken van K en Na
aan een W-oppervlak. Hierbij wordt bijzondere aandacht geschonken aan de effecten,
welke veroorzaakt worden door oppervlakte-verontreinigingen. De tendens, dat het
karakter van de binding van de verontreiniging aan het oppervlak de interaktie
domineert, wordt hiermede bevestigd. Dit wordt geillustreerd door de verblijftijd-
metingen van K op W. Bovendien wijzen de resultaten van hoofdstuk 5 op gelocali-
seerde adsorptie in het geval van Na op gecarboniseerd W. Bij K op W daarentegen
(hoofdstuk 4), moet aangenomen worden dat K zich vrij langs het oppervlak kan be-
wegen. Ook blijkt er op grond van deze metingen een verband tussen τ_o en Q_i te
bestaan.

Tenslotte moet de aandacht gevestigd worden op een fundamenteel verschil tus-
sen de metingen beschreven in de hoofdstukken 1, 2 en 3 en die in de hoofdstuk-
ken 4 en 5. Voor edelgas-interakties is de gemiddelde verblijftijd enkele groot-
te-orden kleiner dan die voor alkali-ion desorptie. Verder is in het laatste ge-
val de energie-overdracht tussen het invallende atoom en het oppervlak volledig.
Het ad-ion is in thermisch evenwicht met het oppervlak, terwijl in het geval van
edelgasverstrooiing de energie-overdracht zeer gering is (vergelijk He op LiF).
Desalniettemin bestaat de indruk dat een kwalitatieve vergelijking tussen de re-
sultaten van desorptiemetingen met niet-reactieve verstrooiingsexperimenten zeer
instructief is, voor wat betreft microscopische details van de wisselwerking tus-
sen atomen en oppervlakken. Differentiële metingen aan gas-oppervlakte interak-
ties zullen hiervoor belangrijke informaties opleveren.

CURRICULUM VITAE

Mr. Joe N. Smith Jr. attended the California Institute of Technology, Pasadena, California, and received the Bachelor of Science and Master of Science degrees from that Institute in 1958 and 1959 respectively.

Since 1959, Mr. Smith has been a member of the scientific staff of the Atomic Physics Laboratory of Gulf General Atomic Inc., San Diego, Calif., where he has been engaged primarily in fundamental research concerned with the interaction of atomic and molecular beams with solid surfaces. This work has included studies of molecular dissociation and reconstitution, chemical reaction, energy transfer and adsorption-desorption phenomena but, in the main, has been concerned with non-reactive scattering from single crystal surfaces.

During this period Mr. Smith has served as principal investigator on numerous research contracts conducted for the U.S. Airforce Office of Scientific Research. Further he has served on the papers selection committee for several international symposia, has served as co-chairman of a conference on the Fundamentals of Gas-Surface Interactions and was co-editor of the proceedings of that conference, published by Academic Press (N.Y.). In addition he currently performs services as referee for the Journal of Chemical Physics and for Surface Science.

Mr. Smith is a member of the American Physical Society and is listed in American Men of Science and Who's Who in the West. At present he is on a one year's leave of absence from Gulf General Atomic and holds the position of visiting scientist at the FOM-Institute for Atomic and Molecular Physics, Amsterdam, where he is again engaged in basic research on gas-surface interactions in collaboration with Professor dr J. Los.

bundel, de verhouding is van de atoom-oppervlakte interactietijd en de karakteristieke vibratietijd van het oppervlak. Naarmate deze verhouding groter wordt neemt de energie-overdracht toe, aangezien gedurende de interactie van het atoom met het oppervlak meermalen overdracht van een fonon plaats kan vinden.

In hoofdstuk 3 wordt de verstrooiing van edelgassen aan LiF besproken. De resultaten tonen eveneens aan dat atomaire verstrooiing aan oppervlakken in het thermische energie-gebied erg gevoelig is voor de periodiciteit en de amplitude van de wisselwerkingspotentiaal langs het oppervlak. Hetzelfde geldt voor anisotropieën in de elastische eigenschappen van het kristal. Bovendien wordt gesuggereerd, dat er een sterke vibratiekoppeling is van het gasatoom loodrecht op het kristaloppervlak. Voor deze koppeling is een schatting van de interaktietijd van veel belang. Evenwel, door de aard van het experiment moet het bij een schatting blijven.

In de hoofdstukken 4 en 5 worden de verblijftijdmetingen besproken van K en Na aan een W-oppervlak. Hierbij wordt bijzondere aandacht geschonken aan de effecten, welke veroorzaakt worden door oppervlakte-verontreinigingen. De tendens, dat het karakter van de binding van de verontreiniging aan het oppervlak de interaktie domineert, wordt hiermede bevestigd. Dit wordt geïllustreerd door de verblijftijdmetingen van K op W. Bovendien wijzen de resultaten van hoofdstuk 5 op gelocaliseerde adsorptie in het geval van Na op gecarboniseerd W. Bij K op W daarentegen (hoofdstuk 4), moet aangenomen worden dat K zich vrij langs het oppervlak kan bewegen. Ook blijkt er op grond van deze metingen een verband tussen τ_o en Q_i te bestaan.

Tenslotte moet de aandacht gevestigd worden op een fundamenteel verschil tussen de metingen beschreven in de hoofdstukken 1, 2 en 3 en die in de hoofdstukken 4 en 5. Voor edelgas-interakties is de gemiddelde verblijftijd enkele grootte-orden kleiner dan die voor alkali-ion desorptie. Verder is in het laatste geval de energie-overdracht tussen het invallende atoom en het oppervlak volledig. Het ad-ion is in thermisch evenwicht met het oppervlak, terwijl in het geval van edelgasverstrooiing de energie-overdracht zeer gering is (vergelijk He op LiF). Desalniettemin bestaat de indruk dat een kwalitatieve vergelijking tussen de resultaten van desorptiemetingen met niet-reactieve verstrooiingsexperimenten zeer instructief is, voor wat betreft microscopische details van de wisselwerking tussen atomen en oppervlakken. Differentiële metingen aan gas-oppervlakte interakties zullen hiervoor belangrijke informaties opleveren.

CURRICULUM VITAE

Mr. Joe N. Smith Jr. attended the California Institute of Technology, Pasadena, California, and received the Bachelor of Science and Master of Science degrees from that Institute in 1958 and 1959 respectively.

Since 1959, Mr. Smith has been a member of the scientific staff of the Atomic Physics Laboratory of Gulf General Atomic Inc., San Diego, Calif., where he has been engaged primarily in fundamental research concerned with the interaction of atomic and molecular beams with solid surfaces. This work has included studies of molecular dissociation and reconstitution, chemical reaction, energy transfer and adsorption-desorption phenomena but, in the main, has been concerned with non-reactive scattering from single crystal surfaces.

During this period Mr. Smith has served as principal investigator on numerous research contracts conducted for the U.S. Airforce Office of Scientific Research. Further he has served on the papers selection committee for several international symposia, has served as co-chairman of a conference on the Fundamentals of Gas-Surface Interactions and was co-editor of the proceedings of that conference, published by Academic Press (N.Y.). In addition he currently performs services as referee for the Journal of Chemical Physics and for Surface Science.

Mr. Smith is a member of the American Physical Society and is listed in American Men of Science and Who's Who in the West. At present he is on a one year's leave of absence from Gulf General Atomic and holds the position of visiting scientist at the FOM-Institute for Atomic and Molecular Physics, Amsterdam, where he is again engaged in basic research on gas-surface interactions in collaboration with Professor dr J. Los.

although the lattice dimensions of alkali-halide crystals and metal crystals are nearly the same, diffraction of light gas atoms from surfaces of the former has been studied extensively whereas diffraction from the harder surfaces has not yet been observed. There are physical reasons why diffraction from metal crystals may not occur or may not be observable.

J.E. Lennard, in *Fundamentals of Gas-surface Interactions* (Academic Press, N.Y., 1967) p. 295.

R.L. Palmer, J.N. Smith, H. Saltsburg and D.R. O'Keefe, J. Chem. Phys. DDC 746, 40 (1970).

II

From preliminary results already obtained it seems probable that measurements of the residence time for ion desorption can be utilized as a new technique for the study of adsorption.

Chap. 2, this thesis.

III

The application of the method of continuous deposition of metal surfaces which has been successfully applied to molecular beam scattering studies can also be a powerful tool in the study of heterogeneous catalysis.

J.N. Smith, H. Saltsburg and R.L. Palmer, in *Rarefied Gas Dynamics, Symposium* (Academic Press, N.Y., 1969) p. 1141.

IV

In his studies of sodium desorption Kaminsky used the evaporation of alkali halides (for example KCl) to produce the incident beam, in mass analysis, he reports the composition of the incident beam that desorbs 745 K atoms. This conclusion is false as can be shown by comparison with evaporation studies of the alkali-halides.

J.H. Perreault and R.A. Chupka, J. Chem. Phys. 26, 862 (1957).
M. Kaminsky, Ann. der Physik 18, 55 (1960).

CURRICULUM VITAE

Mr. Joe E. Smith Jr. attended the California Institute of Technology, Pasadena, California, and received the Bachelor of Science and Master of Science degrees from that Institute in 1958 and 1959 respectively.

Since 1961, Mr. Smith has been a member of the scientific staff of the Atomic Physics Laboratory of Gulf General Atomic Inc., San Diego, Calif., where he has been engaged primarily in fundamental research concerned with the interaction of atomic and molecular beams with solid surfaces. This work has included studies of molecular dissociation and recombination, chemical reaction, energy transfer and adsorption-desorption phenomena but, in the main, has been concerned with non-reactive scattering from single crystal surfaces.

During this period Mr. Smith has served as principal investigator on several research contracts conducted for the U.S. Airforce Office of Scientific Research. Further he has served on the paper selection committee of several international symposia, has served as co-chairman of a conference on the fundamentals of Gas-Surface Interactions and was co-editor of the proceedings of that conference, published by Academic Press (....). In addition he currently performs services as referee for the Journal of Chemical Physics and for Surface Science.

Mr. Smith is a member of the American Physical Society and is listed in American Men of Science and Who's Who in the West. At present he is on a one year's leave of absence from Gulf General Atomic and holds the position of visiting scientist at the FOM-Institute for Atomic and Molecular Physics, Amsterdam, where he is again engaged in basic research on gas-surface interactions in collaboration with Professor Dr J. Los.

STELLINGEN

I

Although the lattice dimensions of alkali-halide crystals and metal crystals are nearly the same, diffraction of light gas atoms from surfaces of the former has been studied extensively whereas diffraction from the latter surfaces has not yet been observed. There are physical reasons why either atom diffraction from metal crystals may not occur or may not be observable.

J.C. Crews, in Fundamentals of Gas-surface interactions, (academic press, N.Y., 1967) p. 480.
R.L. Palmer, D.R. O'Keefe, H. Saltsburg and J.N. Smith Jr., J. Vac. Sci. and Tech. 7, 91 (1970).

II

From preliminary results already obtained it seems probable that measurements of the residence time for ion desorption can be utilized as a new technique for the study of adsorption.

Chap. V, this thesis.

III

The application of the method of continuous deposition of target surfaces, which has been successfully applied to molecular beam scattering studies, can also be a powerful tool in the study of heterogeneous catalysis.

J.N. Smith, H. Saltsburg and R.L. Palmer, in Rarefied Gas Dynamics, 6th Symposium (academic press, N.Y., 1969), p. 1141.

IV

In his studies of surface ionization Kaminsky used the evaporation of alkali-halides (for example KCl) to produce the incident beam. By mass analysis, he reports the composition of the incident beam (for example 74% K atoms). This conclusion is false as can be shown by comparison with evaporation studies of the alkali-halides.

J.Berkowitz and W.A. Chupka, J. Chem. Phys. 29, 653 (1958).
M. Kaminsky, Ann. der Physik 18, 53 (1966).

V

It has been shown that the scattering of light atoms is a very sensitive
measure of the perfection of a solid surface. Further, there are physical
grounds for suggesting that atom scattering is a more sensitive test of
surface perfection than is low energy electron diffraction (LEED).

J.N. Smith Jr. and H. Saltsburg, J. Chem. Phys. $\underline{40}$, 3585 (1964).

VI

Many of the contributions to the American way of life due to the Red Indian
have been widely recognized. The influence of the existence of the Iroquois
Nation on the creation of the original American Republic and its constitu-
tion deserves more attention however.

For example, see The Indian Heritage of America, Alvin M. Josephy, Jr.,
(Alfred A. Knopf, N.Y., 1968).

VII

Gasser, et al. have studied the reaction $H_2 + D_2 \rightarrow 2\ HD$ as catalyzed by Ni
and conclude that the reaction proceeds via a precursor state in which an
incident D_2 (or H_2) molecule reacts directly with an adsorbed H (or D) atom.
Their data are insufficient to prove this conclusion.

R.P.H. Gasser, K. Roberts and A.J. Stevens, Surf. Sci. $\underline{20}$, 123 (1970).

VIII

It has occasionally been suggested that a scientific approach to the evalu-
ation of the merits of creative art could be developed. This suggestion is
not only absurd but, if pursued, could easily lead to destructive changes
in all areas of human ethical and moral behaviour.

For example, see The Scientific Attitude, C.H. Waddington, Penguin Books,Ltd.
London (1941).

IX

From recent experimental results of changes in the critical temperature of
superconducting thin films, as a function of film thickness, a strong effect
of surface photon frequencies is inferred. A direct experimental test of this
inference might result from simultaneous atomic beam scattering studies from
surfaces of such films.

M. Strongin et al., Phys. Rev. Letters $\underline{21}$, 1320 (1968).

.-.-.-.-.